ROUND

HOLLOW STRUCTURAL SECTIONS

SUBJECTED TO INELASTIC STRAIN REVERSALS

ROUND
HOLLOW STRUCTURAL SECTIONS
SUBJECTED TO INELASTIC STRAIN REVERSALS

by

MAGDI ANTOINE CHIDIAC, B.Sc.

A Thesis
Submitted to the School of Graduate Studies
in Partial Fulfilment of the Requirements
for the Degree
Master of Engineering

McMaster University
March, 1976

MASTER OF ENGINEERING (1976)
(Civil Engineering)

McMASTER UNIVERSITY
Hamilton, Ontario

TITLE: Round Hollow Structural Sections Subjected to Inelastic Strain Reversals

AUTHOR: Magdi Antoine Chidiac, B.Sc. (Cairo University)

SUPERVISOR: Dr. Robert M. Korol

NUMBER OF PAGES: x, 179

ABSTRACT

A research programme is presented to more fully understand the behaviour of Round Hollow Structural Sections subjected to inelastic strain reversals. An attempt is made to establish a preliminary guideline for choosing a reasonable value for the slenderness ratio (D/t) that qualifies the Round HSS for cyclic loading.

An experimental programme on nine sections was performed to evaluate the loss in load capacity due to inelastic cyclic loading and to construct the load-deflection hysteresis loops.

Three different limiting cyclic deflections were imposed to the smallest D/t section and a comparison was made between the performance of the tube in each case.

Prasad's computer program was used to select the strain value at which local buckling will appear and to calculate the half buckle wave-length. The results were compared to the experimental results obtained by the author.

A comparison is made between two Round HSS having different diameters and thicknesses but the same D/t ratio.

A comparison is made between the behaviour of Round HSS and Square HSS subjected to the same cyclic loading programme.

An attempt is made to suggest a reasonable curve relating the number of cycles to failure and the D/t ratio.

ACKNOWLEGMENTS

I wish to express my sincere and profound gratitude to my research supervisor, Dr. R.M. Korol, not only for his guidance, but also for his inspiration, patience, encouragement and advice inside and outside this research work. I would like to thank Dr. A.C. Heidebrecht for his interesting discussions and for all the references he gave me. Also, I would like to thank the staff of technicians of the Applied Dynamics Laboratory (A.D.L.) who helped in carrying out the experimental work.

This investigation was made possible through the financial assistance of Dr. Korol's research fund and the teaching assistantship offered by the Civil Engineering Department at McMaster University, to whom I am very grateful. Test specimens were fabricated and donated by the Steel Company of Canada and Prudential Steel Company of Calgary, to whom I extend my sincere thanks. I am very grateful to DOFASCO for obtaining the test specimens from Prudential.

This work is dedicated to my wife, Andrée, in recognition of the sacrifices which she has made during the period of this investigation. I would like to thank her for typing the thesis, for her encouragement and patience.

I would like to thank my mother who dedicated herself to my education, and also for her encouragement to pursue my graduate studies.

TABLE OF CONTENTS

LIST OF FIGURES

LIST OF TABLES

CHAPTER 1

INTRODUCTION

1.1 Problem of the Day

In the last few years, many scientists and technologists have spent much of their time exploring the process that occurs in the earth's crust and analysing resulting earthquakes and their effects.

Major quakes have demonstrated in recent years that we are living in a period of increasing earthquake activity. In this case, the loss of life is regarded to be of great importance. The highest number of deaths was in Peru in 1970, where 70,000 persons lost their lives (15), in spite of the fact that the earthquake had a moderate magnitude. The Guatemala earthquake (February 4, 1976) is the most recent and dramatic quake, where 22,000 people died, 75,000 injured and more than one million homeless. The extent of the damage was large due to the aftershocks which were intermitent for a period of two weeks.

Furthermore, a considerable number of structural failures can be expected, depending upon the location and the earthquake itself. The longer the vibrations persist

the greater the damage. The first vibrations may loosen or weaken some members which can subsequently fail if the vibrations continue. Tall buildings require about 20 to 30 seconds before they oscillate at maximum amplitude and if the earthquake lasts only a few seconds, maximum stress will not be reached within the structural members. Aftershocks of sufficient magnitude cause damage, because they may lead to the collapse of buildings which have been weakened sufficiently by the first shocks. The earthquake of 1960 in Chile, which had a main shock of M 8.5 (11), was followed by a considerable number of aftershocks. Each aftershock was more intense than the earthquake which ruined Managua in December 1972, where the magnitude was M 6.2, the duration of the quake was 42.5 seconds and the damage cost was 1000 million dollars (12). If this Chilean quake had occurred in California, it would have devastated a very large part of the state.

The San Fernando quake had a magnitude of only M 6.6 and lasted just 12 seconds. The average damage to light industrial buildings was 20% in the earthquake area of high intensity and the average damage to brick buildings was more than 18%. The total damage was estimated to be 500 million dollars (13).

The quake in Caracas in 1967 with a moderate magnitude of M 6.4, produced damage averaging 10% to some 250 high-rise buildings of 10 stories and more (10).

The quake in Alaska (1964) resulted in enormous damage to high-rise buildings due to its large magnitude of M 8.4 and its large duration, in spite of the fact that those buildings had been built according to the latest earthquake specifications (14). The average damage to private property amounted to about 40%. The total damage cost was approximately 311 million dollars and the number of deaths was 125.

From the previous discussion about the consequences of former earthquakes, it appears that in recent earthquake design, the role of the structural engineer is of great importance. Thus, the earthquake-resistance design requirements of the National Building Code of Canada 1975 provide minimum standards to safeguard the public against major structural failure and consequent loss of life. The designed structure should be able to resist minor earthquakes without damage and resist major catastrophic earthquakes without collapse.

Earthquake design will not be discussed in detail, but the fact that any member may be subjected to a repeated and reversed load, is of a great importance. The designer must take into consideration those members and their connections which must be capable of resisting repeated and reversed loads for a large number of cycles, large deflections and high inelastic strains.

In designing conventional buildings against major

earthquakes, it is an accepted design philosophy to allow inelastic deformations in the frames. This is largely dictated by economic considerations, as a structure capable of resisting a severe earthquake in an elastic manner would be excessive in cost (16). The extent of the allowable inelastic deformations is a very difficult, non-deterministic problem. In practice, some reasonable drift limitations for a strong motion earthquake are often imposed, and the design is carried out on this basis. Further, at least until some further research is completed, there is great reluctance on the part of designers to allow inelastic cyclic action in the columns. On the preceding basis, dissipation of energy through inelastic deformations are desirable only in the girder, and there is considerable interest in the actual behavior of the regions (plastic hinges) in which such deformations take place.

One of the main problems that can affect the cyclic program, is the appearance of local buckling in the compressive part of the members. The higher the deflection, the higher the inelastic strain and the greater will be the effect of local buckling. Local buckling will depend on the slenderness ratio b/t of the members. Any increase of the b/t ratio with a high inelastic strain, will decrease the number of cycles needed to cause local buckling.

A limited number of research programmes and experiments were done on members and connections subjected to cyclic loading. In the next few pages, a review of work involving repeated and reversed loads, is presented.

Firstly, cyclic loading is described for rolled steel sections (H shape), then its effect is related to the connections between rolled shapes (beams and columns). Finally, the investigation on square HSS undertaken at McMaster is recounted to be followed by the work of the author for circular hollow sections.

1.2 Literature Review

In February 1965, an experimental study on small rolled structural steel cantilever beams, subjected to cyclic reversed loading, was reported by Bertero and Popov (1). The maximum strain at the clamped end was carefully controlled and varied between ± 1.0 and ± 2.5 percent. The maximum control strain for every cycle was kept constant throughout the series of cycles applied to each tested beam. The b/t (flange width to thickness) ratio for the eleven tested beams was 10.5.

Local buckling was detected after 70 cycles at 1% controlled strain. But for strains greater than 2%, local buckling was noted just after or during the first cycle.

When the maximum imposed cyclic strain was set at 1%, fracture of the beam occurred after 650 cycles. However, as soon as the strain was increased, the fatigue life of the beams rapidly decreased. For the specimen tested under a control strain of 2.5%, fracture occurred after 15 cycles.

The unsymmetrical severe distortions of the flanges tend to induce torsional displacements of the section and local reduction in the flexural stiffness of the member which increased as the number of cycles increased. Except for 1% strain, the stresses induced in the distorted flanges caused the early formation of cracks that finally led to the fracture of the beam.

The authors concluded that this drastic drop in the low cycle fatigue endurance of the beams was not directly related to the deterioration of the mechanical properties of the material itself at the clamped edge. Instead, the principal reason for this phenomenon was attributed to the early development of local buckling in the beam flanges.

To assess the effect of the local buckling more fully, the results of the experiments done by Benham and Ford (2), on the material itself can be compared with those of Bertero and Popov (1). The former found that by strain cycling a specimen between ± 2.43% strain, in tension and in compression, the number of cycles required to produce failure was greater than 400.

It is possible that the initiation of local buckling of the flanges was precipitated by a combination of residual stresses and initial imperfections. But in the opinion of Bertero and Popov, the principal reason for the rapid deterioration in beam capacity is associated with the induced inelastic curvature of the flanges. This curvature persists during the unloading process. A kink remains even under zero load. The compressive and tensile forces, or both, which develop during the succeeding loading cycles, acting on the slightly kinked flanges of a beam, give rise to a force component that acts perpendicularly to the flange and further distorts the cross section. If the induced stresses are sufficiently large, this distortion becomes plastic. Once

this process begins, the wrinkle of the flange tends to become increasingly larger as the number of cycles increases. A rather similar phenomenon occurs with the cyclic loading of circular sections and will be discussed subsequently.

In none of the eleven Bertero and Popov experiments was local buckling detected during the first half cycle. To avoid premature local buckling of the flange subjected to a static loading, their work had the effect that recommendations are given in the ASCE manual of 1971 (3) that the b/t ratio must not exceed 17. For cyclic loading this ratio must be reduced.

Popov and Pinkney (4), carried out a cyclic loading program on cantilever beams with different types of connections to stub columns. Their work was a continuation of the preceeding work (1), and its main purpose was to obtain information on the behaviour of H shaped beams and their connections during cyclic loading.

The b/t ratio for all the specimens was equal to 14. The cyclic loading program was such that a sequence of increasing deflections was applied, with an arbitrary number of cycles at each amplitude limit. In some cases, a constant amplitude was applied throughout the test. The number of cycles to failure strongly depended on the extent of the tip deflection imposed, and was as low as 5, and as high as 120. Failure was mainly due to flange buckling.

The behaviour of most of the specimens was satisfactory

throughout the cyclic test, and from their conclusions the following points were relevant to the work done by the author:

1. Beam sections, with b/t = 14, were capable of resisting the severe effects of cyclic loading without premature failure. On the other hand, local buckling of the compression flange was a major reason of complete failure of connections.
2. Local buckling did not precipitate an immediate loss of load-carrying capacity. Indeed, the ability to buckle and thus distribute damage may be of significance in prolonging the life of a member.
3. The number of repeated and reversed loadings which can be sustained appears to be in excess of that which may be anticipated in actual service.
4. The load-deflection hysteresis loops are highly reproducible during cyclic loading, which means that a considerable amount of energy is absorbed.

Hence the behaviour of a beam itself subjected to cyclic loading is the first step to be investigated, the next step must be the investigation of the behaviour of the beam and its connections, where local buckling may cause problems.

Repeated and reversed loading tests at constant deflection amplitudes were conducted on rolled steel cantilever beams by Takanashi (5).

The following conclusions were drawn:

1. Stable hysteresis loops cannot be obtained after severe lateral buckling caused by cyclic loading.
2. There exists some critical magnitude of amplitude, within which the hysteresis loops are stable under cyclically reversed loadings. Once the amplitude is beyond this magnitude, the load capacity of the beam reduces with each cycle.

Vann, Thompson, Whalley and Ozier (8) published the results of their work on the behaviour of wide flange cantilever beams subjected to cyclic loading, in June 1973.

The b/t ratio used in all the tests was equal to 16 or 10.5. Intermediate lateral bracing was used for some specimens.

For the unbraced beams, it was found that short beams with thick plate elements exhibited stable loops. But short and thin plate elements exhibited decaying hysteresis loops. A short cantilever having thin plate elements (b/t = 16) and cycled to a ductility factor of 7.2, failed after 12 cycles and the loss in load capacity was 48%. Losses may be attributed to web buckling induced by local flange buckling. A long cantilever having thick plate elements (b/t = 10.5) and cycled to a ductility factor of 11.1, failed after 20 cycles. But the losses were due to lateral torsional buckling rather than web buckling.

For the lateral braced beams, the hysteresis loops

did not remain stable due to buckling of the unbraced flange. As the cycling progressed the loops became nonsymmetric, having a larger peak when the braced flange was in compression.

When axial load was superimposed on the cyclic loading, a small increase in load capacity with cycling was observed, followed by more rapid decreases than for a similar specimen without axial loading.

The following conclusions were put forward:

1. At very large amplitudes of cyclic deflection, cantilever beams with b/t close to the limits prescribed for plastic design, may exhibit unstable hysteresis loops. The deterioration is severe only, when local buckling is combined with web buckling or with lateral torsional buckling.
2. Addition of an axial load tends to induce more rapid deteriorations.
3. Generally, the members resisted fracture and sustained a useful amount of load capacity, for a greater number of large deflection cycles than would be expected in an earthquake.

Nashid (9) studied the behaviour of HSS subjected to inelastic strain reversal. Seven simple beams of square cross section were tested, covering a range of b/t from 16 to 38. The limiting deflection for the cyclic program was that obtained at 2% strain.

For b/t = 16, loss in load capacity was 16% after 20 cycles. For b/t = 36, the loss was 55%, caused by cracks which occurred after 10 cycles.

The appearance of a large local buckle in the first half cycle, caused a large degree of inelastic strain. Nashid suggested further research with a control strain less than 2%.

It was concluded that a b/t ratio of about 22, guarantees a reasonable level of performance. Nashid suggested the following limitation for the width-thickness ratio (b/t) for cyclic loading:

$$b/t \leqslant 155/\sqrt{\sigma_y}$$

1.3 Current Work

The main purpose of this investigation is, to more fully understand the behaviour of round HSS subjected to high inelastic strain reversals. This study can be useful in the design of earthquake resistant structures, because it will provide some insight into the ability of closed sections to withstand severe loading reversals and to absorb energy through inelastic load excursions.

The sections used in this investigation, covered the range of compact sections and non-compact sections.

It should be noted that the research program was not devised to demonstrate the value of round hollow sections as coupled shear wall beams (which require much more capacity), but as elements in a building, which while designed to carry static live and dead loadings, act in a secondary capacity to resist earthquake and other dynamic forces.

One of the main purposes of the study was to obtain a certain value of the D/t ratio, for which

1. the section can be cycled to a large value of inelastic strain ($\Delta = 3\Delta_p$) without the appearance of any local buckling, or
2. little deterioration in beam capacity occurs after 20 cycles of loading.

CHAPTER 2

EXPERIMENTAL PROGRAM

2.1 Testing Material

A total of nine tests was performed on round HSS supplied by:

1. The Steel Company of Canada Ltd.,
2. Prudential Steel Company of Calgary.

All sections investigated were cold-formed sections. The slenderness ratio, D/t, for the tested round HSS was chosen so as to provide a range for compact and non-compact sections.

2.2 Material Properties

A typical stress-strain curve obtained from a tensile test is shown in Figure 2.1. The yield stress, σ_y, is the stress corresponding to a total strain of 0.5%. This stress usually corresponds closely to the constant stress at yielding and is close to the stress obtained by

the conventional 0.2% offset strain method.

Round HSS material properties as concluded by Hudoba (17), do not vary significantly along the periphery of the cross-section. Hudoba found that for a tensile test, the material coupons, cut from each specimen at right angles to the seam and in the longitudinal direction of the beam, as shown in Figure 2.2a, are representative of the material properties. The tensile specimens were cut conforming with ASTM specifications (18), at 90 degrees to the weld. Two thirds of both ends were flattened, due to the deficiency of curved grips to properly clamp the specimen. Figure 2.2b shows the shape and dimensions of the tensile specimens.

The extensometer was used for all the specimens, and the strain gauges were used for 5 specimens, two gauges per specimen. Strain gauges were mounted on both sides of the tensile specimens to separate the effect of any eccentricity, and the mean value was calculated. For tube T3, an S-1 type electronic extensometer was used in addition to the two strain gauges. Figure 2.3 shows the difference between the stress-strain relations obtained by the strain gauges and the extensometer. The only difference between the two curves is the slope of the elastic part, the modulus of elasticity obtained by the extensometer was four times the value obtained by using the strain gauges ($E_{ext.}$ = 120,000 and $E_{s.g.}$ = 30,000 ksi). The difference in the elastic zone was due to some slippage between the

tensile specimen and the extensometer itself. It was noticed that both procedures gave the same yield stress, which was the primary purpose of the tensile tests. After yielding both curves were the same. Therefore, extensometer can be used to obtain the exact stress-strain curve, but the slope of the elastic zone must be corrected, i.e. by dividing the obtained modulus of elasticity by 4.

The tensile tests were performed in the hydraulic "Tinius Olsen" testing machine at a common constant slow strain of 100 micro-inches/inch/second.

Table 2.1 gives the cross-sectional area of the specimens, the maximum load, the load at failure, the ultimate stress and σ_y the stress corresponding to a strain of 0.5% for every specimen.

The overall view of all tensile test coupons is shown in Figure 2.4. The pieces of sections from which the coupons were cut can be seen in the background.

2.3 Testing Arrangement

2.3.1 Test Set Up

The test set up was designed to allow for a simply supported beam of variable span (72,80 and 88 inches), by using four end brackets with three consecutive holes, as in Figure 2.5a.

The cyclic program was done by means of the MTS system (Material Testing Systems) with hydraulic jack, where its ram was mounted at midspan of the beam. Details of the test set up are shown in Figures 2.5a and 2.5b.

For the first four tubes, six strain gauges were mounted on half the periphery of the tube, spaced by a vertical distance equal to D/6, and longitudinally displaced 2 inches from midspan. Refer to Figure 2.6. For the remaining five tubes no strain gauges were used, due to the appearance of local buckling during the half first cycle, which gave incorrect and misleading strain readings in subsequent cycles.

Deflections were measured by means of two dial gauges installed 4 inches from midspan, and two other dial gauges at each end support. Their positions are shown in the photographs labelled Figures 2.7 and 2.8. The accuracy of each dial gauge was ± 0.001 inch.

2.3.2 Preparation of Specimens for Testing

All the specimens were cut to the appropriate length shown in table 2.5 plus 2 inches at each end. Two holes of 1 13/16 inch were made at each end of the tube, so that a supporting bar could pass through.

Every hole was reinforced by a curved steel plate 4x4 inches, having the same curvature of the tube and the same sized opening, to prevent any failure

at the support due to bearing stresses or crushing stresses. The reinforcing plates were welded inside or outside the tube depending on the clearance between the supporting brackets and the tube.

2.3.3 Mounting of Strain Gauges

The surface preparation and installation of gauges were made as recommended in the instruction bulletin B-137-3 August 1974 provided by the manufacturer "Micro-Measurements" (19).

The electric strain gauges used were: EP-08-500 BH-120 option W, manufactured by Micro-Measurement Co., Romulus, Michigan, with the following specifications:

Resistance in ohms	120.0 ± 0.30%
Gauge factor at 75° F	2.055 ± 0.50%
Strain limits	Approximately 15%

For the gauge installation M-Bond GA-2 adhesive was used. This is a 100% solid epoxy system which has a preferred cure schedule of 40 hours at 75° F.

2.3.4 Supporting Elements

It is evident from Figures 2.5a and 2.5b that four (W 14x87) columns were used to support the various components of the experimental set-up. One Column was positioned at each end where the brackets were bolted, and two at midspan to hold the hydraulic jack. The columns were 4.5 feet

apart, and every column was prestressed to the floor by two 2.5 inch diameter bolts. Figure 2.9 shows photographs of the overall set up of the test.

Two bars of 1 3/4 inch diameter and 2 feet length were used as supporting elements, one at each end. Stress-proof Round Steel bars were used, which provide a yield strength of 100 ksi (20).

Each bar was supported on two steel end brackets (24x28x1 inches). The bracket in turn was connected to the column by 12 bolts of one inch diameter. The bracket was also provided with three equally spaced holes of 1 13/16 inch diameter, to provide for the three different required spans.

2.3.5 Steel Collars

Steel collars were used for loading purposes at mid-span, to guarantee a well distributed line load on the whole cross section and hence to prevent areas of stress concentration which could lead to premature local buckling.

To represent the actual behaviour of a simple beam during loading, the tube must be free to buckle in any direction. By using the steel collar the tube will be prevented from buckling inside the collar. This type of collar was used to simulate a nearly approximate fixed end condition

at midspan since buckling would be inhibited inside the collar and where flattening of tube would normally not occur. The slope of the tube at midspan would be zero as well as the horizontal displacement due to symmetry. As such, the simple beam system may be considered as two cantilever beams, with both ends being deflected relative to midspan. By making that assumption, the collar acts as a supporting element with the load being considered to be applied at each end.

For all tests, the collars were 24x24 inches and 3 inches wide, with a circular hole at the centre slightly greater than the diameter of the tube to provide reasonable clearance. The space between the collar and the tube was filled with a thin galvanized sheet metal 3 inches wide, which could be bent easily around the tube.

The top edge of the collars was provided with five threaded holes, 4 inches apart so that the collars could be firmly connected to the loading plates. Dimensions of the collars are given in Table 2.2 and details are shown in Figures 2.5a and 2.10.

2.3.6 Loading Plates

Two circular loading plates were used to connect the steel collar to the load cell, as in Figure 2.10.

The lower plate was 20 inches in diameter and 2 inches thick. This plate was provided with:

a) Eight holes of 1 1/16 inches located at a periphery of 16 inches diameter, equally spaced.

b) Three holes along the diameter of the plate 4 inches apart; the upper part of the three holes was 2 inches diameter and the lower part was 1 1/16 inch diameter, so that the countersunk bolts could be used.

The upper plate was 20 inches diameter and 2 inches thick, with the same eight holes along the periphery as in the lower plate. This plate was connected to the load cell by means of a 5 inch diameter female thread welded to the top of the plate.

The lower plate was bolted to the collar by using three countersunk bolts of one inch diameter and 4 inches in length.

The lower plates and the collar, were connected to the upper plate and the load cell by means of eight bolts

of one inch L9 Lamalloy high tensile steel. From these eight bolts, six connected the two circular plates together, and the remaining two bolts penetrated to the collar itself through the two plates. The different kinds of bolts are described in Table 2.3

2.4 Description of Test Apparatus

2.4.1 Electronic Controller

The controlling unit used to govern the hydraulic jack is Model 406.11 Controller produced by the MTS system. It is an electronic sub-system, designed to adjust the position of the ram and to readout functions (i.e. stroke travel or load) in an electrohydraulic testing machine.

Included with the 406.11 Controller are:

a) Servo Controller

b) AC Transducer Conditioner (LVDT)

c) DC Transducer Conditioner (Load Cell)

d) Feedback Selector

e) Limit Detector

The system's hydraulic actuator applies a mechanical input to the specimen and to a transducer connected to the load cell in order to evaluate the amount of load applied.

The feedback selector allows selection of either transducer connected to the LVDT system indicating the

hydraulic jack's stroke reading, or the external transducer conditioner signal received from the load cell indicating the load reading.

The servo controller accepts two signals:

a) Program input (command)

b) Feedback

The command signal represents the desired variable and the feedback signal represents the actual variable as sensed by the selected transducer. In the test programme undertaken, the signal variable was a certain increment of load. If the desired value of load (command) and the feedback value (actual amount of load calculated from the load cell) are not equal, the servo controller develops a control signal to correct the difference. The control signal is applied to the servo valve of the actuator. The servo valve opens in the direction required to decrease the difference between command and feedback.

The Limit Detector monitors the output of a selected transducer and indicates if its output exceeds preset upper and lower limits. If desired, an exceeded limit can also cause the system failsafe interlock to open, stopping the test.

2.4.2 Hydraulic Jack

The hydraulic jack is of 250 kips capacity, with a peak to peak ram stroke of eight inches. The ram travel is

controlled by the LVDT system according to the command signal sent from the controller unit. The jack weighs 1600 lbs. and is manufactured by the MTS systems Corporation.

2.4.3 Load Cell

The load cell can be used for both tension and compression purposes with a maximum capacity of 450 kips. Load value is indicated by means of an electronic transducer connected to the controller unit, in the form of DC voltage. The cell weighs 140 lbs. and has two threaded ends of 5 inches diameter and 5 3/4 inches height.

2.4.4 Steel Coupler

A steel coupler was used to connect the load cell to the hydraulic jack. The coupler had two consecutive internal threaded holes. The lower hole was 5 inches in diameter and the upper one was 4 inches in diameter.

2.4.5 The LVDT (Linear Variable Differential Transformer) System

Differential transformers are electronic devices for translating the displacement of a magnetic armature into an AC voltage which is a linear function of the displacement. This device, after being calibrated, is used to indicate the hydraulic jack's stroke reading as mentioned earlier.

2.5 Preparation of Test Apparatus

The hydraulic jack was calibrated for stroke readings against the DC voltage signals representing the set point commands applied to the controller. The three variables, stroke, DC voltage and the set point changes proved to be linearly related with considerable accuracy.

The load cell was calibrated in the 120 kips Tinius Olsen testing machine, for both tensile and compressive load values in the range of ± 120 kips. Load readings and the DC voltage readings of the cell's electric transducer were also of a linear relationship.

2.6 Testing Procedure

The load was applied to the specimens by means of a gradual increase of the stroke of the jack. A static load test was carried out on each specimen before and after the cyclic program. Subsequent cyclic loading was begun after the attainment of a deflection equal to three times the elastic limit deflection during the first cycle, where the load was applied downward. The resulting value of the midspan deflection was maintained during subsequent loading throughout the cyclic test, being measured from the previous position of zero load.

For the first, fifth, tenth, fifteenth and twentieth cycles a minimum of twenty readings were recorded. For the other intermediate cycles four main points were investigated, the two peak points of maximum tension (when the load is applied downward) and maximum tension (when the load is applied upward), and the two points of zero load. At each of these stages, detailed readings of load, stroke, dial gauges and strain gauges were recorded. The cyclic program was carried out for twenty cycles unless premature failure (cracks) of the specimen occurred.

The tested sections are listed in Table 2.4, with all their structural properties. The elastic modulus of all sections was assumed to be 30,000 ksi, while the measured values ranged between 28,500 and 31,000 ksi. The minimum yield stress was assumed to be 50 ksi for the preliminary calculations. Table 2.5 shows the elastic and plastic properties of the tested beams corresponding to the exact value of yield stress. The plastic properties obtained in Table 2.5 were the guide lines to select the limiting cyclic deflection for each tube ($\Delta = 3\Delta_p$). The lengths of the tubes were chosen to provide a reasonable limiting deflection which will fall within the ranges of the available dial gauges (± 1.0 inch).

Tensile Specimen Numbers	Round HSS		Dimensions of Tensile Specimens (inches)	Area of Specimens (inches)	P max. (Kips)	P failure (Kips)	σ_u (Ksi)	σ_y (Ksi)
	Diameter OD (inch)	Thickness t (inch)						
T1	8.625	0.120	1.518X0.122	0.1852	12.40	10.60	66.95	51.40
T2	8.625	0.156	1.500X0.156	0.2340	15.50	12.80	66.24	51.50
T3	8.625	0.188	1.500X0.188	0.2820	18.16	15.20	64.40	51.50
T4	10.750	0.219	1.500X0.219	0.3290	23.35	19.50	70.97	51.70
T5	12.750	0.250	1.530X0.252	0.3860	25.00	21.00	64.77	52.40
T6	14.000	0.250	1.485X0.241	0.3580	24.80	19.75	69.27	46.80
T7	8.625	0.188	1.500X0.188	0.2820	19.04	15.80	67.51	55.50
T8	8.625	0.188	1.500X0.188	0.2820	19.04	15.80	67.51	55.50
T9	6.640	0.108	1.475X0.105	0.1550	10.18	8.50	65.70	46.50

Table 2.1
Tensile Test Data

Collar Numbers	Tube Diameters OD (inches)	Collar Dimensions (inches)	Hole Diameters D_c (inches)	Weight of Collars lbs.
1	14.000	24X24X3	14.20	355
2	12.750	24X24X3	12.95	378
3	10.750	24X24X3	10.95	410
4	8.625	24X24X3	8.80	438
5	6.640	24X24X3	6.80	458

Table 2.2

Dimensions of the Steel Collars

Type of Bolts	Diameter of Bolts (inch)	Number of Bolts Used	Length of Bolts (inch)	Nuts	Counter Sunk Bolts
a	1	2	7	No	No
b	1	6	7	Yes	No
c	1	3	4	No	Yes

Table 2.3

Bolts Used To Connect The Loading Plates To The Collar

Tube Number	Outer Diameter (inches) OD	Wall Thickness (inches) t	Diameter Thickness Ratio D/t	Area ($inches^2$) A	Moment of Inertia ($inches^4$) I	Section Modulus ($inches^3$) S	Plastic Sec. Modulus ($inches^3$) Z	Shape Factor s
T1	8.625	0.120	72	3.20	29.00	6.73	8.75	1.300
T2	8.625	0.156	55	4.15	37.30	8.63	11.20	1.298
T3	8.625	0.188	46	4.98	44.40	10.30	13.40	1.300
T4	10.750	0.219	49	7.25	100.00	18.70	24.30	1.299
T5	12.750	0.250	51	9.82	192.00	30.10	39.10	1.299
T6	14.000	0.250	56	10.80	255.00	36.50	47.30	1.296
T7	8.625	0.188	46	4.98	44.40	10.30	13.40	1.300
T8	8.625	0.188	46	4.98	44.40	10.30	13.40	1.300
T9	6.640	0.108	61	2.22	11.83	3.56	4.63	1.300

Table 2.4

Structural Properties Of The Hollow Structural Sections.

Tube Number	Span (inches) L'	Yield Load (kips) P_p	Yield Moment (kip-ft) M_y	Yield Deflection (inches) Δ_y	Plastic Load (kips) P_p	Plastic Moment (kip-ft) M_p	Elastic Defection at Mp (inches) Δ_p	$\frac{1}{2}\Delta_p P_p$ (kip-inch) W_p
T1	72	19.22	28.82	0.172	24.99	37.47	0.223	2.786
T2	72	24.70	37.00	0.172	32.00	48.10	0.223	3.568
T3	72	29.50	44.20	0.172	38.40	57.50	0.224	4.300
T4	80	48.30	80.60	0.172	62.80	104.70	0.223	7.000
T5	88	71.70	131.40	0.177	93.13	170.74	0.230	10.689
T6	88	77.62	142.40	0.144	100.60	184.50	0.187	9.406
T7	72	31.80	47.60	0.185	41.30	62.00	0.240	4.956
T8	72	31.80	47.60	0.185	41.30	62.00	0.240	4.956
T9	72	9.20	13.80	0.200	11.96	17.90	0.262	1.567

Table 2.5

Elastic and Plastic Properties of Tested Tubes.

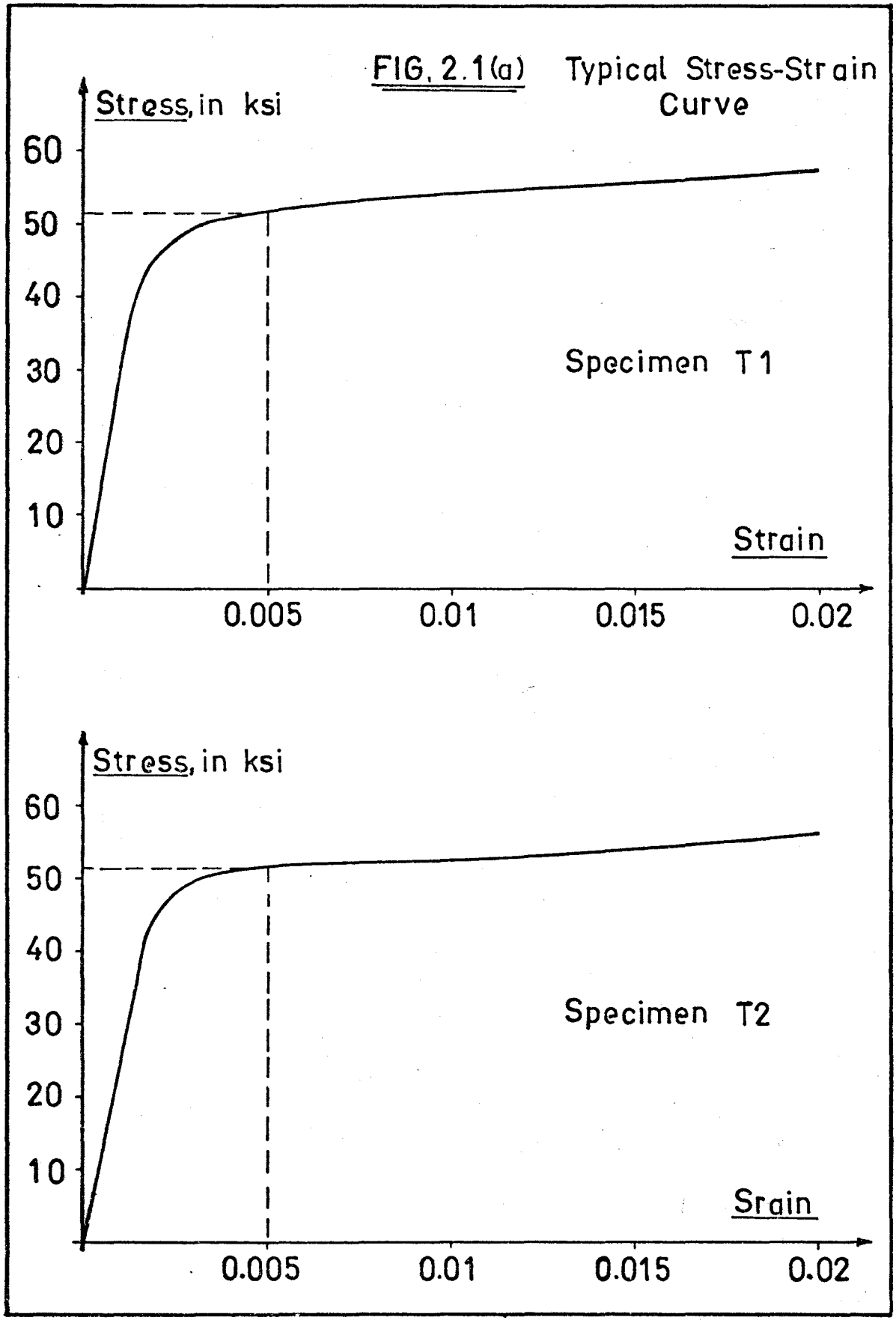

FIG. 2.1(a) Typical Stress-Strain Curve

FIG. 2.1(b)

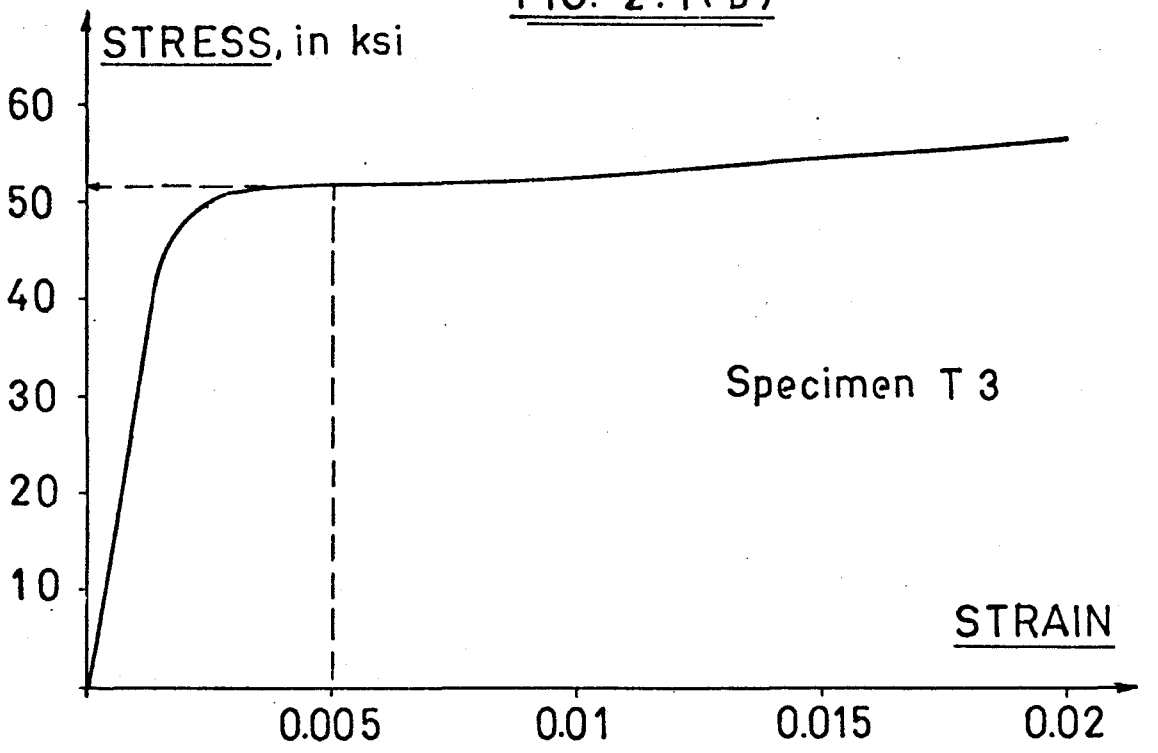
STRESS, in ksi
60
50
40
30
20
10
Specimen T 3
STRAIN
0.005
0.01
0.015
0.02

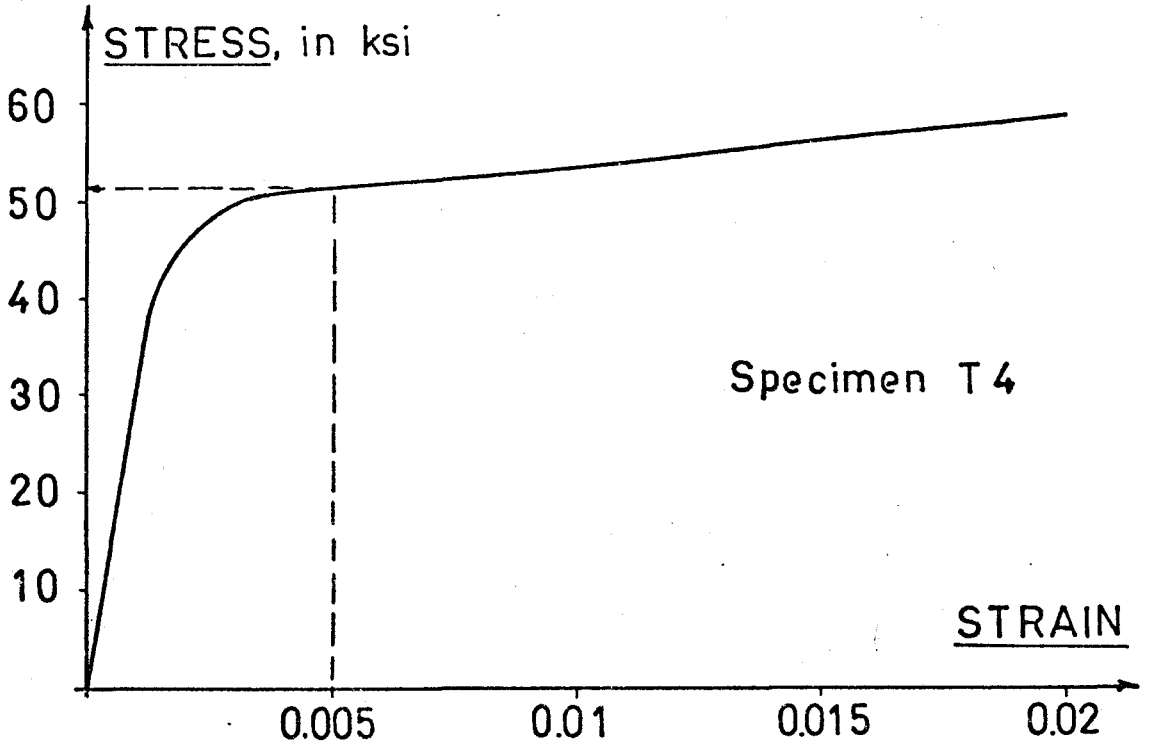
STRESS, in ksi
60
50
40
30
20
10
Specimen T 4
STRAIN
0.005
0.01
0.015
0.02

FIG. 2.1(c)

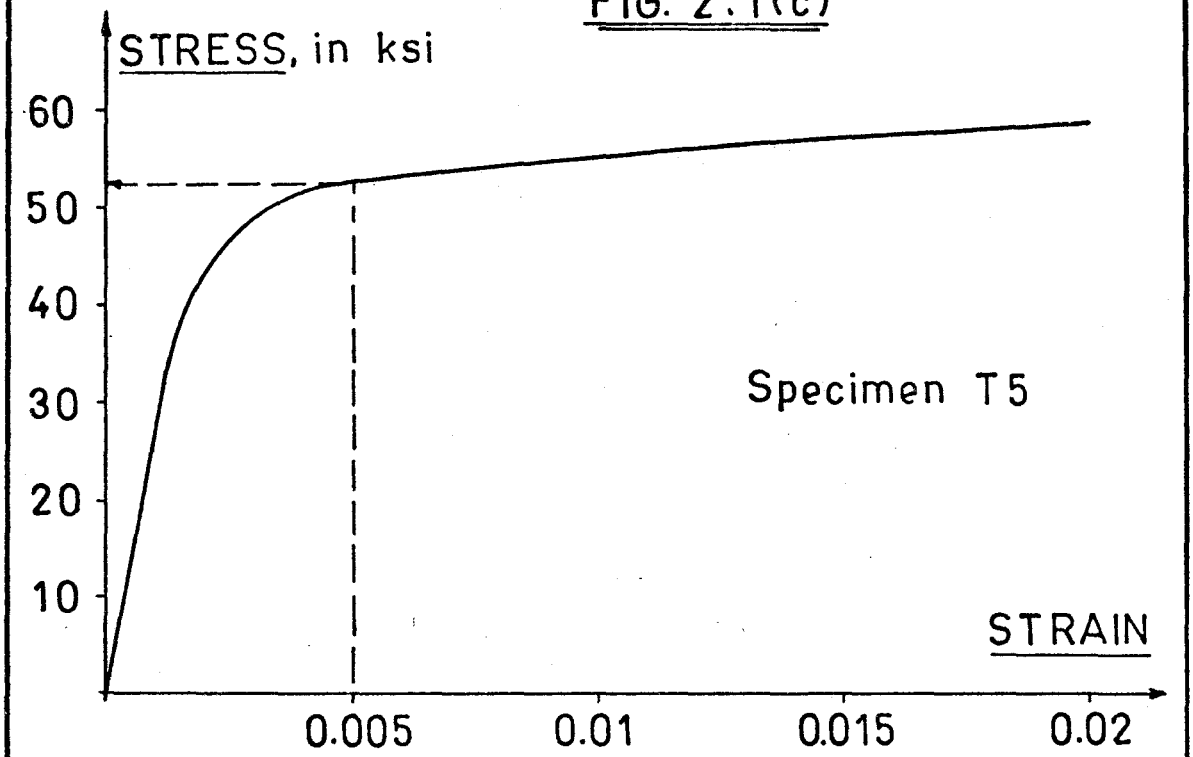
STRESS, in ksi
60
50
40
30
20
10
Specimen T5
STRAIN
0.005
0.01
0.015
0.02

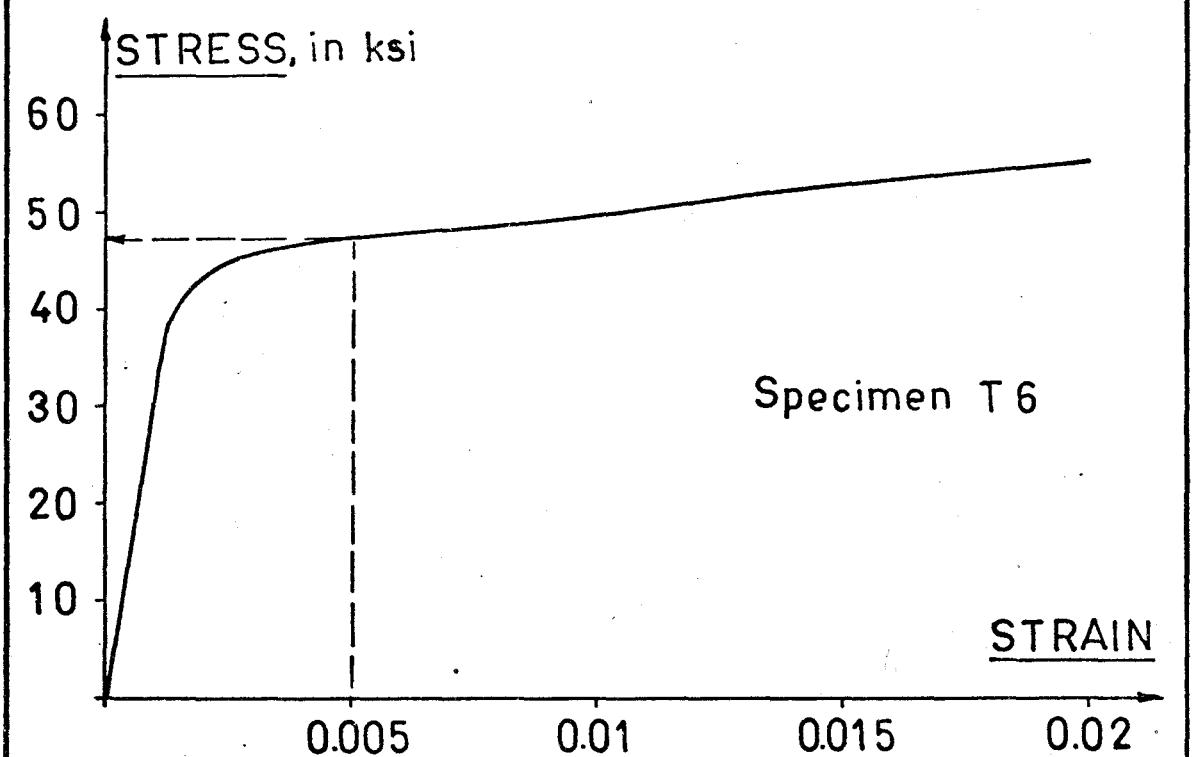
STRESS, in ksi
60
50
40
30
20
10
Specimen T6
STRAIN
0.005
0.01
0.015
0.02

FIG. 2.1(d)

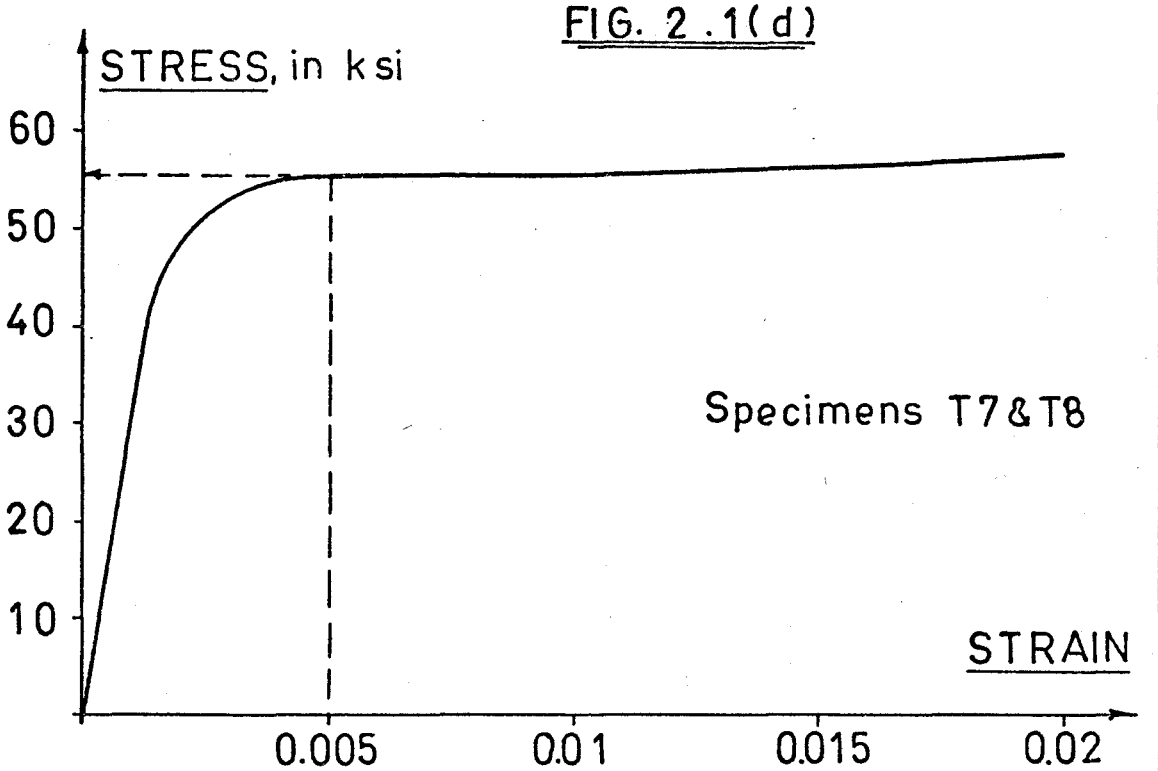
STRESS, in ksi
60
50
40
30
20
10
Specimens T7 & T8
STRAIN
0.005
0.01
0.015
0.02

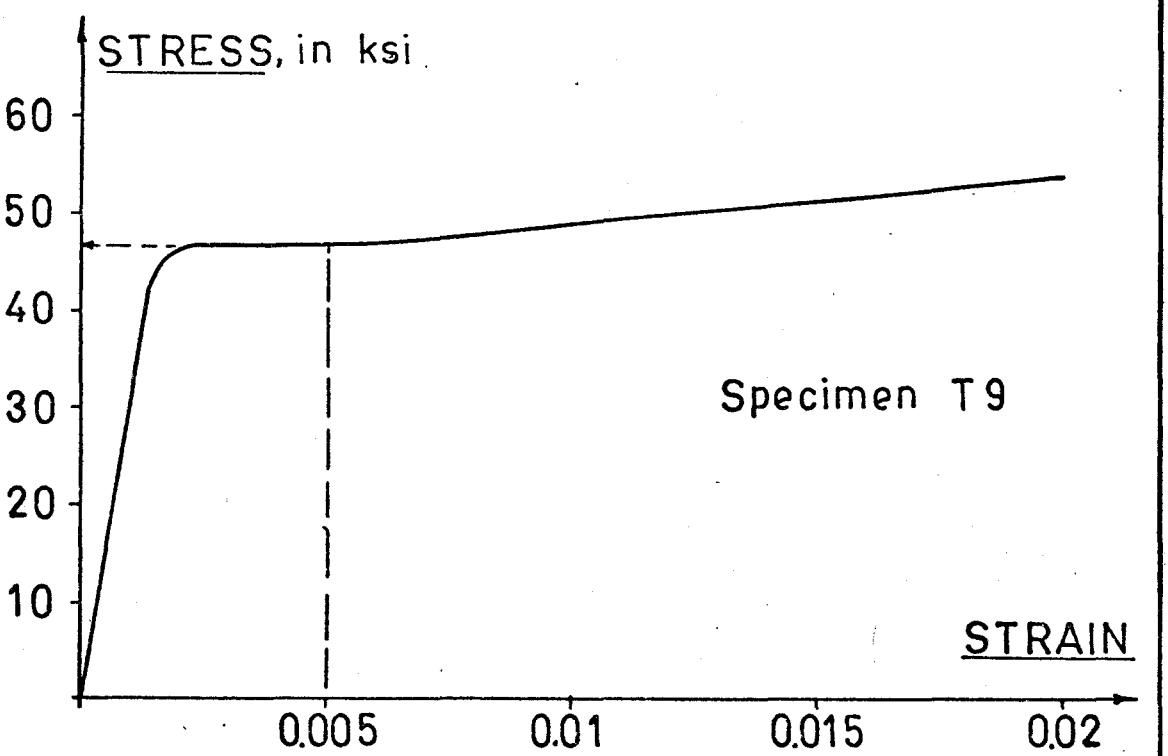
STRESS, in ksi
60
50
40
30
20
10
Specimen T9
STRAIN
0.005
0.01
0.015
0.02

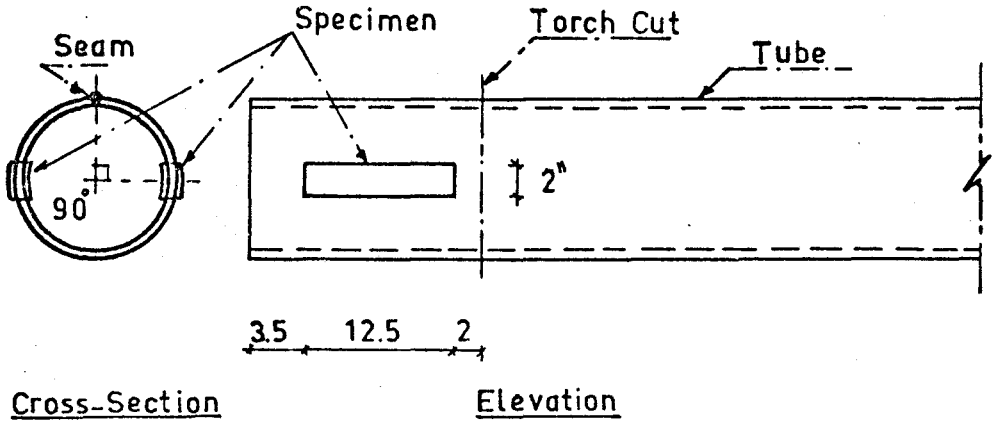

FIG. 2.2 a Tensile Test Specimens and Their Locations in the Tube

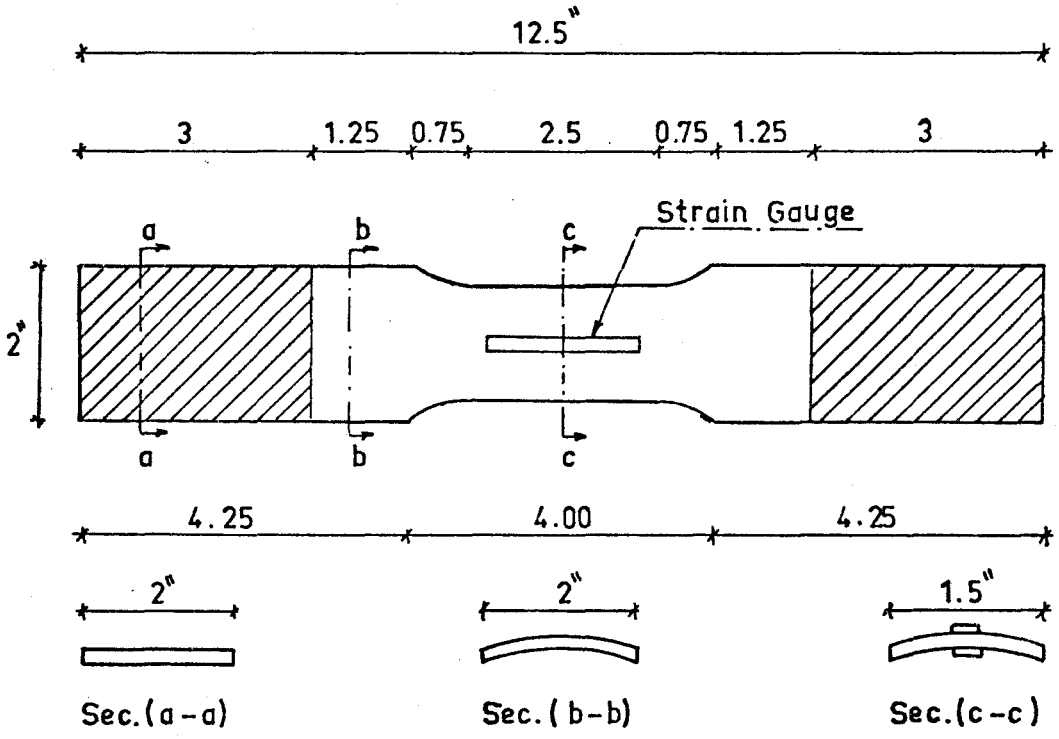

FIG. 2.2 b Dimensions of the Tensile Specimens with Flattened Ends

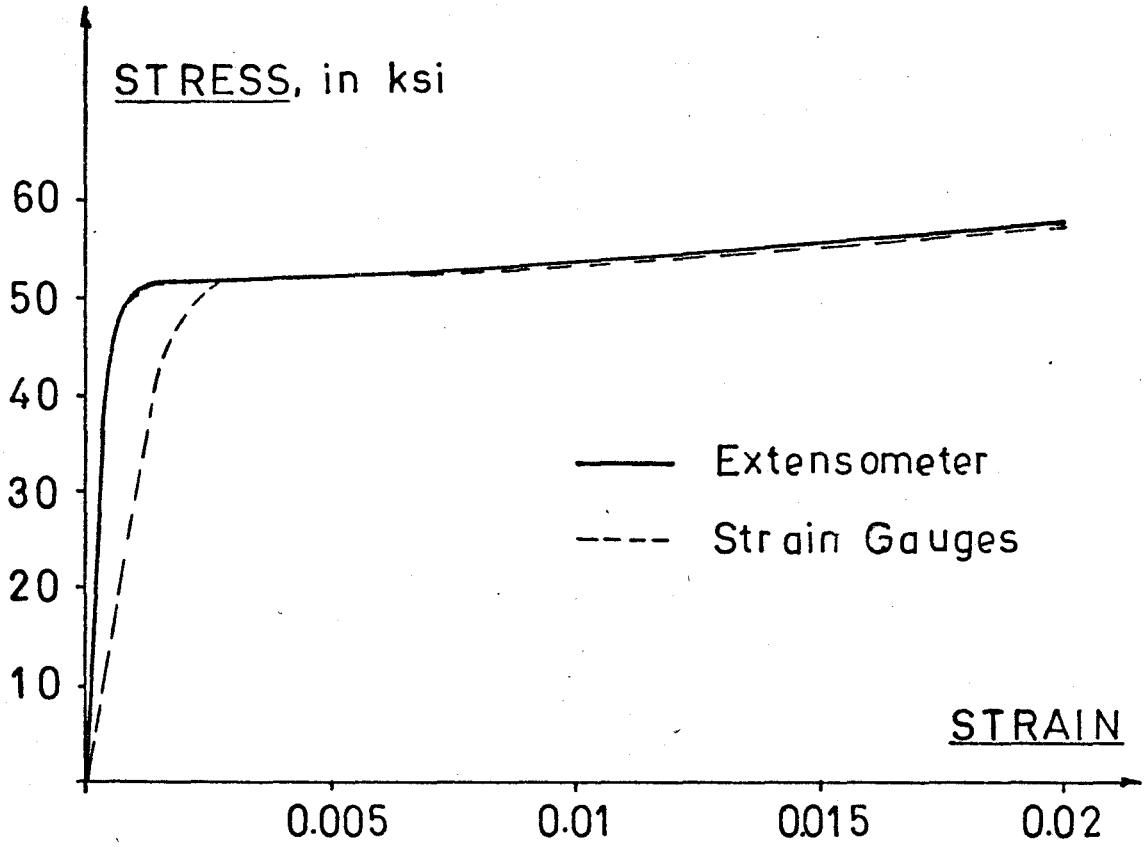

FIG. 2.3 Stress-Strain Curve for Specimen T 3 (8.625 OD X 0.188) By Using Strain Gauges and Extensometer

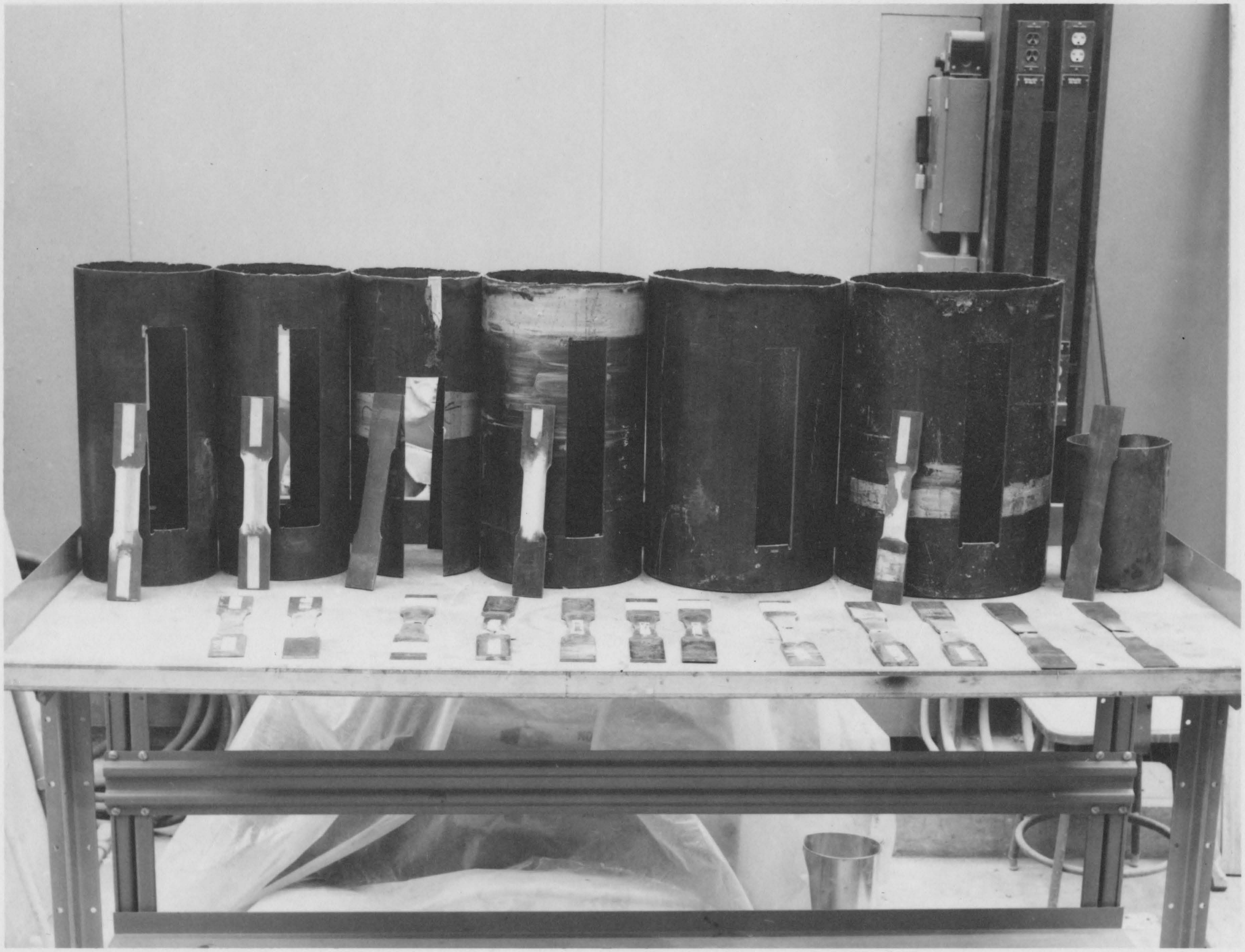

FIGURE 2.4 Tensile Test Specimens.

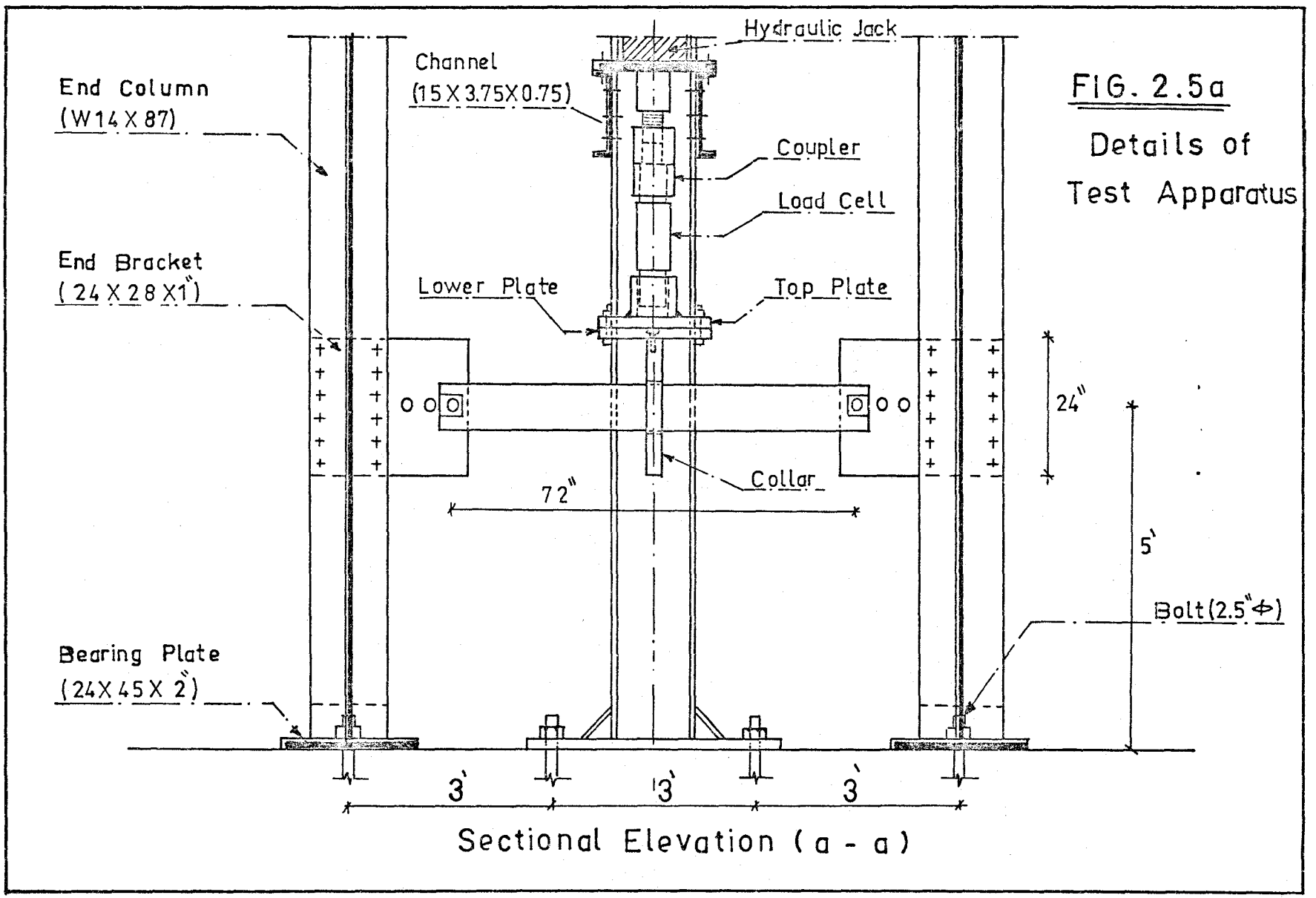

FIG. 2.5a

Details of Test Apparatus

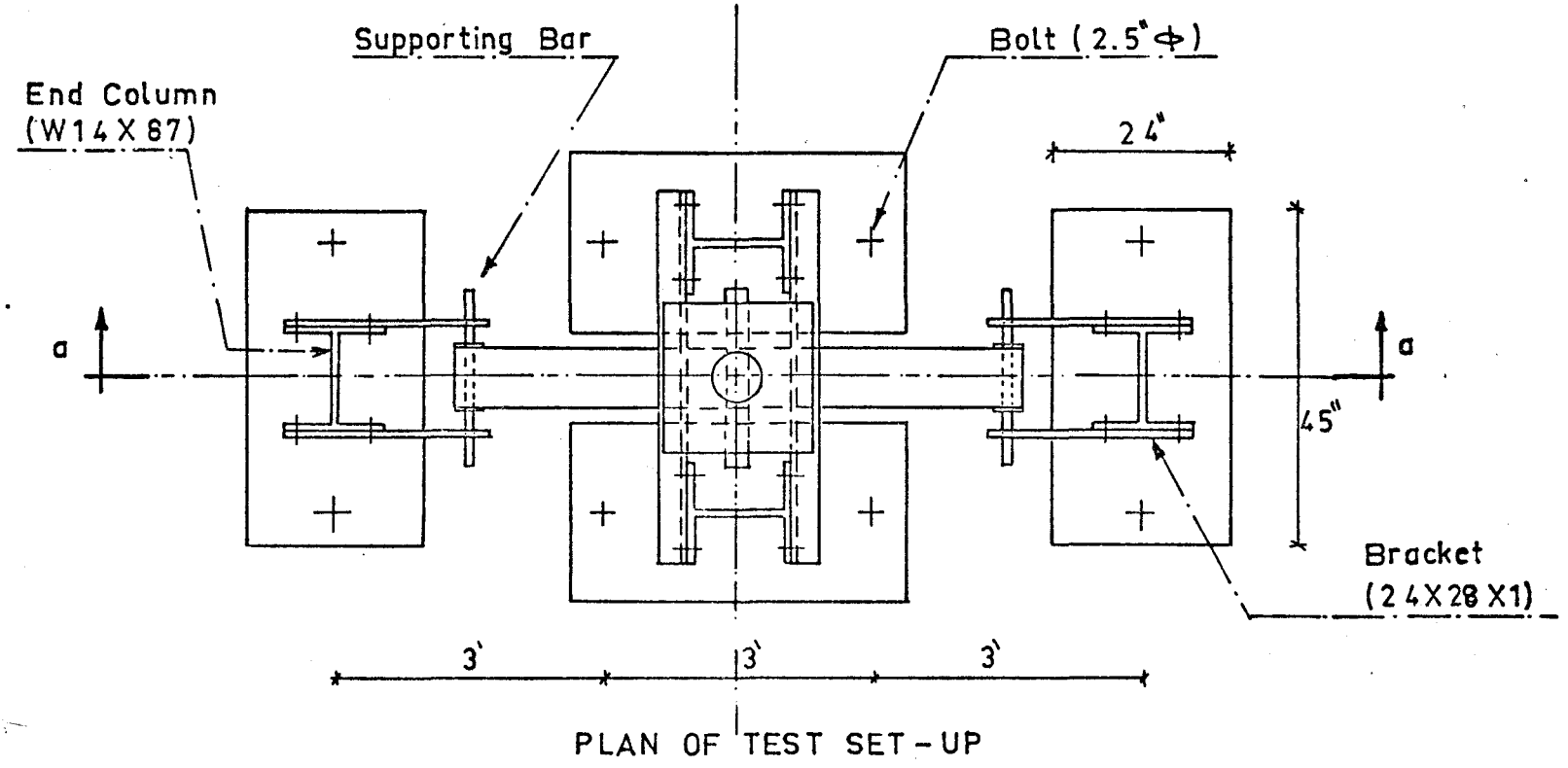

FIG. 2.5 b Details of Test Apparatus

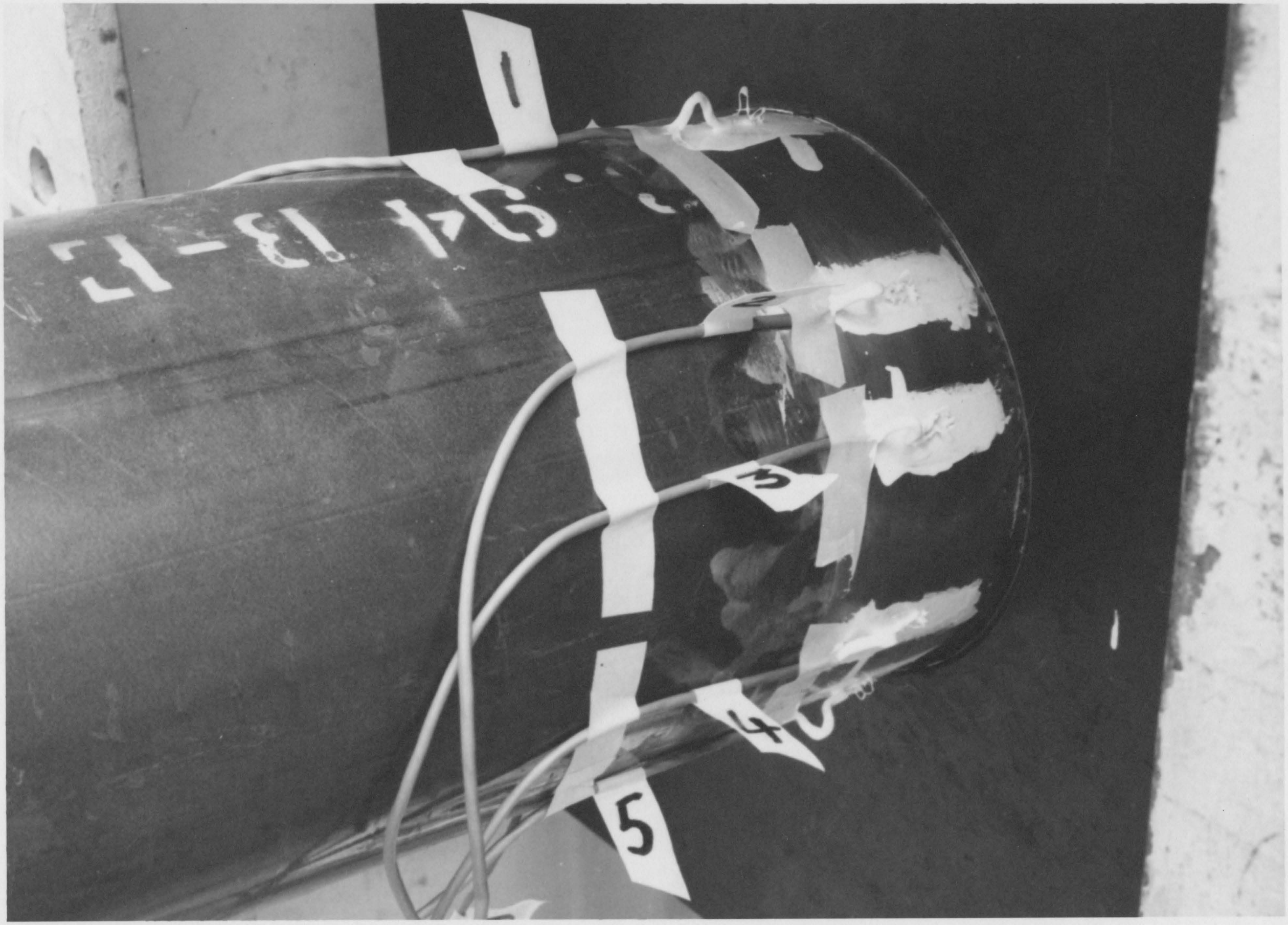

FIGURE 2.6 Position of Strain Gauges.

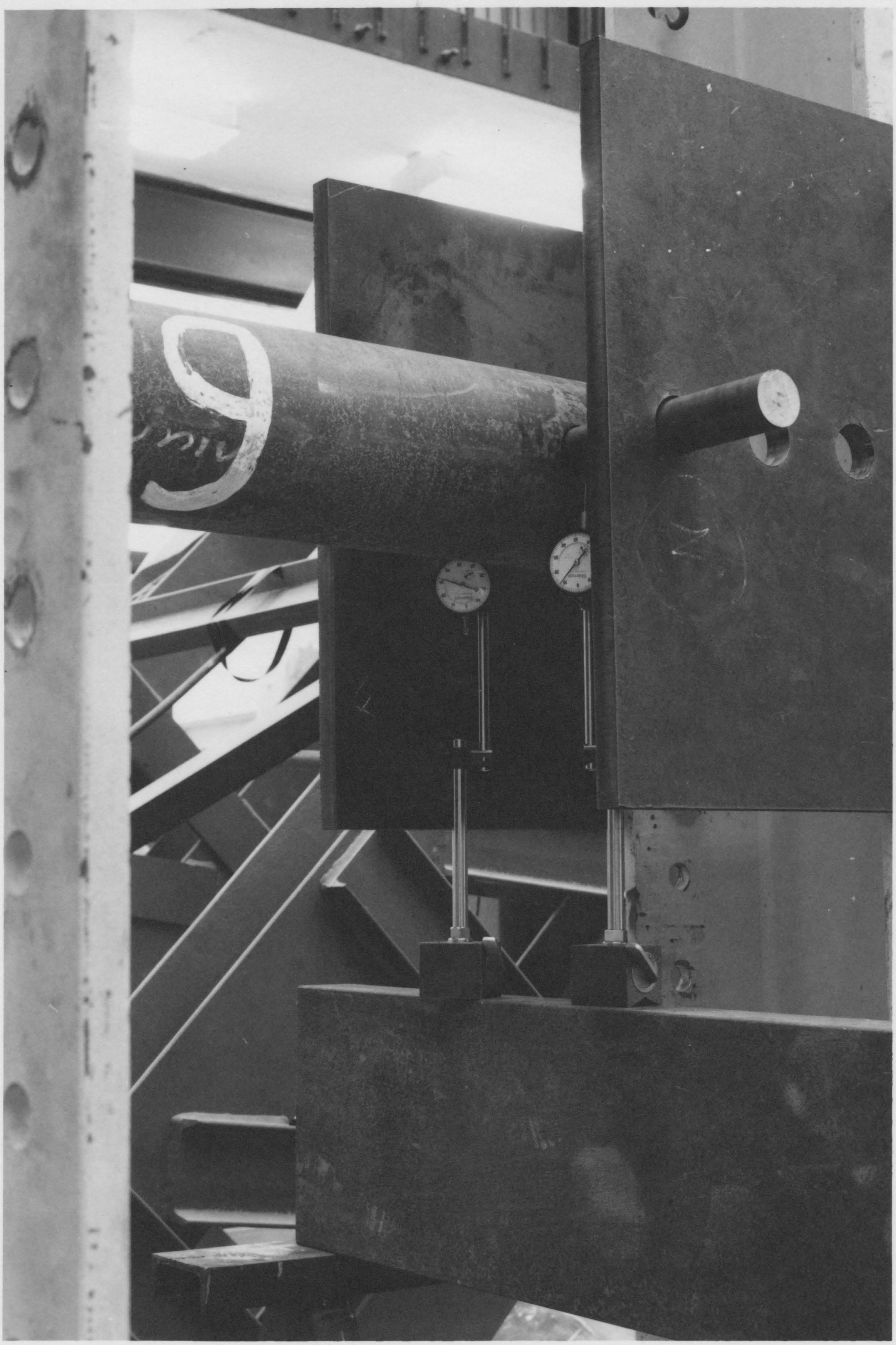

FIGURE 2.7 Dial Gauges at End Supports

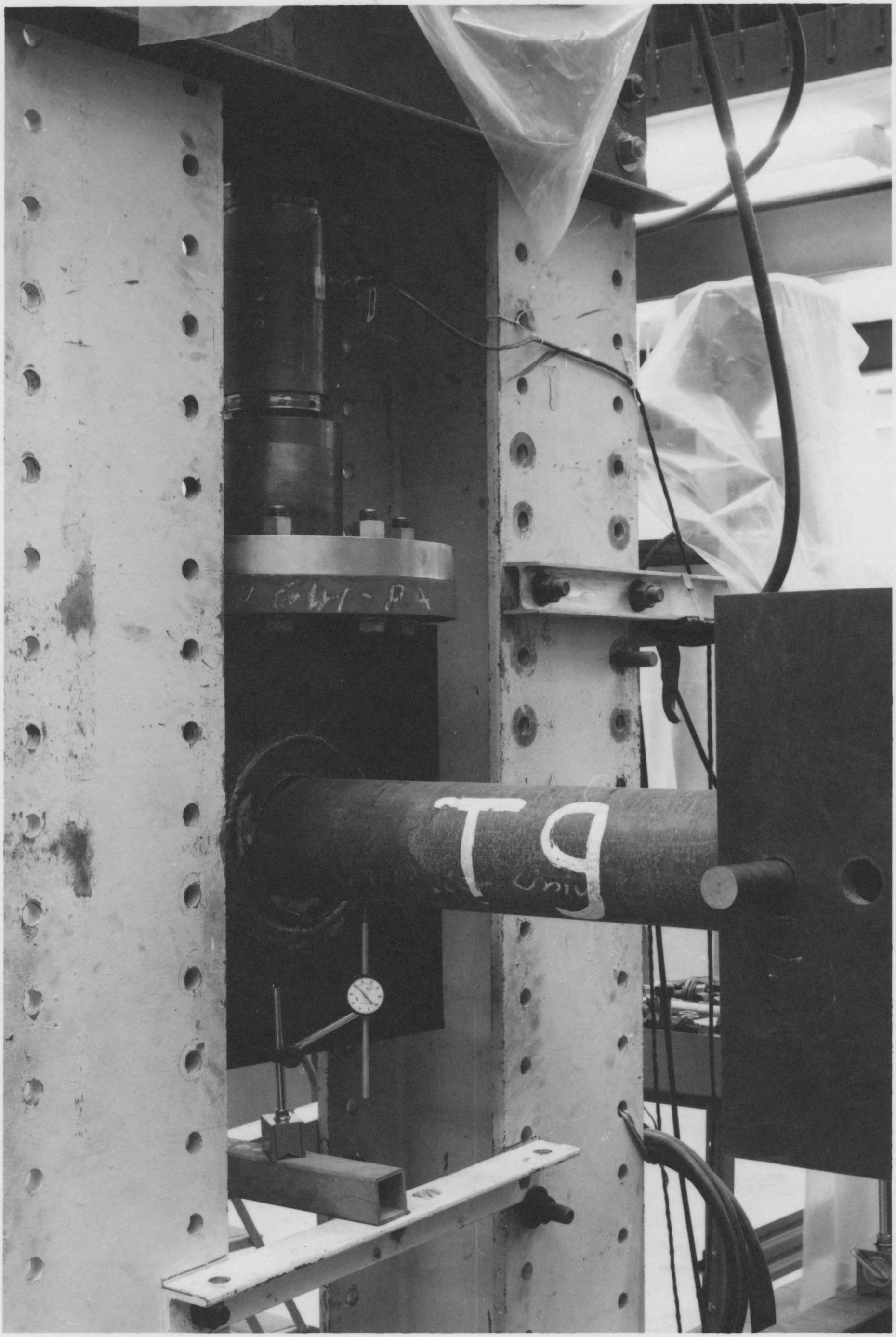

FIGURE 2.8 Transmission of Load from Jack to Tube.

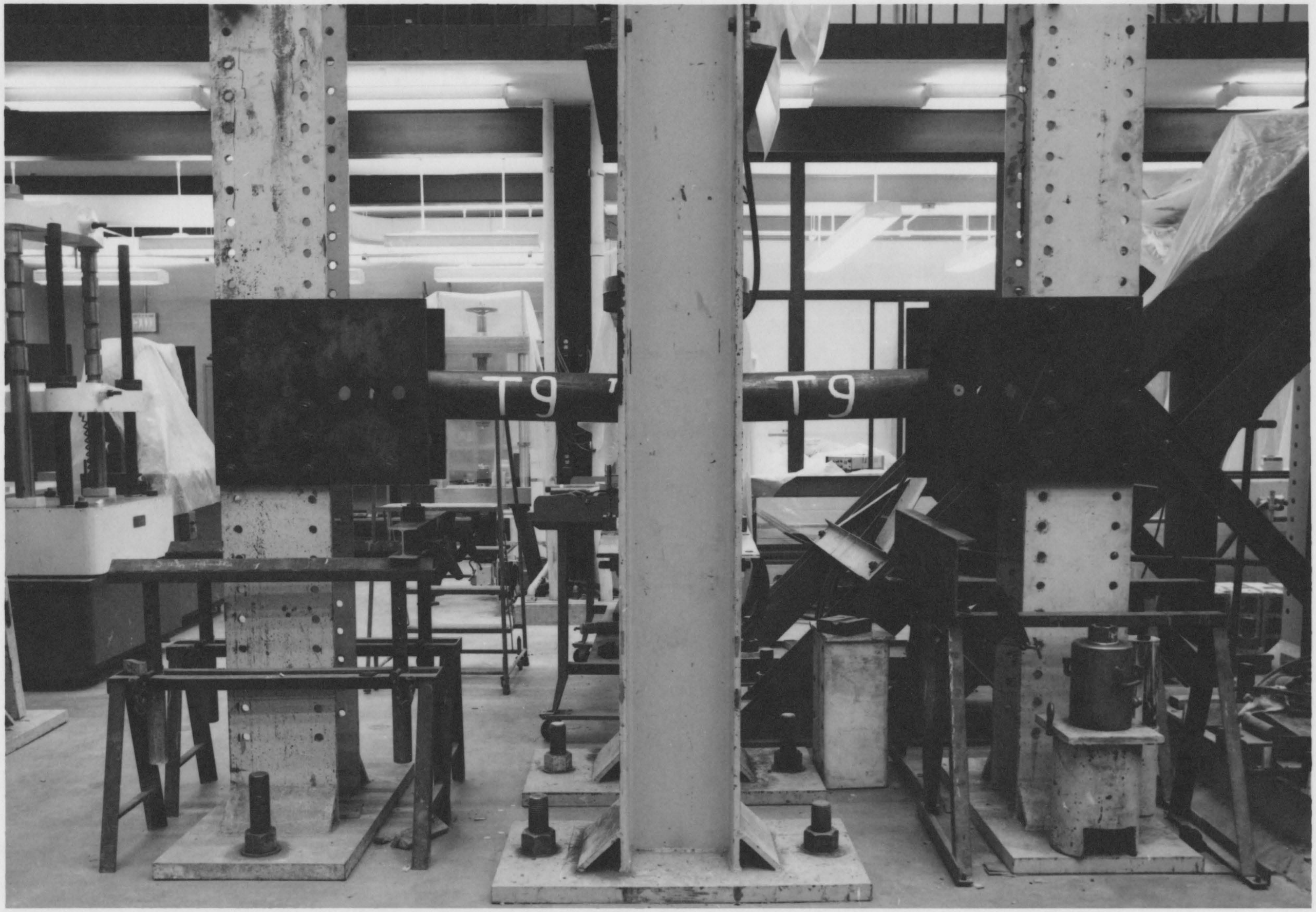

FIGURE 2.9 Overall View of Test Apparatus.

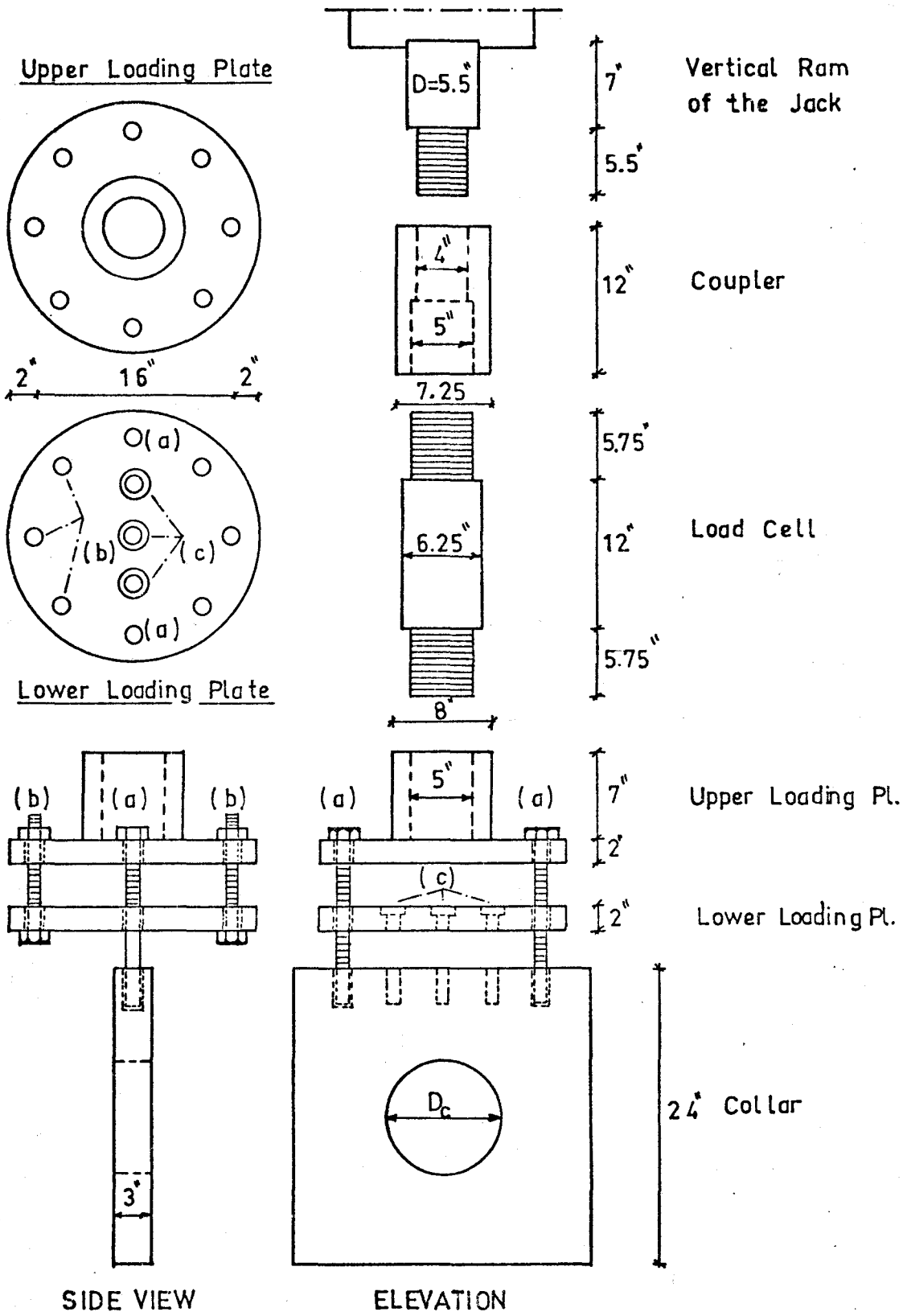

FIG. 2.10 Connections betw. the Jack & Collar

CHAPTER 3

EXPERIMENTAL RESULTS

3.1 Introduction

This chapter contains the experimental records and results of the tested beams. For each beam the graphical relationship, and photographs showing the shapes of local buckling, are presented.

The limiting deflection "Δ" for the cyclic program was almost equal to $3\Delta_p$ (the reasons for which $3\Delta_p$ was not exactly reached for the 7 tubes will be discussed later in clause 3.7) for all beams except tube T3 and T8. The limiting deflections for T8 and T3 (both 8.625 OD x 0.188) were equal to twice and seventeen times Δ_p respectively. Since T7 was the same size round, a comparison is made of the behaviour among T3, T8 and T7, the latter having been cycled to three times Δ_p. All beams were loaded up to twenty cycles except beam T3 which developed cracks during the first half of the second cycle.

Strain gauges were used for tubes T1, T2, T3 and T4 only to draw the relationships between moment and curvature, but due to local buckling which appeared in the first half cycle, all the strain readings after the first half

cycle made little sense and hence were not deemed reliable. For this reason, strain gauges were not used for the other tubes. A comment on this subject will be made later in this chapter.

The test results are presented in forthcoming sections.

3.2 Static Loading Curves

Fig. 3.1-a through 3.1-i show the detailed static load deflection relationship for each beam prior to and following the 20 cycle loading program. However, because cracks occurred in beam T3 after one and one half cycles, Fig. 3.1-c shows the relation for the first two half cycle in compression (load applied downward).

The behaviour after twenty cycles is important since it represents the possible resistance to static loading situations after cyclic loading has occurred, such as might occur from an earthquake.

From the tests it was observed that, the load capacity deteriorated considerably as a function of the D/t ratio after the cyclic testing. The percentage of losses in tube capacity in comparison to the static capacity before cycling ranges between 16.4% for D/t = 46 and 41.3% for D/t = 72, for the uncracked beams during twenty cycles. A marked drop of 48% was recorded for T3 after one and one half cycles.

Fig. 3.2 shows the relationship between the loss in capacity and the D/t ratio. Observe that a straight line correlation exists for the results except those of tubes T3 and T8 which were governed by different limiting deflections and are shown by the solid circle and triangle respectively. The straight line relationship applies from D/t = 49 to D/t = 72.

The loss in load capacity for tube T7 (D/t = 46) was considerably smaller than for the other specimens. If the straight line in Fig 3.2 were to be extended to D/t = 46 the resulting loss in capacity would be about 29%. The actual loss for section T7 was 16.4%. A small part of the difference can be accounted for, by the limiting deflection for T7 being $2.82\Delta_p$ as opposed to $3\Delta_p$ for the other six specimens shown in table 3.5. (The reason for this difference will be discussed later in clause 3.7). It appears that the prime reason for the major difference is likely due to a superior performance of this tube with a subsequent transition of the curve for values of D/t less than 49.

Comparing the 16.4% losses with the 8.5% losses after 20 cycles for the same tube when cycled to $1.85\Delta_p$, it seems that 16.4% represents a lower bound on the actual behaviour of the tube at $\Delta = 2.82\Delta_p$. The capacity loss between D/t = 46 and D/t = 49, may be represented by a dotted smooth curve as suggested in Fig. 3.2, inserted because of a lack of test data in that range. Referring to the

behaviour of tubes T8 and T3 and to the experimental data obtained by Nashid (9) for Square HSS, it appears that in spite of the single test point, the dotted curve represents a logical transition zone for the behaviour of Round HSS. More test data is obviously necessary to confirm the new behaviour. It can be observed that the behaviour of tube T7 was much more satisfactory from the standpoint of maintaining load capacity after cyclic loading, than the remaining six tubes.

The principal reason for the deterioration in tube capacity was caused by the appearance of local buckling. Local buckling occurred in the first half cycle for tube T7, but the loss in capacity was considerably smaller than for tubes with larger D/t. Hence it appears that the deterioration in tube capacity for D/t = 46 will be less than 17% after twenty cycles ($\Delta = 2.82\Delta_p$). To be on the conservative side the author proposes a 20% loss be assumed. Hence, Round HSS will be considered to have failed after twenty cycles, if the loss in capacity is larger than 20% taking into account that local buckling does not preclude failure.

All the beams were able to carry loads with higher values than the calculated plastic loads during the first half cycle, because of strain hardening. For tube T1 (D/t = 72), the calculated plastic load was equl to 24.99

kips and the maximum load applied during the first half cycle was equal to 27 kips. Specific values of plastic load for all tubes, are given in Table 2.5.

3.3 Effect of Local Buckling

It was hoped that one of the nine beams could sustain the 20 cycles program without the appearance of local buckling. However, this was not the case even for tube T8 which was cycled to 1.85 Δ_p only.

For all beams local buckling occurred in the first half cycle, except in tube T8 where it appeared in the second half cycle. Every beam had two local buckles, one at each side of the load. Generally the one to develop initially was very large relative to that which formed on the opposite side of the specimen. The latter was often so minute that it could be detected only by touching the surface The major buckle was located at the right side of the collar for some tubes, and at the left side for the others. If it formed on the observer's right side of the collar, it continually formed there during compressive loading of subsequent cycles.

The height of the half buckle wave was very small for T7 and T8, in comparison with the remaining tubes. The lengths of the half buckle wave were measured after 20 cycles

and are recorded in Table 3.1. The measurrements were done by 3 independant observers with an accuracy of ± 0.04", by using calipers. As was mentioned earlier, local buckling was the principal reason for the loss in tube capacity for all tubes and this deterioration increased with the D/t ratio. From Fig. 3.2, it is observed that the effect of local buckling on the tube capacity is reduced considerably at D/t equal to 46. As was mentioned previously further experimental work is required to confirm behaviour in this lower range of D/t. The shape and size of all nine buckle waves are shown in the photographs labelled Fig. 3.16 through Fig. 3.23.

Fig. 3.3a through Fig. 3.3h all show two curves. The upper one represents the relationship between the loss in tube capacity for downwards loading and the number of cycles. The lower curve represents the relationship between the loss in tube capacity for upwards loading and the number of cycles.

Fig. 3.4 shows the relation between D/t and the loss in tube capacity after 5,10, 15 and 20 cycles. It is observed that every tube after 5 cycles, lost 50% of its total losses after 20 cycles. For D/t = 46 the loss after 5 cycles was 8.5% and for D/t = 51 the loss was 19%. The figures give an indication concerning D/t which separates those Round HSS which can withstand significant cyclic loading without undue damage, from those which cannot.

Some of the buckling information thought to be

important is given in Table 3.1.

The following statements are based on test observations for 3 tubes in each case:

1. For a constant tube diameter, if D/t increases, the half buckle wave-length will decrease but the height as observed will increase (T1, T2 andT7), for $\Delta = 3\Delta_p$.
2. For the same D/t ratio but variable limiting deflection, the half buckle wave-length will decrease with an increase in the limiting deflection (T3, T7 and T8).
3. A higher height for the buckle wave, means greater deterioration in tube capacity for a constant diameter (T1, T2 and T7), for $\Delta = 3\Delta_p$.

Prasad (6) conducted a research programme to assess the capability of Hollow Structural Sections for design in flexure, under static loading. He attempted to relate the tube slenderness ratio (D/t) and yield strength to the rotation capacity and moment resistance of round sections subjected to bending moment. The main point of the investigation was that, the occurrence of local buckling in the compression flange and the consequent reduction in moment resistance are the critical factors which separate the sections into categories governed by allowable stress or plastic methods of design. His work included an experimental programme as well as an analytical study.

A special computer prgram to evaluate the

limiting D/t ratio for a preassigned value of critical buckling strain was developed using the technique of finite difference. Reference is made to Appendix 1 for the basic equations used by Prasad.

The input data consists of the following:

1. the material properties of the tube (Ramberg-Osgood stress-strain relationship),
2. the number of terms needed for convergence in equation (16),
3. the preassigned value of critical buckling strain,
4. the number of elements into which the circumference of the tube is divided, i.e., N,
5. an array of values of D/t and $m\pi R/L$ (half buckle wave-length parameter).

For each trial value of D/t and $m\pi R/L$ the resulting determinant given by equation (22) was calculated. The resulting grid of determinants was used to estimate the limiting D/t ratio for the preassigned value of critical buckling strain.

The author employed Prasad's program for 3 tubes (T1, T2 and T3), in order to obtain a critical value of strain at which local buckling appeared. The results will be compared with the values obtained from strain gauge data prior to the appearance of local buckling, and from the observation of buckle half wave-lengths subsequently.

A simple equation suggested by Ramberg-Osgood

for describing the stress-strain curve in terms of three parameters, was described in detail by Shanley (7)

$$\frac{E\,\epsilon}{\sigma_{0.7}} = \frac{\sigma}{\sigma_{0.7}} + \frac{3}{7}\left(\frac{\sigma}{\sigma_{0.7}}\right)^{n}$$

where

E = Modulus of Elasticity of the material.

$\sigma_{0.7}$ = Stress value obtained by drawing a straight line through the origin at some selected slope equal to 0.7 E.

σ = Stress at any point.

ϵ = The corresponding strain to the stress σ.

n = Parameter which controls the shape of the stress-strain diagram.

By using Prasad's computer program, the first step was to find a suitable value for the parameter n, so that the stress-strain curve for each specimen, could be matched with a theoretical expression.

The method used to obtain the "best fit" value of the parameter n, is suggested by Ramberg-Osgood (21).

By drawing a straight line from the origin of tensile test curve with a slope equal to 0.85 E, the intersection with the curve gives a new value of stress, $\sigma_{0.85}$. Dividing the value of $\sigma_{0.7}$ by $\sigma_{0.85}$, a new parameter "Δ" is obtained.

$$\Delta = \frac{\sigma_{0.7}}{\sigma_{0.85}}$$

From their investigation, Ramberg and Osgood obtained a curve which relates the values of Δ and the parameter n. Knowing the value of Δ for any material, the value of n can be obtained directly as reference to Fig. 3.5 will indicate. Table 3.2 shows the different values for $\sigma_{0.7}$, $\sigma_{0.85}$, Δ, n and σ_y for tubes T1, T2 and T3. Most of these values were used as input for the computer as well as the modulus of elasticity (E = 30,000 ksi) and the number of elements into which the circumference of the tube was divided (N = 360). The results are shown in Table 3.3. For tube T1, local buckling occurred when the strain was approximately 0.0075 which is higher than that obtained by the computer (0.0064). At the limiting deflection for T1, the strain recorded was equal to 0.021. This value is equal to approximately three times the theoretical predicted strain (0.0064), hence a large buckle was to be expected and in fact occurred. It can be seen that the results are consistent, hence the computer program predictions are on the conservative side.

The values of the dimensionless ratio $m\pi R/L$ are also given in Table 3.3. Substituting in the above ratio for m = 1 and R which represents the radius of the tube, the value of the half buckle wave-length "L" is obtained. The values of "L" obtained from the tests are compared with those obtained form Prasad's computer program in Table 3.4. $"L"_{exp.}$ was measured after 20 cycles

making the assumption that the buckle wave-length remains the same after local buckling occurred. This assumption was made because it was difficult to make accurate measurements at the time of the formation of the buckle and also because $L_{exp.}$ was almost the same during the 20 cycles. $L_{theo.}$ represents the theoretical length of the buckle the instant it occurs. Hence, by comparing the results of tube T1 ($L_{exp.}$ = 1.25 ± 0.04" and $L_{theo.}$ = 1.29") it appears that there was no appreciable difference between the value of L obtained theoretically at incipient buckling and the measured value for $\Delta = 3\Delta_p$.

For T7 (D/t = 46 and $\Delta = 2.82\Delta_p$), $L_{exp.}$ was equal to 1.58 ± 0.04" which is very close to Prasad's predicted value of 1.69 inches. For tube T3 (D/t = 46 and $\Delta = 17\Delta_p$) considerable reduction in the buckle wave-length occurred for $L_{exp.}$ (0.93 ± 0.04 inches) due to the very high inelastic strain. Hence it appears reasonable to compare the theoretical half buckle wave-lenght with the experimental value if deformation is not excessive.

3.4 Hysteresis Loops

Fig. 3.6a through 3.6i show the shape of the load deflection hysteresis loops for the first, fifth, tenth, fifteenth and twentieth cycles, except for beam T3 which cracked after one and one half cycles. The following observations are noted:

1. In all the beams, there is a noticeable difference between the first and the subsequent loops. This comment was made also by Nashid (9).
2. Loops for cycle 2 to cycle 20 had almost the same shape, except that when the number of cycles increased the loops tended to become flatter, and a considerable drop in load capacity was observed.
3. The hysteresis loops tended to shift horizontally to a considerable extent with the result that progressive residual deflection was noted after the first cycle.
4. A permanent kink was formed at midspan for all the beams, except for beams T7 and T8. The formation of the kink was caused by an increase in permanent residual displacement. The kink is shown in Figures 3.16b, 3.18 and 3.21.
5. All the loops following the first cycle, tended to rotate around the z-axis (perpendicular to the page), except for beams T7 and T8 where horizontal shifting occurred without rotation, the losses in tube capacity being less. This rotation may be caused by the kinking action, where a difference in tube levels occurred near the buckle zone after the first cycle. During the second cycle, the buckled section will be subjected to:
   a. A compressive moment resulting from the load

applied at the center of the beam.

b. The longitudinal fibre force will cause an additional moment due to the difference in tube level.

It can be seen that, for a certain value of load, two different deflections may be obtained in the first and the second cycle. Due to the extra moment and the weakness of the buckled section, the larger deflection obtained in the second cycle may cause the rotation of the hysteresis loops when a kink is formed.

6. The flexural capacity was fairly stable throughout the tests which did not have cracks at the buckle section.

7. Tube T3 was cycled up and down to the maximum stroke of the jack, (± 4 inches), which gave a limiting deflection equal to seventeen times Δ_p. Due to the large amount of residual displacement, namely 3.3 inches with a correspondingly very high local strain, failure (cracks) occurred in the second cycle.

3.5 Strain Gauges and Moment-Curvature Relationship

Strain gauges were mounted in order to measure

the strain at six points over half the periphery of each tube. Once the strains for the unbuckled section are known, the curvature may be obtained by dividing the extreme fibre strain by the radius of the tube. When local buckling occurred in the zone of the gauges, the strain readings were not representative of the behaviour of the unbuckled section.

Hence, rather than using the moment-curvature relation for each tube tested, the load-deflection characteristics were deemed to be a much more accurate representation of the behaviour and were used for comparison for all the tests.

3.6 Stability of the Load Levels

The relation between the load levels and the number of excursions is shown in Figures 3.7a to 3.7h. There was a continuous reduction in load level with the increase of number of excursions. The higher the D/t ratio the higher the reduction in load level would be expected. The plastic load value was reached only in the first half cycle for all tubes except for T7 and T8. For tube T7 the plastic load was exceeded in the first three half cycles, and in the first four cycles for T8. The reduction in load level was larger when the load was applied downward.

3.7 Deflection Characteristics

Figures 3.8a to 3.8h show a diagramatic sketch of the midspan deflection with consecutive cycles for all the tubes except for T3. For each cycle four important points were plotted. The first point represents the peak negative deflection, the second one the deflection at zero load, the third point the peak positive deflection and the last one represents the deflection at zero load.

The residual negative deflection is consistent in all of the tests, where downward deflection is being defined as negative. Deflection was controlled in such a way as to maintain the first peak deflection attained in the first half cycle, denoted as Δ in Fig. 3.8, through all the cycles. The deflection was specified as three times the deflection corresponding to P_p. However small vertical displacements at both supports had to be accounted for. This displacement was caused by:

1. Deflection of the supporting bar itself.
2. Deflection of the bracket as it forms a cantilever from the column.
3. The hole in the bracket was slightly oversized relative to the supporting bar to permit easy positioning. This small clearance permits the bar to move. The vertical displacement at each end was measured by two dial gauges which were located near the

connection between the pipe and the supporting bar.

Knowing the displacement at the supports, the deflection at midspan was corrected at every reading. For this reason it was too difficult to maintain Δ exactly equal to $3\,\Delta_p$ throughout the twenty cycles. Table 3.5 shows the average Δ obtained during the twenty cycles for the nine tubes. The magnitude of the positive deflection was very small in all the beams in comparison with the negative deflection. The positive deflections decreased with the increasing number of excursions and in some tubes (T2 and T4) they were completely eliminated in the later excursions of the test.

3.8 Cumulative Energy Dissipation

Energy dissipation is a measure of the cumulative damage. A decrease in the rate of energy dissipation, for a certain structural member means that it is not fully participating in resisting the straining actions. Thus the adjacent members are required to absorb the excess in energy input.

The area enclosed by a hysteresis loop defines the energy dissipated by a member per cycle, and this quantity is of great importance in earthquake engineering. Here, the energy dissipated per single load excursion is designated by W, and the corresponding residual deflection,

Δ_W, is the width of the loop at zero load.

The area of all the loops was calculated for every test, and the cumulative energy dissipation, $\sum W$, was calculated and plotted against the number of excursions in Figures 3.9a to 3.9d. If the loop areas are the same, a straight line will be obtained, otherwise a curved line results.

It was noticed that for tubes of the same diameter, any decrease in thickness would decrease the amount of $\sum W$; this is illustrated for beams T1, T2, and T7 in Fig. 3.9a. When fracture is imminent, a larger drop in peak load values and smaller areas for loops will be obtained. For tube T3, fracture occurred after three excursions and the areas of the first, second and third loops were 128, 186 and 132 kip.inches respectively. Hence, a tendency of flatness of the relationship between the cumulative energy dissipation, $\sum W$, and the number of excursions or a change in slope may result, as in Fig. 3.9d.

By drawing an horizontal straight line at any value of $\sum W$ in Fig. 3.9d, the number of excursions may be known for different values of μ (Δ/Δ_p). For $\sum W = 95$ kip.inches, the number of excursions obtained for T7 and T8 ($\Delta = 2.82$ & $1.85\Delta_p$), were 22 and 8 respectively, which represents a ratio of 2.75 between the number of cycles required for the same value of $\sum W$. The same ratio is obtained for $\sum W = 60$, 140 and 160. Hence tube T8 would be expected to reach a

value of $\sum W = 420$ after 110 excursions, while the same value of $\sum W$ was reached by T7 after 40 excursions. By cycling the same tube with other values of μ (4,5,...,10), new ratios will be obtained and the history of this section will be more covered.

3.9 Effect of Slenderness Ratio on Total Energy Dissipation

The total energy dissipated, $\sum W$, by each specimen is a direct indication of its capability of resisting cyclic effects generated during an earthquake. Both the total nergy and the corresponding number of excursions can be obtained from Figures 3.9a to 3.9d.

The value of σ_y was not constant for all the tubes, ranging between 46.5 and 55.5 ksi. Hence, it will be convenient to define a dimensionless energy ratio "e" based on the energy dissipated during a single cycle. If P_p is the computed plastic load, Δ_p is the corresponding elastic deflection and W is the actual energy dissipated per single cycle, hence:

$$e = W / \tfrac{1}{2} P_p \Delta_p$$

$$\sum e = \sum W / \tfrac{1}{2} P_p \Delta_p$$

Figure 3.10 shows the relation between the

accumulated energy ratio, $\sum e$, and the D/t ratio. A smooth curve connecting the points was obtained, except for the value where D/t = 46, which was far removed from the curve. The principal reason for this is that the limiting deflection for T7 ($\Delta = 2.82\,\Delta_p$) was smaller than the limiting deflections for all the other tubes, where Δ was slightly larger than $3\,\Delta_p$ as it can be seen in Table 3.5. A comparison is made in Fig. 3.11, between the cumulative energy ratio and the number of cycles for different values of D/t and $\mu = 3$. From the curve it appears that any increase in the D/t ratio decreases the accumulated energy ratio $\sum e$, for a constant value of μ.

3.10 Residual and Cumulative Residual Deflections (4) and (9)

During the cyclic programme, different types of deflection were measured:

1. Δ_m = Maximum deflection at midspan, measured from the original zero position.
2. Δ'_o = Residual deflection at midspan measured from the origianl zero position.
3. Δ'_w = Residual deflection at no load position, which means the width of the loop.
4. Δ_p = Elastic deflection corresponding to the plastic load P_p.

All the above deflections are plotted against the number of cycles for each tube in Figures 3.12a to 3.12h. It can be seen from the Figures that Δ'_w was constant during the cyclic programme for tubes with small D/t (T4, T5 T7 and T8), but for the remaining tubes where D/t was greater than 55, there was an increase in the value of Δ'_w. The curves representing Δ'_m and Δ'_o were almost parallel. The larger the value of D/t, the smaller will be the difference between Δ'_o and Δ'_w after 20 cycles. Hence, the width of the loop and the drop in load capacity will be larger, as well as the total energy dissipated.

The ratio of total deformation to elastic deformation at yield, has been variously defined as that ratio for strains, rotations and displacements. The value of the ductility factor thus varies widely, depending upon the definition used. Another source of confusion arises over whether the ductility factor is measured consistently from the initial configuration of the system, or from the immediately preceding no-load configuration. Popov and Pinkney (4), suggested that the ratio of the residual plastic deformation to elastic deformation at yield, will represent a more logical measure. This ratio will be referred to as the " deflection plasticity ratio ", or simply the " plasticity ratio ", denoted by

$$\pi_d = \Delta'_w \;/\; \Delta_p$$

The plasticity ratio will indicate the residual deflections as well as the permanent damage. Popov and Pinkney (4), found that the accumulated energy ratio, $\sum e$, was proportional to $\sum \pi_d$ in their experiments. This phenomenon is to be expected for Round HSS and will be checked later.

The cumulative plasticity ratio $\sum \pi_d$, is plotted against the number of excursions in Figures 3.13a to 3.13d. This relationship, being close to a straight line, indicates that we have an approximately constant residual deflection for most of the specimens.

From Fig. 3.13a it can be seen that for the same tube diameter (8.625 inches) and different thicknesses (0.12, 0.156 and 0.188 inches), any decrease in thickness will cause an increase in the slope of the straight line for a constant limiting deflection Δ, which means that a higher value of $\sum \pi_d$ will result in larger deterioration in load capacity and a smaller amount of energy dissipation. It is to be noted that the span for all tubes in Fig. 3.13a was the same, equal to 72 inches.

The curves for T5 and T6 were drawn in Fig. 3.13b, while that for T4 was drawn in Fig. 3.13c. Different figures were necessary due to the different spans required, 88, and 80 inches respectively.

Fig. 3.13d shows the difference between the behaviour of the same size tube cycled with $\mu = 17$, $\mu =$

2,82 and μ = 1.85. As indicated in the figure, the results show that the higher the value of μ, the higher will be the value of $\sum \pi_d$. When the fracture is imminent for Δ = 17, a larger Δ_u is obtained as well as a change in the slope of the curve relating $\sum \pi_d$ and the number of excursions.

Drawing an horizontal straight line from any value of $\sum \pi_d$, and dividing the number of cycles obtained for T8 by the one obtained for T7, a ratio of 2.65 is obtained.

Fig. 3.14 shows the relation between $\sum e$ and $\sum \pi_d$ after 20 cycles. It can be seen that there is some proportionality between the two parameters, even by using different values of μ.

Figures 3.2 and 3.9a to 3.13d, may be useful for earthquake design before or after the earthquake.

During the design, the engineer could follow a procedure such as:

1. From Fig. 3.2 a section which will have a small amount of loss in load capacity after being cycled (10%-20%).
2. From Fig. 3.10 and 3.11, the corresponding amount of energy dissipation for the chosen section.
3. From Fig. 3.9 and 3.13, the value of $\sum W$ or $\sum \pi_d$ after any number of cycles. If the curve is extended to failure, the engineer will know the maximum amount of $\sum W$ for this section and may have an approximate estimate for the life of the section.

After an earthquake, Fig. 3.12 may be very useful. Knowing the acceleration and the time of the earthquake, the response of any structure may be known by using a dynamic analysis computer program. From this analysis, the number of cycles as well as the deflection values may be known. The mean deflection may be calculated and the corresponding value of μ will be known. Knowing the value of μ, the corresponding series of curves will be selected. The plastic residual deflection Δ_o is measured from the structure. Hence, the number of cycles may be checked form Fig. 3.12 depending of the D/t ratio, and the values of maximum deflection and cumulative energy dissipation will be selected. Extending the curve in Fig. 3.9 to failure, the value of $\sum N$ obtained from Fig. 3.12 may be located and an approximate value of the remaining life may be known as well as the actual damage.

3.11 Discussion and Comments on Failure Shapes

Figures 3.16 to 3.23 show major buckles for all the tubes. The kinking actions and the off line alignement are shown clearly in Figures 3.16b and 3.18a. The tiny buckles which were formed late in the loading pattern are shown in Figures 3.18f and 3.21. Major buckles occurred in the zone where the strain gauges were mounted for tubes T1, T2 and T4 as it is shown in Figures 3.16a, 3.17

and 3.19 . Due to the severe buckle shown in most of the figures, it can be understood why a loss in bond occurred for some gauges after a couple of cycles.

After the cyclic programme, all the beams except T7, T8 and T9 were pushed downward to the maximum stroke of the jack (4 inches). The load was then released (no load position). The load was applied upward for the remaining beams, except where some unusual buckle occurred as in beam T1 or when the procedure was different as in T3.

Cracks occurred in tubes T2 and T5 as it is shown in Figures 3.17 and 3.20. No visual cracks occurred in tubes T4 and T6, even after cycling the tubes to the maximum positive and negative stroke. The two cracks which occurred in tube T3 after one and one half cycles are shown in Figures 3.18a and 3.18b.

The following statements are based on the previous discussions:

1. Tubes with D/t ranging from 46 to 72, sustain a cyclic loading programme, composed of twenty cycles and governed by a limiting deflection $\Delta = 3\,\Delta_p$, without the appearance of any cracks.
2. Larger deterioration in load capacity as well as larger buckles will be obtained by increasing D/t ratio.
3. Once local buckling appeared, prediction that

fracture will occur after a certain number of cycles, becomes very difficult. The reason for this is that the occurrence of fracture will be a combination of:

a. Size of local buckle.

b. Fatigue of the metal itself.

c. Diameter to thickness ratio (D/t).

d. Stiffness of the section itself (I).

e. Location and size of the kink.

4. Benham and Ford (2), pointed out in their investigation on low endurance fatigue of a mild steel, that specimen's failure, subjected to a strain smaller than 4%, is largely a fatigue failure. But for a strain larger than 4%, buckling of the specimen established the limiting condition of failure.

5. Since, in all the tubes, local buckling occurred in the first half cycle at a strain value smaller than 1%, it can be seen that the occurrence of cracks during the following cycles will be attributed to a combination of fatigue and buckling and not to fatigue alone.

6. Assuming that the 7 tubes may be be cycled until the loss of capacity reaches 50% without fracture at $\Delta \simeq 3\,\Delta_p$ and assuming that the rate of deterioration will be constant and the same as it was during the last few cycles for every tube, a relationship for the number of cycle at 50% loss versus D/t may be extrapolated. A dotted curve showing this extrapolation relationship is shown in Fig. 3.15. Another curve is drawn at 20%

loss in load capacity directly using the experimental results, except that for D/t = 46 the result was extrapolated using the previous assumptions.

3.12 Comparison Between Two Different Round HSS Having the Same D/t Ratio

A comparison is shown in Table 3.6 between tube T2 (8.625 OD x 0.156) and tube T6 (14.00 OD x 0.25). Both tubes had almost the same D/t ratio (55 and 56 respectively). It can be seen from the table that the loss in load capacity was the same for both tubes after 20 cycles (34%) as well as after 5 cycles (18%). Also the cumulative plasticity ratio $\sum \pi_d$ was very close for both tubes (78.5 and 83 respectively). In addition the accumulated energy ratio $\sum e$ was virtually the same (102 and 103 respectively).

This comparison is useful, because it appears to the author that having the same D/t ratio from different diameters and thicknesses, the same cumulative plasticity ratio $\sum \pi_d$ and the same capacity loss will be obtained. knowing that any decrease in D/t will increase $\sum e$, it may be logical for earthquake design to choose two smaller tubes rather than one large. The section modulus of the two small tubes will be the same as the large one and D/t of the former tubes may be smaller too. This choice may provide a larger value for $\sum e$ and more flexibility, because the rotation is equal to the outside fibre strain divided by the radius of

the tube. Hence, the smaller the radius, the larger will be the rotation, for a constant value of strain. It is to be noticed that the weight of the beam as well as the cost of connections must be taken into consideration too.

3.13 Comparison Between the Behaviour of Square and Round HSS Under Cyclic Loading

To compare the behaviour of Square and Round HSS subjected to cyclic loading, a Square HSS was chosen from Nashid's (9) experiments. The section was chosen so that its limiting cyclic deflection was close to the one used by the author ($\Delta = 3\ \Delta_p$).

For the Square HSS 10 x 10 x 0.281 inches, b/t = 36 and $\Delta = 3.15\ \Delta_p$, cracks occurred after 10 cycles, $\sum e$ was equal to 110 after 20 cycles and the total loss in load capacity was 55%.

For the Round HSS 10.75 OD x 0.219, D/t = 49 and $\Delta = 3.25\ \Delta_p$, no cracks occurred during the twenty cycles of loading, $\sum e$ was equal to 113 and the loss in load capacity was 31%. A more detailed comparison is given in Table 3.7. It is to be noticed that cracks did not occur in any of the tubes during the twenty cycles of loading, even for D/t = 72.

The section modulus was larger for the Square HSS, and hence, fracture was due to severe local buckling and

and residual stresses. Fracture and deterioration in load capacity for Square HSS may be due to the corners of the sections, which did not form rigid connections between the different plates of the cross-section. Residual stresses exist at the corners due to cold forming, hence an earlier appearance of local buckling may be expected, and its effect may be significant.

From the previous comparison, it is observed that the performance of Round HSS subjected to cyclic loading is better than that of the Square sections for slenderness ratios which are related to code limitation for various categories of design.

3.14 Review of Other Cyclic Loading Results

3.14.1 Rolled Steel Sections

ASCE (3) recommends that for A36 steel, to preclude local buckling for plastic design, $b/t \leqslant 17$. But in the opinion of Bertero and Popov (1), this ratio must be reduced for cyclic reversed loading.

3.14.2 Square HSS

In the CSA Standard S16.1 (22), limiting b/t ratio for plastic design sections may be obtained from the

following equation:

$$b/t \leqslant 160 / \sqrt{\sigma_y}$$

Hence, for σ_y = 50 ksi, the limiting value for b/t will equal 23.

The range of b/t (16 to 38) for Square HSS tested by Nashid (9) provided sections for plastic, compact and non-compact design. The suggested value by Nashid of b/t= 22 was based on a capacity loss of 25% after 20 cycles and on a limiting deflection equal to $4\Delta_p$.

Since the range of D/t (46 to 72) for Round HSS covered by the author provided sections for compact and non-compact design, the suggested value for the limiting value of D/t will be related to that range and to a limiting cyclic deflection equal to $3\Delta_p$.

Based on tube T7 (D/t = 46) where local buckling was permitted to occur with a capacity loss $\leqslant$ 20% after 20 cycles, a tentative limiting value for D/t may be expressed by the following inequality:

$$D/t \leqslant 2350 / \sigma_y \qquad \text{for} \qquad \Delta = 2.82\Delta_p$$

It should be noted that the tentative equation was chosen from one test point at D/t = 46. Hence the reader

is cautioned in choosing a value based on this inequality until the range of D/t closer to 46 will be investigated by further research.

This tentative inequality is supported by:

1. The sudden change in the behaviour of Round HSS for $D/t < 49$. The capacity loss for $D/t \geqslant 49$ was larger than 30% and increased linearly with D/t ratio. A transition zone occurred for $D/t < 49$, and a sudden drop in the relation occurred, where the loss for D/t = 46 was 16.4%.
2. The behaviour pf tube T8 ($D/t = 46$ and $\Delta = 1.85\Delta_p$), where the loss was 8.5% after 20 cycles.

3.15 Static and Dynamic Cyclic Loading

All the cycles during the cyclic loading program were quasi-static and not dynamic, hence readings at intermediate locations were recorded resulting in the attainment of accurate loop shapes.

A comparison between static and dynamic hysteresis curves was done by Hanson (23). He concluded that the major difference between quasi-static and dynamic hysteresis loops, occurred when the response amplitude was close to the initial yield deflection amplitude. For frequencies

about 3 cps. and deflections up to 2 times the initial yield deflection, the dynamic hysteresis loops may be assumed to be the same as the static hysteresis loops for most purposes.

From Henson's conclusion it can be seen that a quasi-static cyclic loading test for the tubes used by the author will give reasonable results very close to a dynamic cyclic loading test.

Tube Number	D/t Ratio	Length of Half Buckle Wave (inches)	Location of Major Buckling			
			Right to the Load	Left to the Load	Upper Periphery	Lower Periphery
T1	72	1.25	X		X	X
T2	55	1.48	X		X	
T3	46	0.93	X		X	X
T4	49	2.13	X		X	
T5	51	2.48		X	X	
T6	56	2.68		X	X	
T7	46	1.58	X		X	
T8	46	1.35		X	X	
T9	61	1.18		X	X	

Table 3.1 Buckle Lengths and Locations

Tube Number	$\sigma_{0.7}$ (ksi)	$\sigma_{0.85}$ (ksi)	Δ	n	σ_y (ksi)
T1	47.0	44.3	1.060	16	51.4
T2	48.0	45.2	1.062	16	51.5
T3	49.8	47.0	1.060	16	51.5

Table 3.2

Values to Obtain "n" in Ramberg-Osgood Equation

Tube Number	Diameter Thickness Ratio D/t	Critical Strain ϵ_c	$\frac{m\pi R}{L}$	Radius (inches) R	Half Buckle Wave-Length (inches) L
T1	72	0.0064	10.5	4.3125	1.29
T2	55	0.0080	9.0	4.3125	1.51
T3	46	0.0100	8.0	4.3125	1.69

Table 3.3

Critical Value of Strain for a Corresponding "D/t" Ratio

Tube Number	D/t Ratio	L Experiment (inches)	L Prasad (inches)	ϵ_c Prasad	ϵ_c Exp.
T1	72	1.25 ± 0.04	1.29	0.0064	0.0075
T2	55	1.48 ± 0.04	1.51	0.0080	0.0088
T3	46	0.93 ± 0.04	1.69	0.0100	0.0106

Table 3.4

Comparison Between Prasad's Prediction and Test Results, For Critical Buckling Strains and Half Buckle Wave-Lengths.

Tube Number	$\Delta_{average}$ (inches)	Δ_p (inches)	Δ/Δ_p
T1	0.661	0.223	2.95
T2	0.702	0.223	3.15
T3	3.900	0.224	17.40
T4	0.725	0.223	3.25
T5	0.731	0.230	3.18
T6	0.660	0.187	3.35
T7	0.675	0.240	2.82
T8	0.438	0.240	1.85
T9	0.827	0.262	3.16

Table 3.5

The Average Limiting Deflection Δ for Each Tube.

Table 3.6

Same D/t Ratio From Different Tubes.

Items for Comparison	Units	Tube T2 D/t = 55	Tube T6 D/t = 56
Diameter	inches	8.625	14.000
Thickness	inches	0.156	0.250
S	$inches^3$	8.630	36.500
Capacity Loss After 20 Cycles	%	33.700	34.100
Capacity Loss After 5 Cycles	%	18.600	18.100
ΣW	kip.inches	364.000	968.000
$\Sigma \pi_d$	——	78.500	83.000
Σe	——	103.000	102.000
σ_y	ksi	51.500	46.800
P_p	lbs.	32.000	100.000
Δ_p	inches	0.223	0.187
L'	inches	72.000	88.000
$\frac{1}{2}\Delta_p P_p$	kip.inches	3.568	9.406

Items for Comparison	Units	Round HSS (10.75" OD x 0.219")	Square HSS (10" x 10" x 0.281")
D/t or b/t	—	49.000	36.000
Area	inches^2	7.250	10.720
S	inches^3	18.700	33.400
Δ_p	inches	0.223	0.316
P_p	lbs.	62.800	79.500
L'	inches	80.000	97.500
Δ / Δ_p	—	3.250	3.150
No. of Cycles	—	20.000	20.000
$\sum e$	—	113.000	110.000
Cracks	—	—	After 10 Cycles
Capacity Loss after 10 Cycles	%	22.000	28.000
Capacity Loss after 20 Cycles	%	31.000	55.000

Table 3.7

Comparison Between the Behaviour of Round and Square HSS.

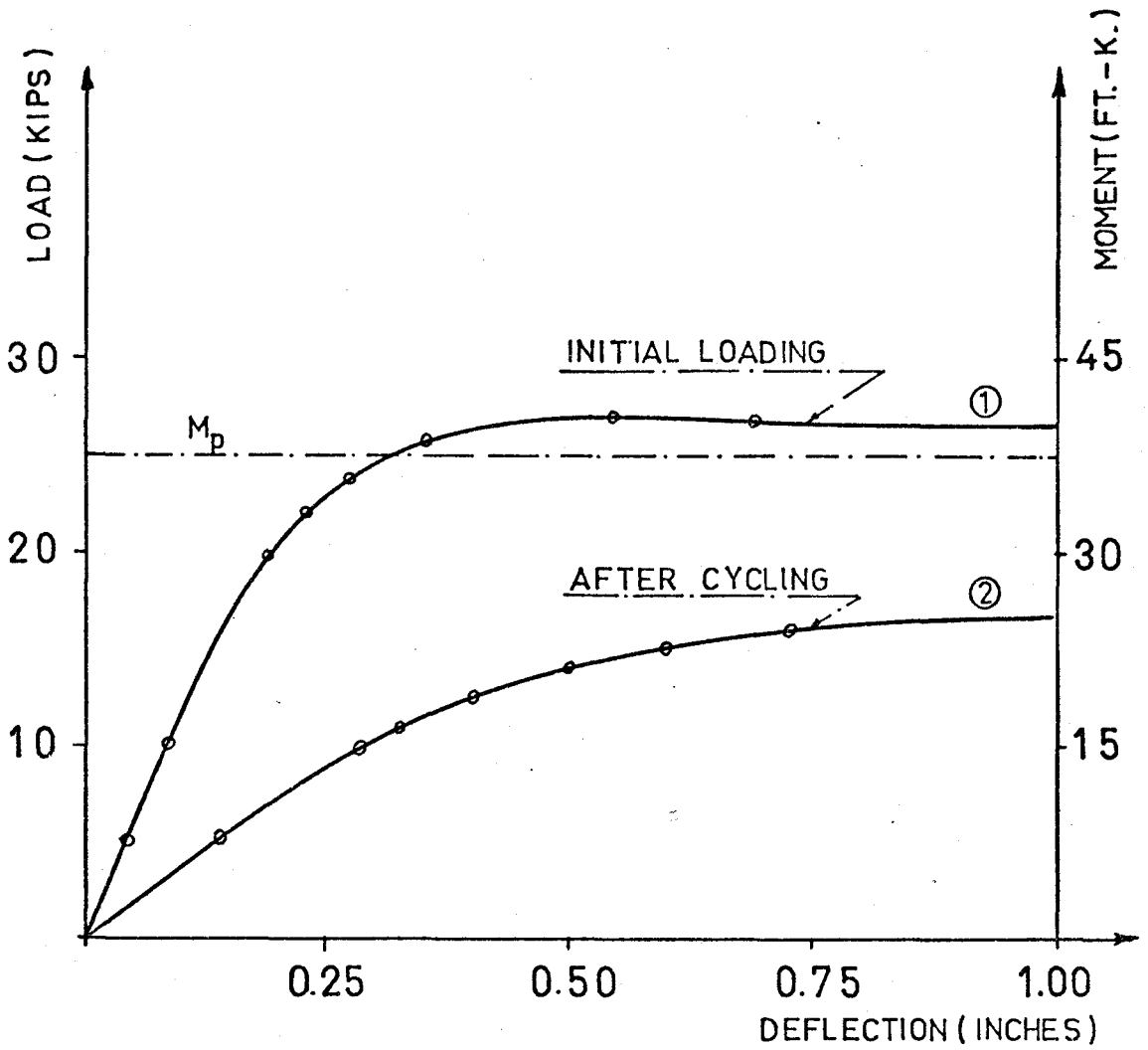

FIG. 3.1-a LOAD DEFLECTION CURVE
FOR D/t = 72
T1 (8.625" OD X 0.12")

CURVE ① = INITIAL LOADING

CURVE ② = AFTER CYCLING

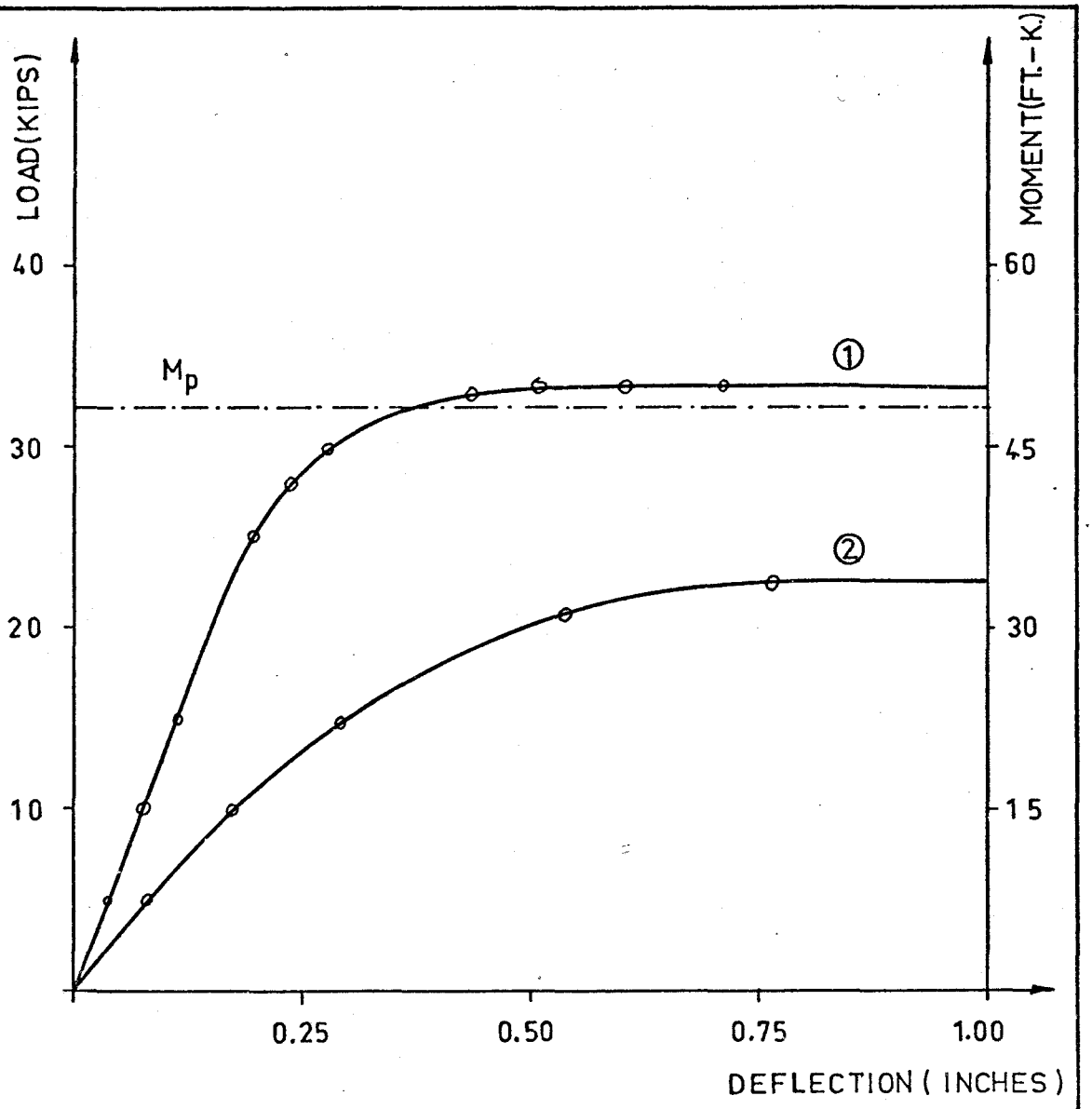

FIG. 3.1-b LOAD DEFLECTION CURVE
FOR D/t = 55
T2 (8.625" OD X 0.156")

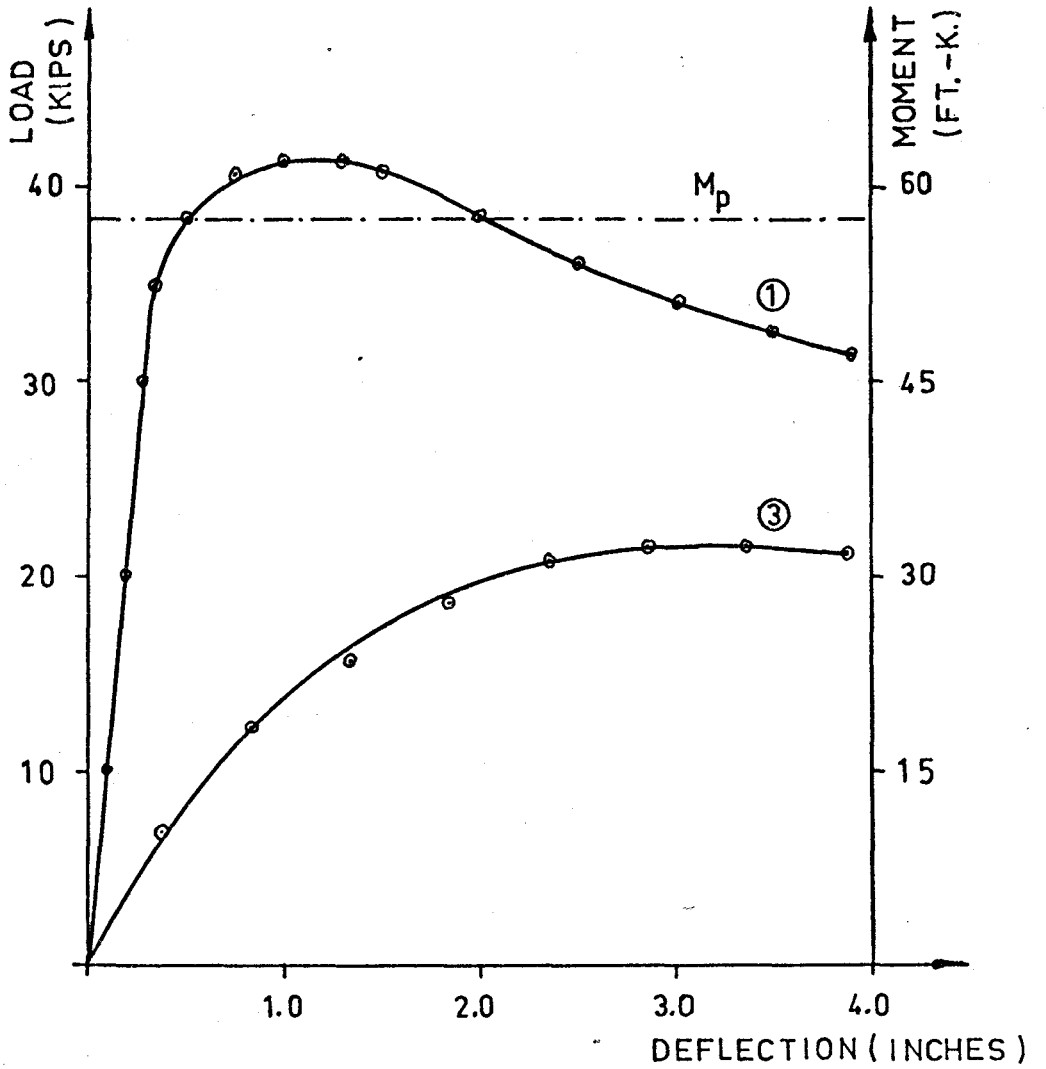

FIG. 3.1-c LOAD DEFLECTION CURVE

FOR D/t = 46

T 3 (8.625" OD X 0.188")

CURVE ③ AFTER ONE CYCLE

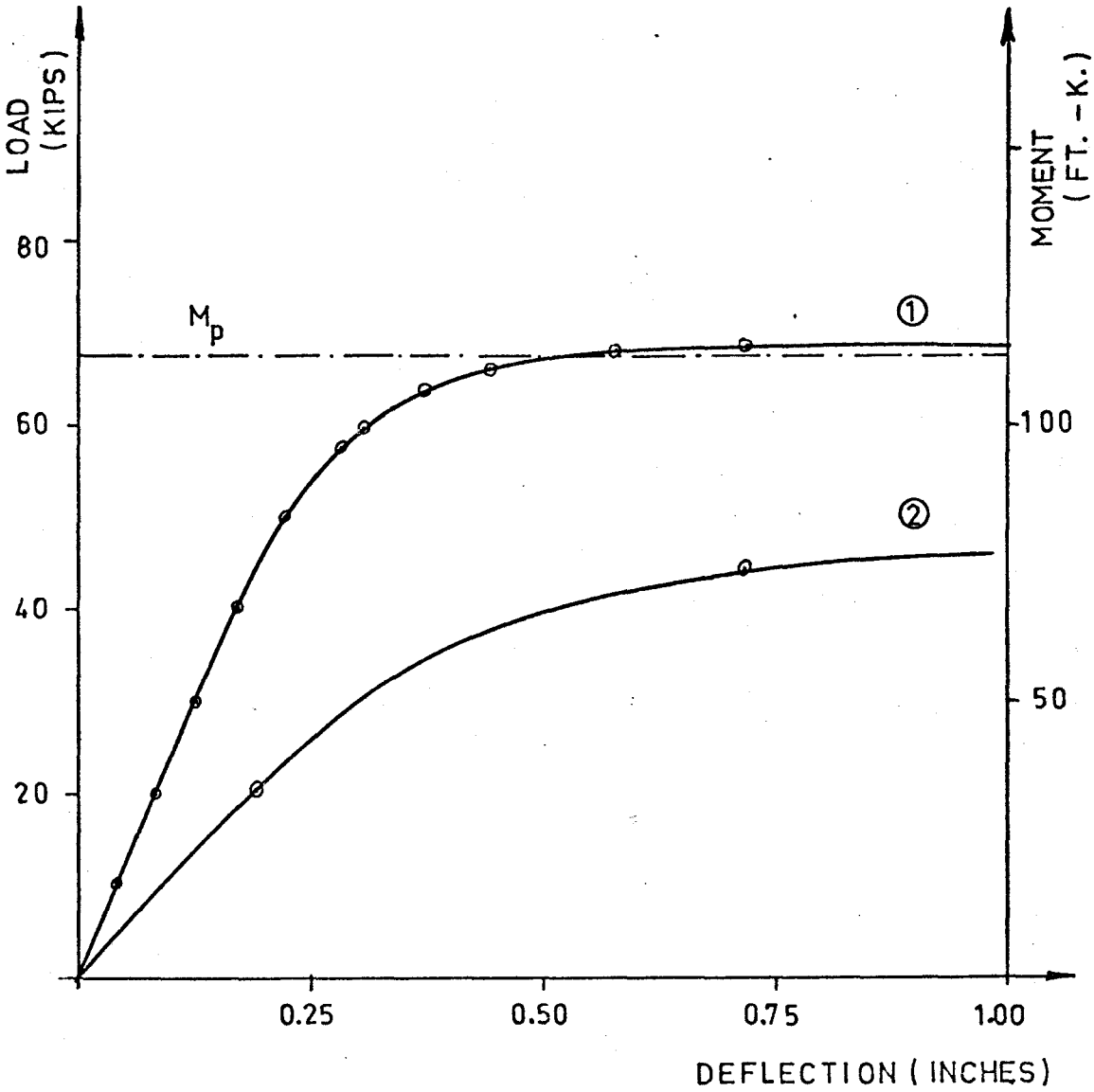

FIG. 3.1-d LOAD DEFLECTION CURVE FOR D/t = 49 T 4 (10.75" OD X 0.219")

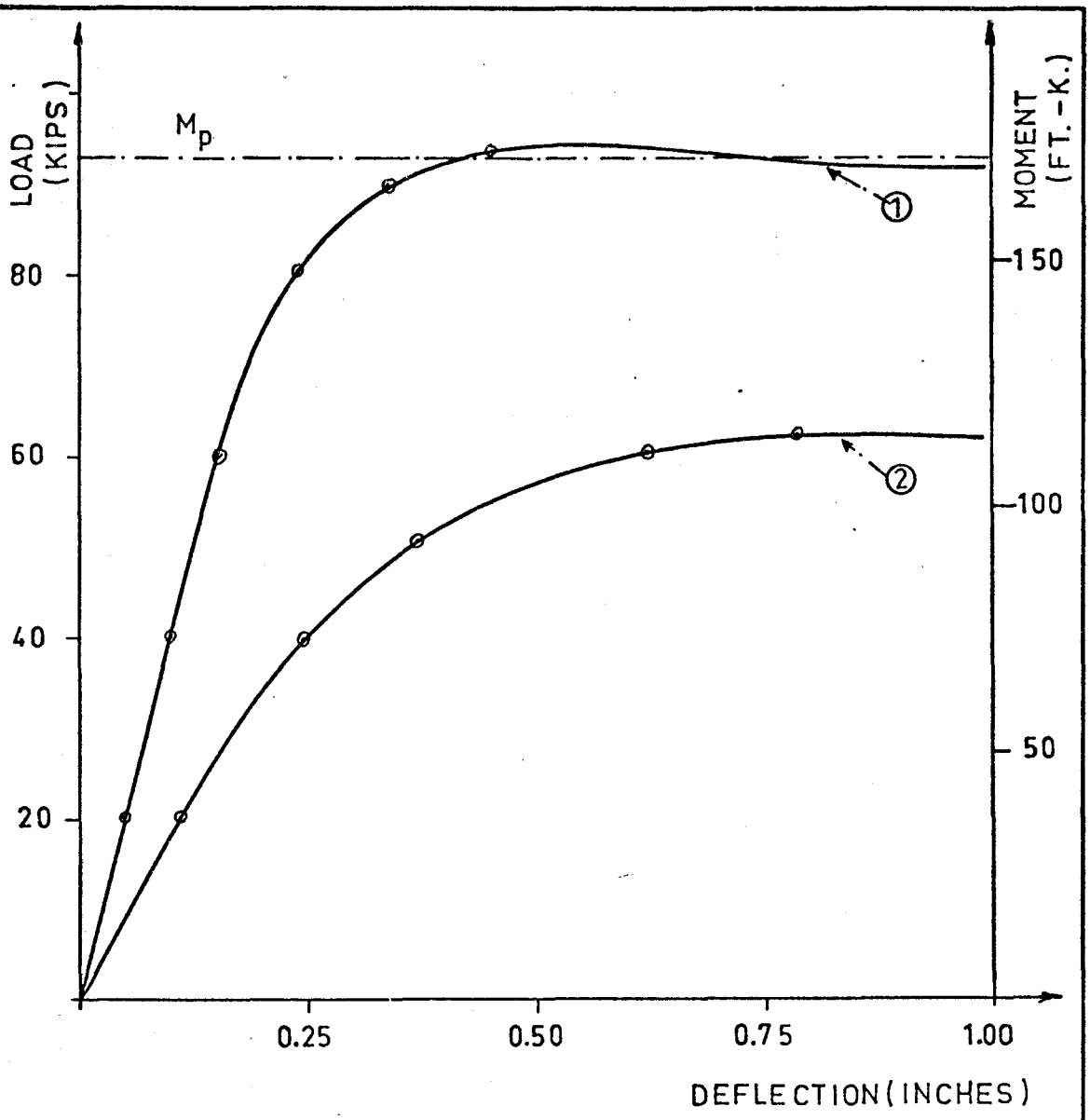

FIG. 3.1-e LOAD DEFLECTION CURVE FOR D/t = 51
T 5 (12.75" OD X 0.25")

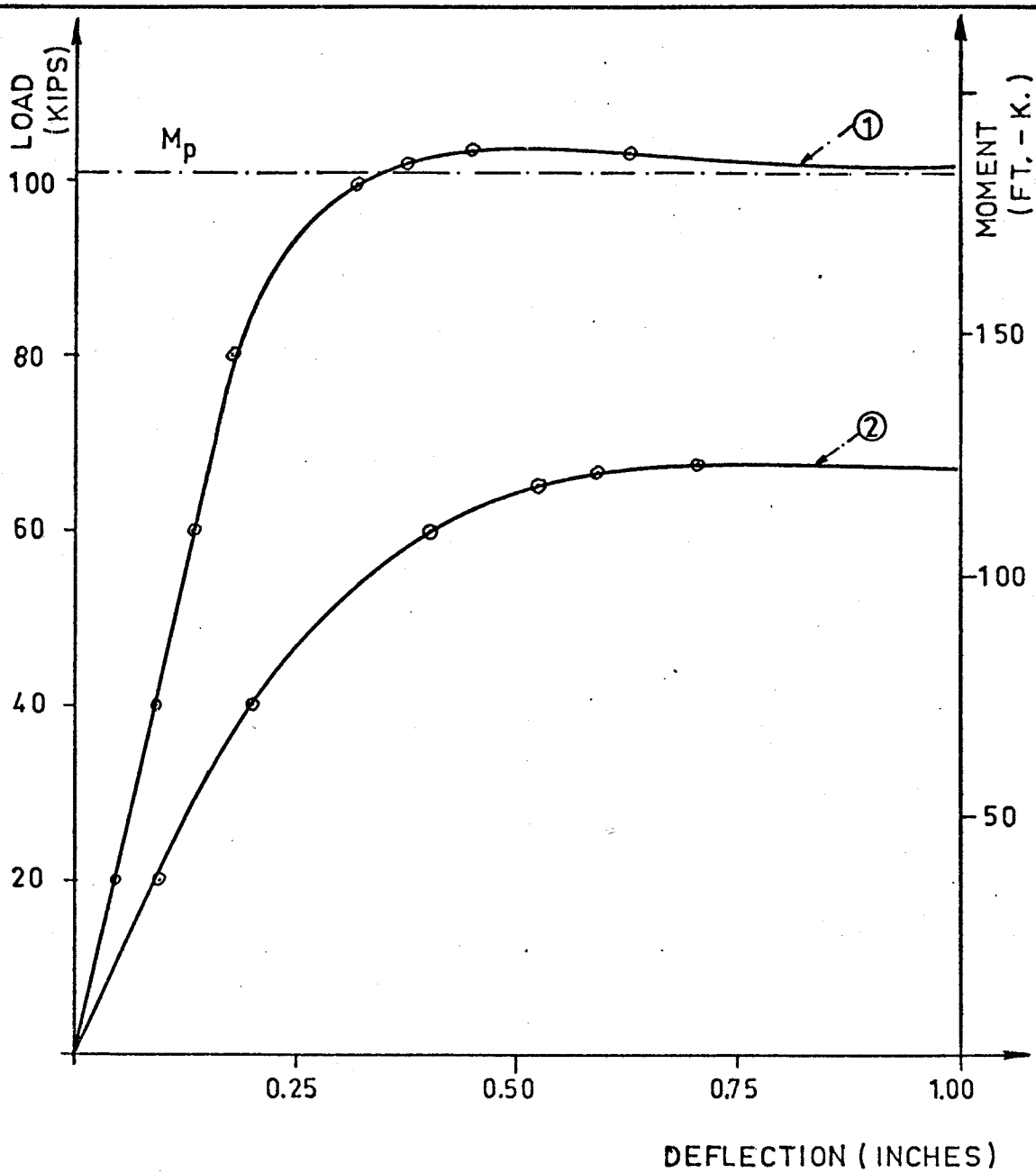

FIG. 3.1 - f LOAD DEFLECTION CURVE
FOR D/t = 56
T 6 (14.00" OD X 0.25")

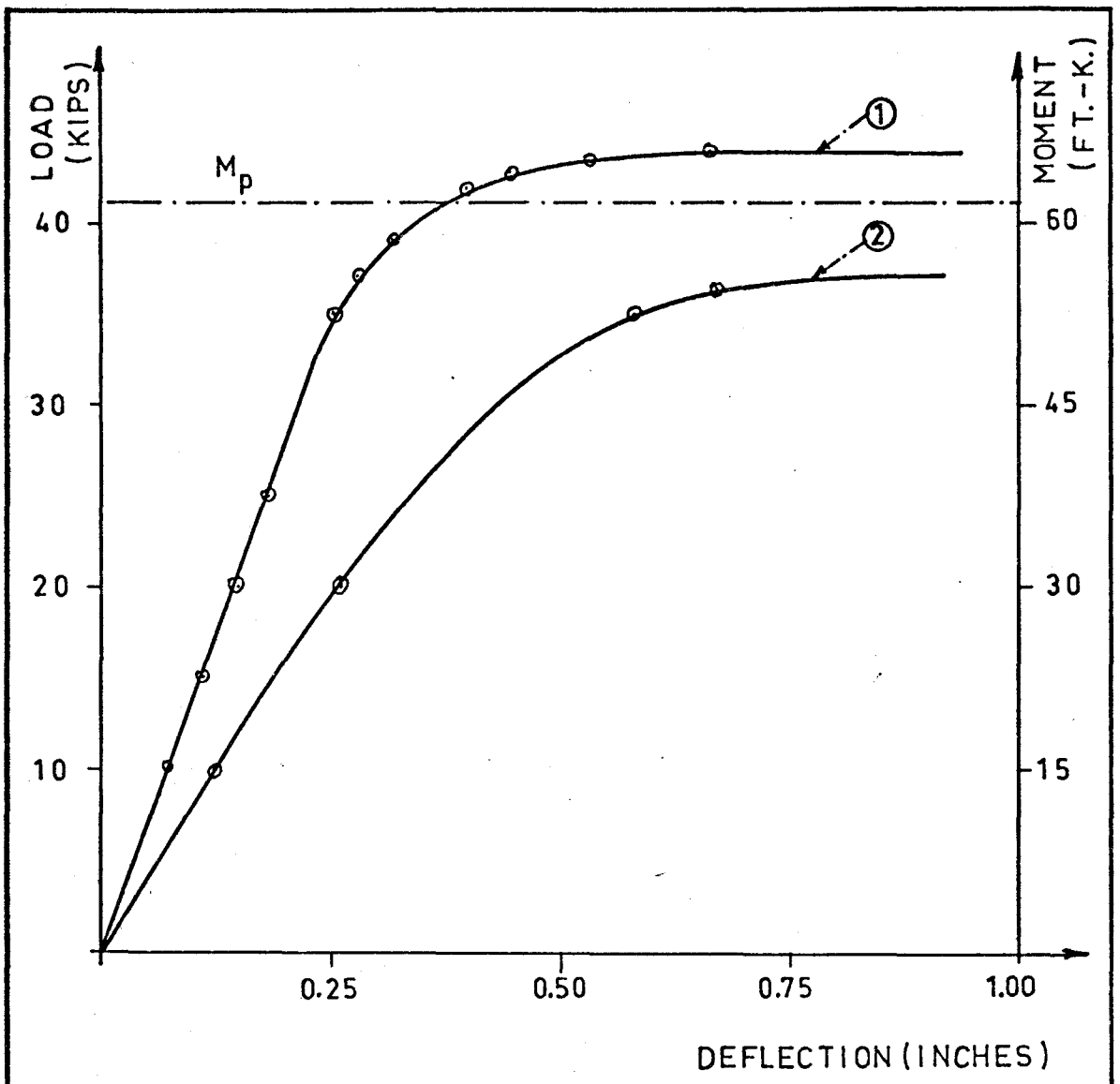

FIG. 3.1-g LOAD DEFLECTION CURVE FOR D/t = 46 T7 (8.625" OD X 0.188")

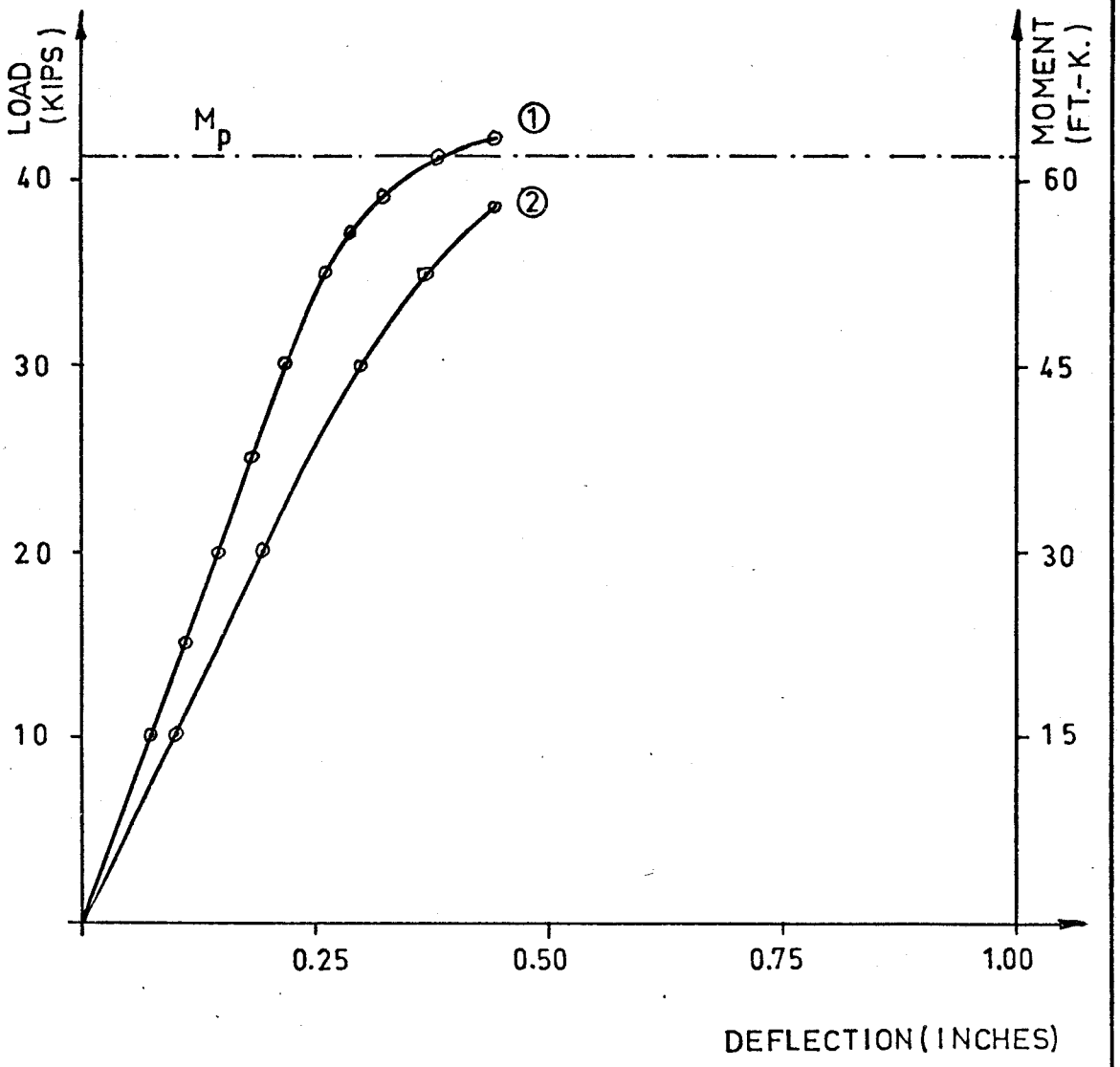

FIG. 3.1-h LOAD DEFLECTION CURVE

FOR D/t = 46

T 8 (8.625" OD X 0.188")

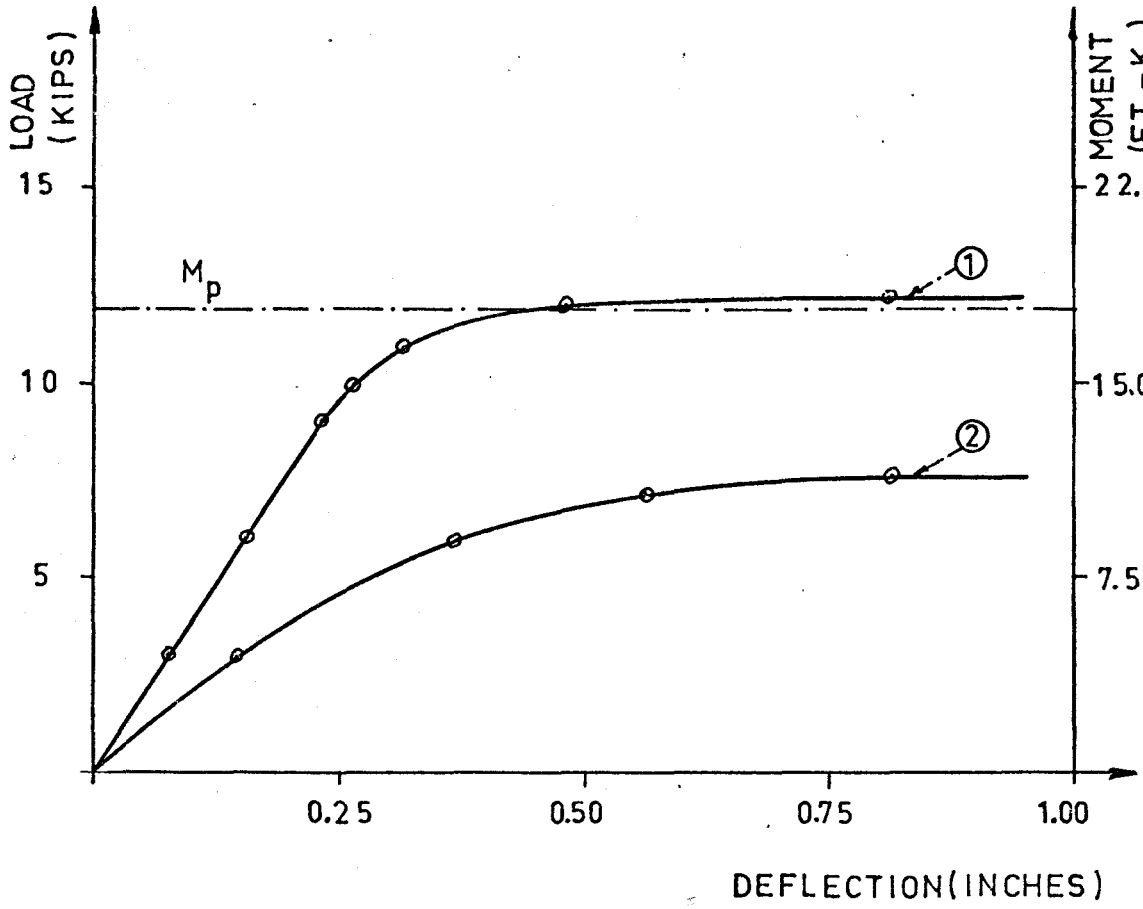

FIG. 3.1 - i LOAD DEFLECTION CURVE FOR D / t = 61

T9 (6.640" OD X 0.108")

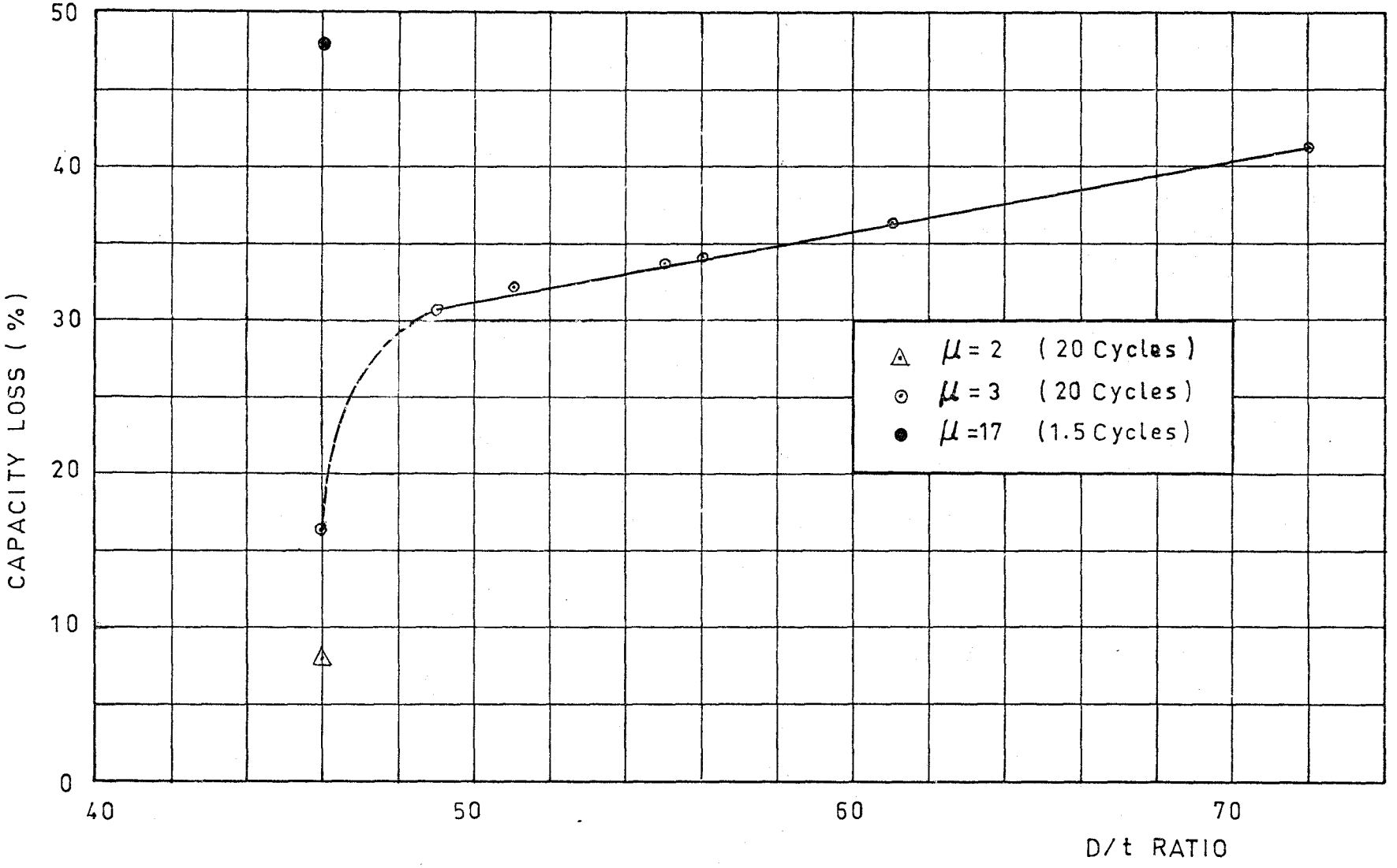

FIG. 3.2 CAPACITY LOSS Vs. D/t RATIO

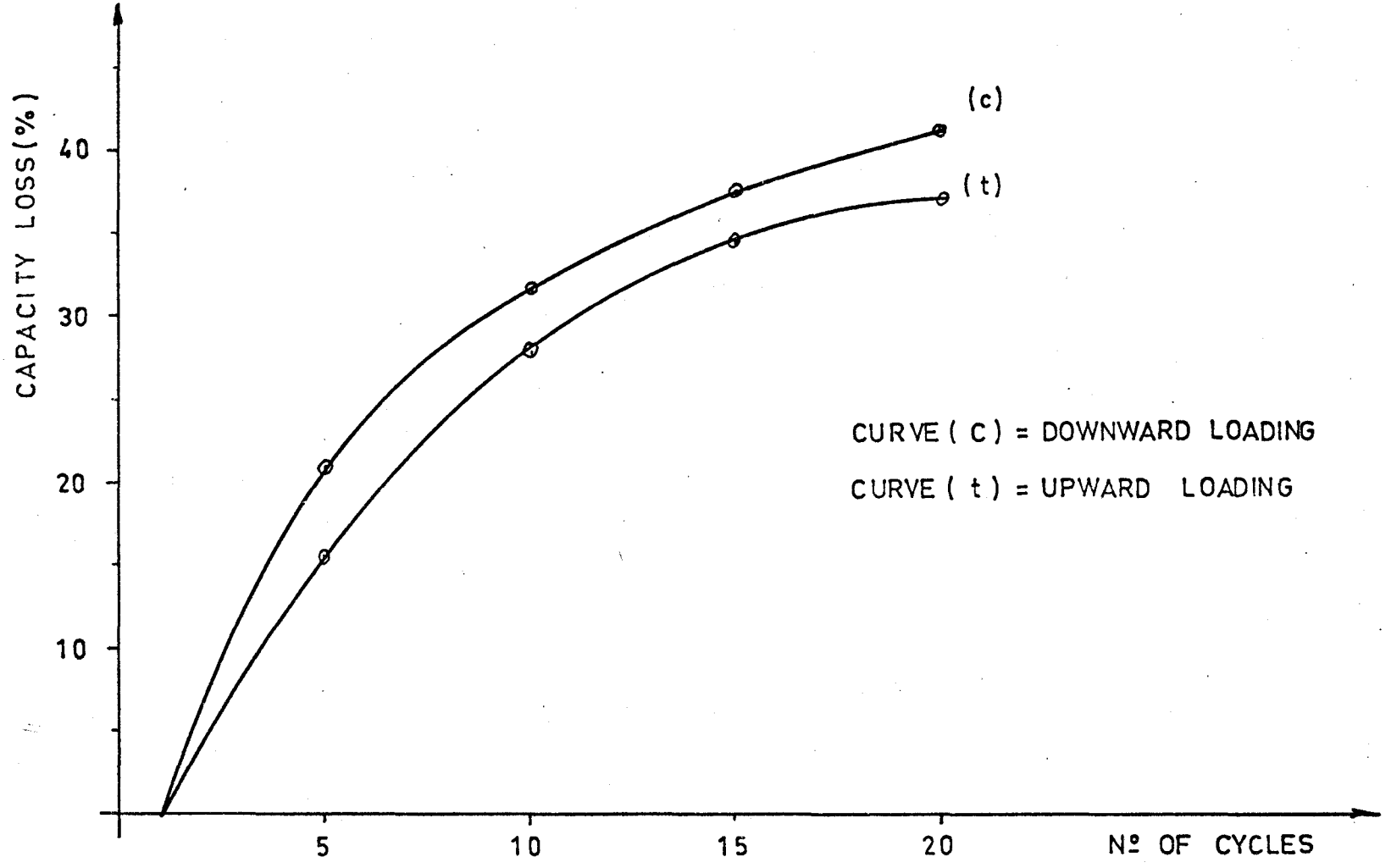

FIG. 3.3-a CAPACITY LOSS Vs. Nº OF CYCLES FOR T1

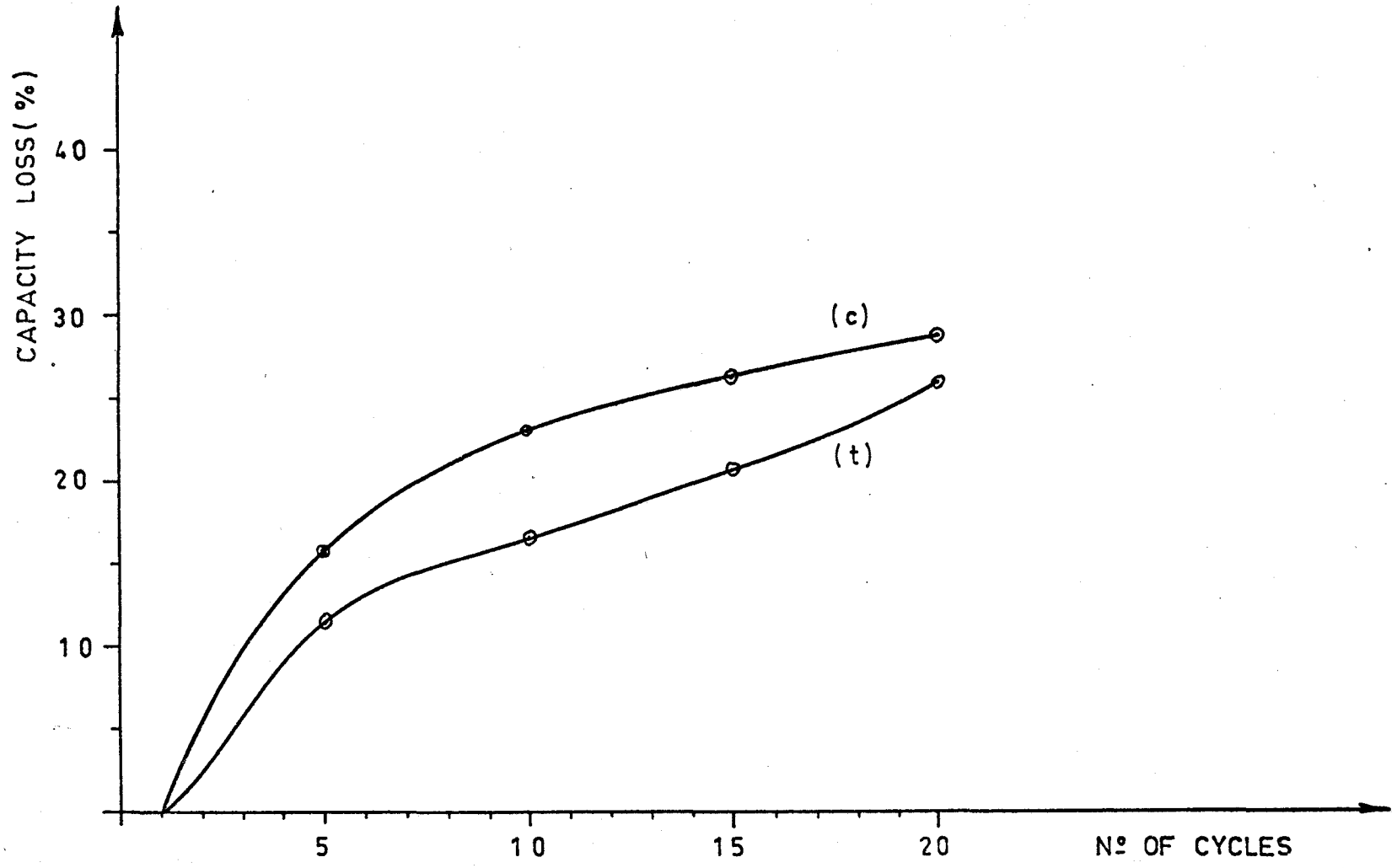

FIG.3.3-b CAPACITY LOSS Vs. Nº OF CYCLES FOR T2

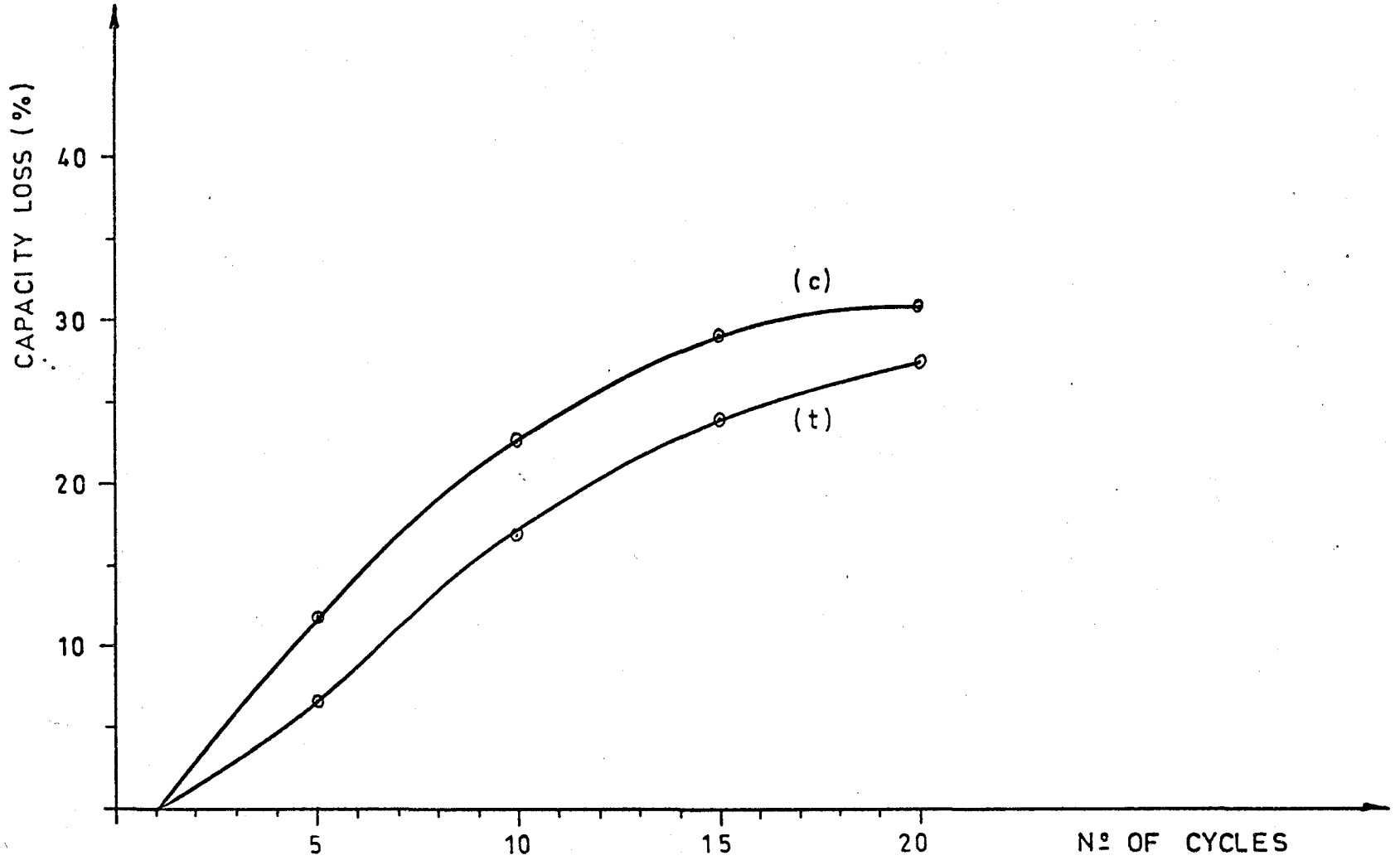

FIG. 3.3-c CAPACITY LOSS Vs. Nº OF CYCLES FOR T4

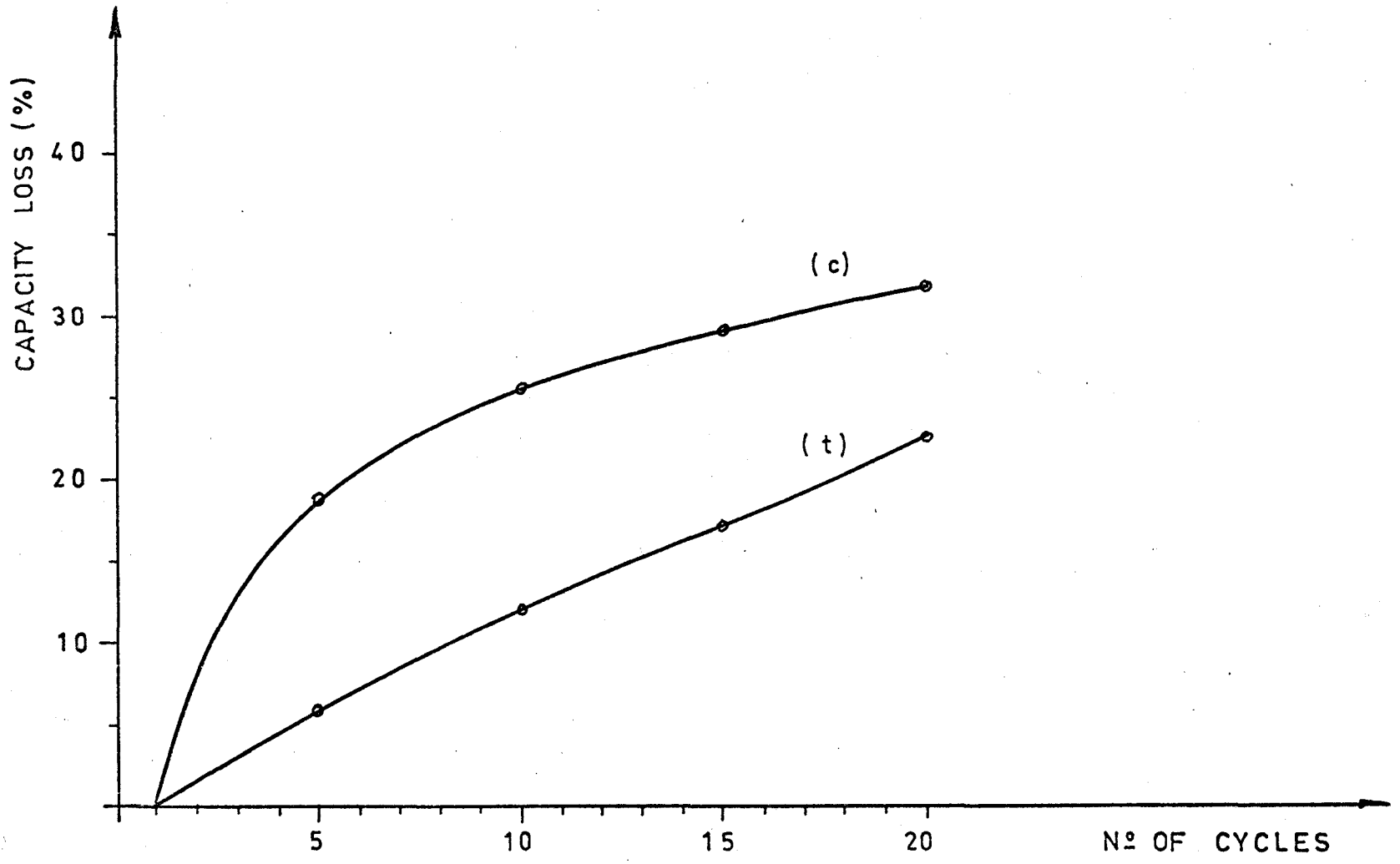

FIG. 3.3-d CAPACITY LOSS Vs. Nº OF CYCLES FOR T5

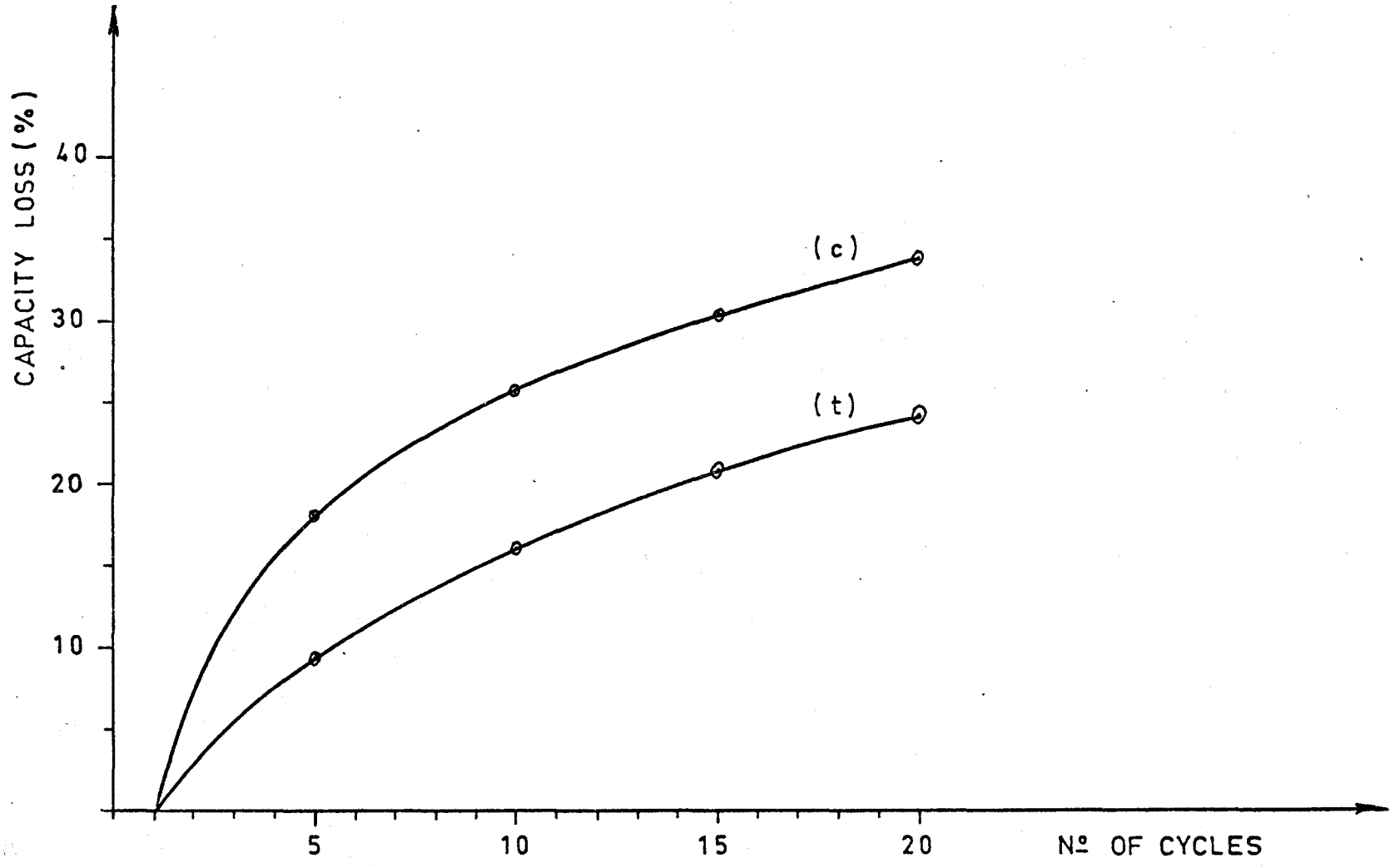

FIG. 3.3-e CAPACITY LOSS Vs. Nº OF CYCLES FOR T6

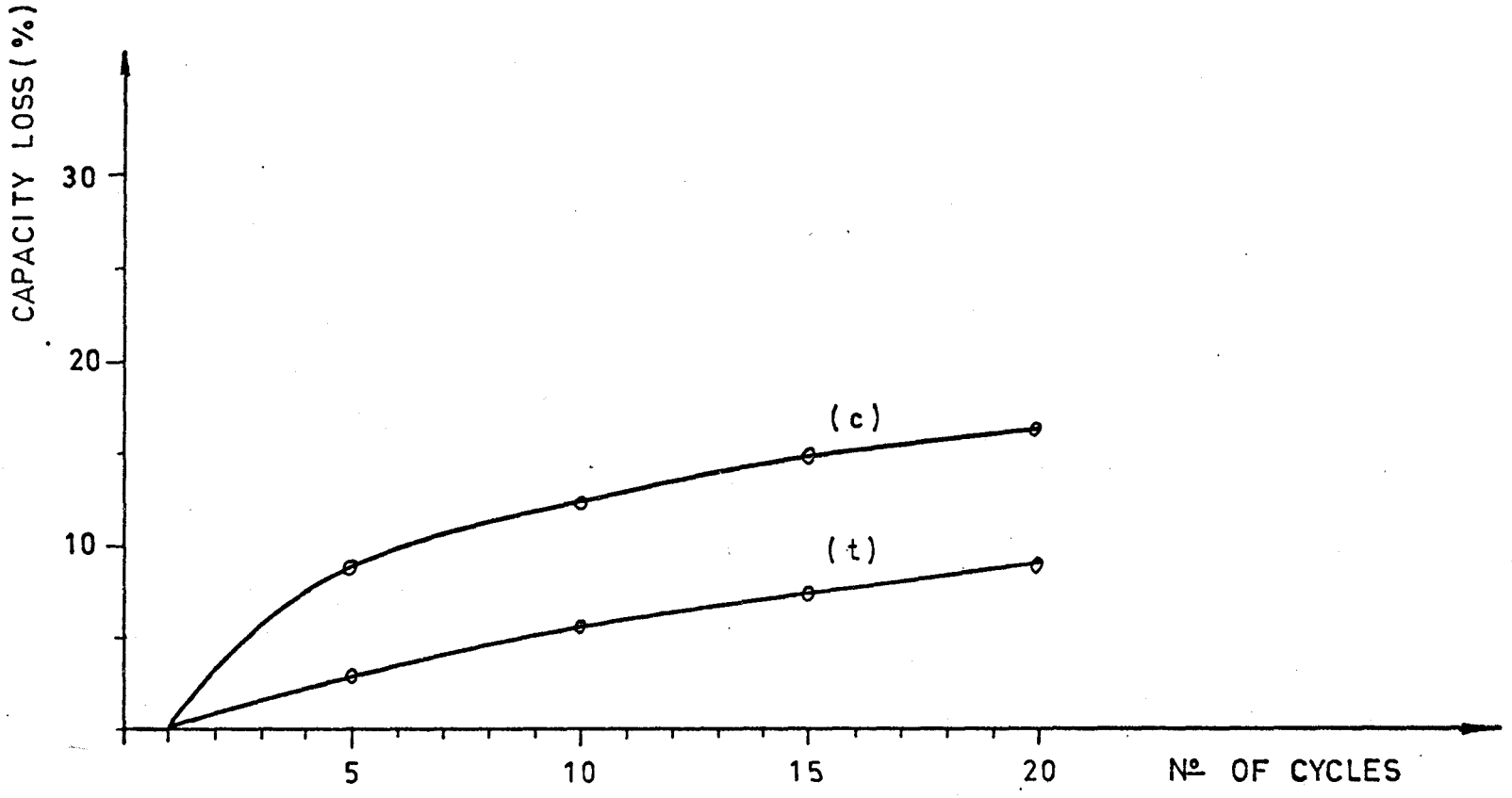

FIG. 3.3-f CAPACITY LOSS Vs. Nº OF CYCLES FOR T7
($\Delta = 2.82\ \Delta_p$)

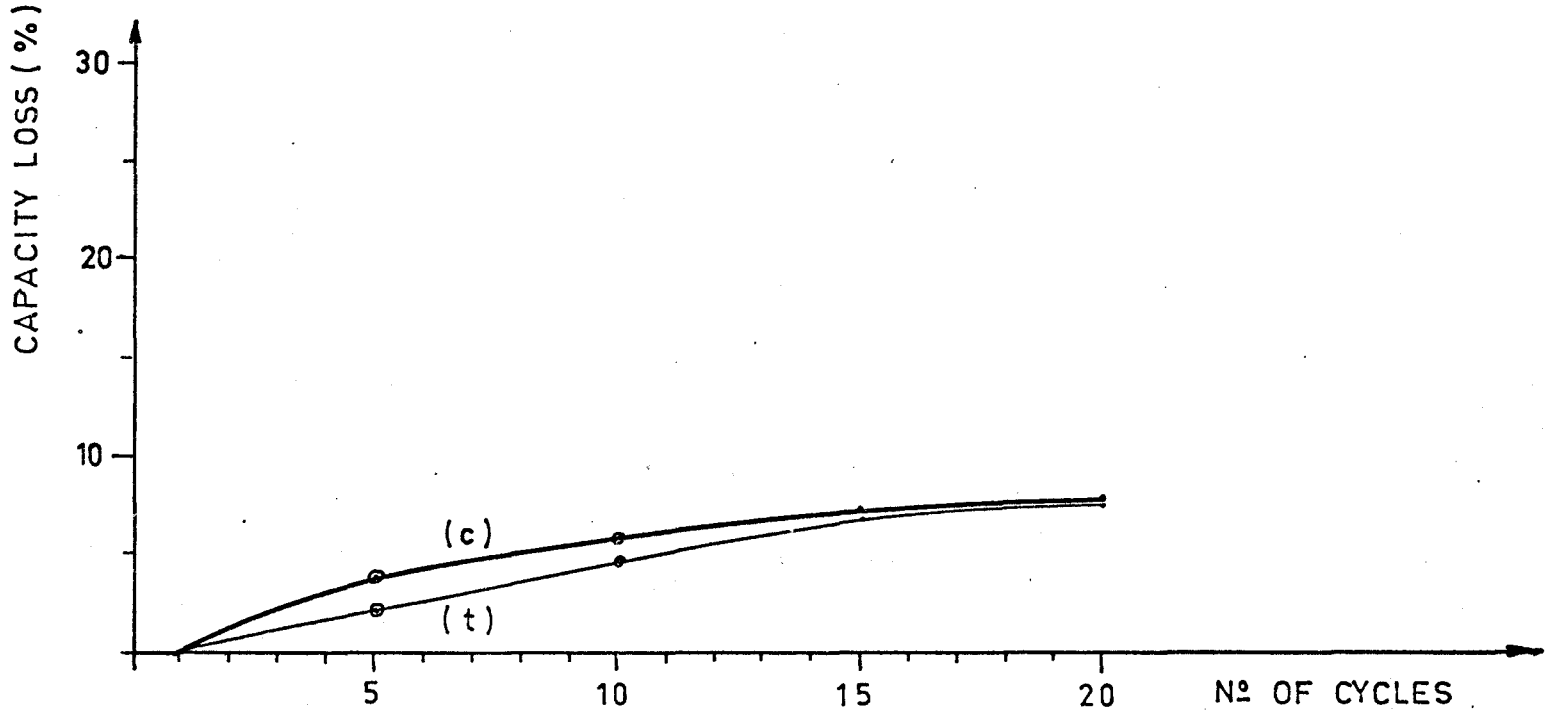

FIG. 3.3-g CAPACITY LOSS Vs. Nº OF CYCLES FOR T8

($\Delta = 1.85\,\Delta_p$)

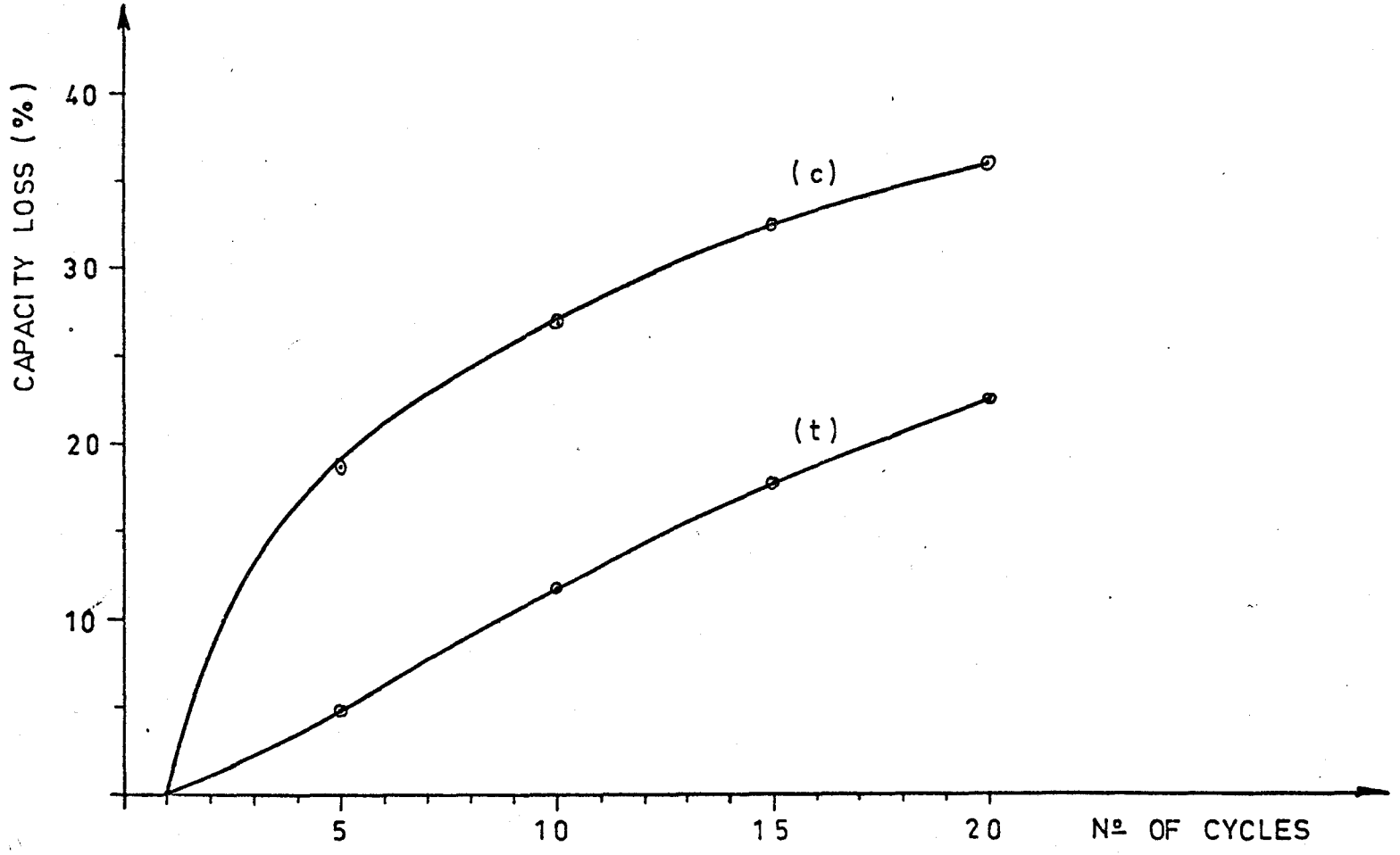

FIG. 3.3-h CAPACITY LOSS Vs. Nº OF CYCLES FOR T9

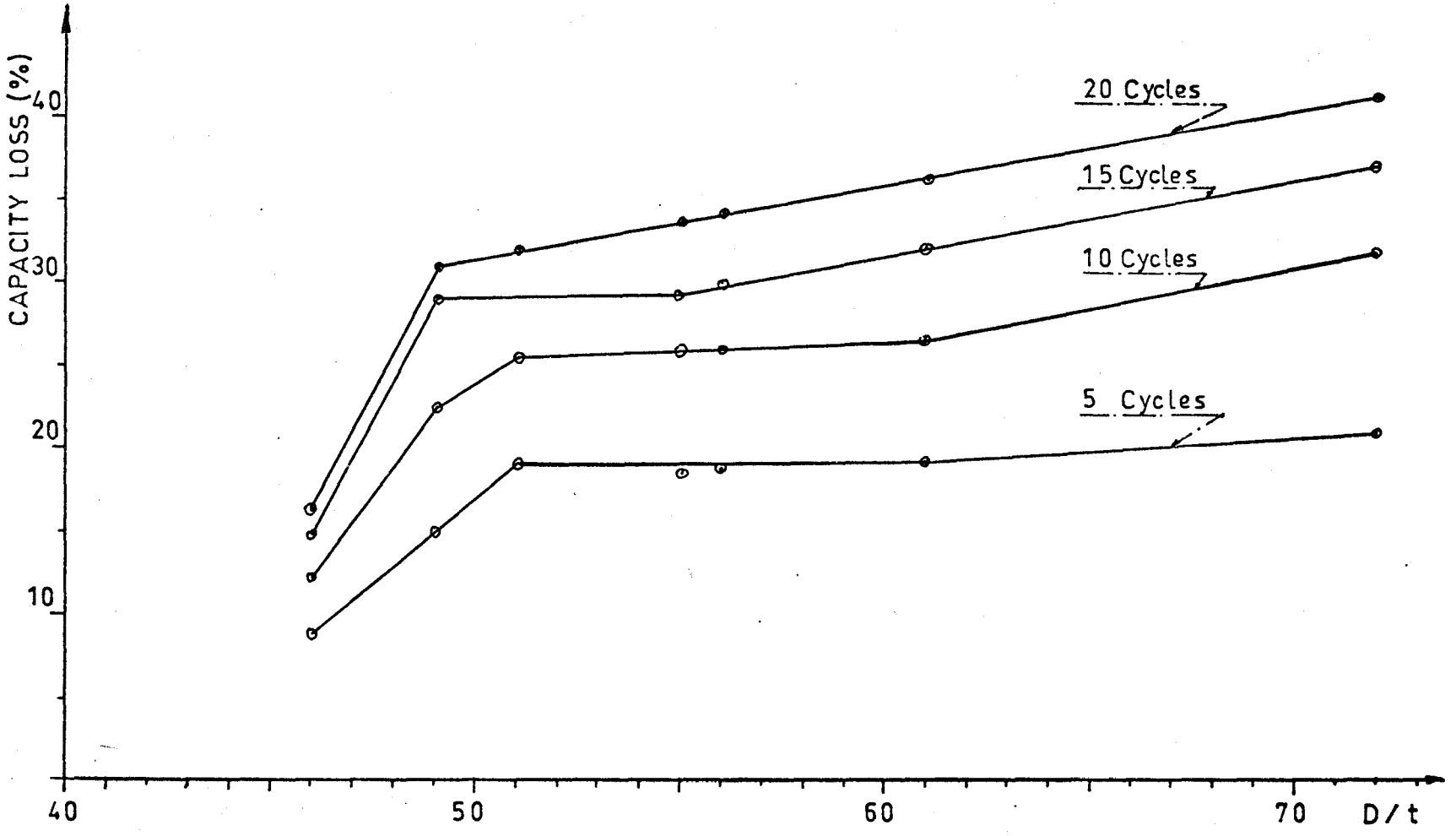

FIG. 3.4 CAPACITY LOSS Vs. D/T RATIO AFTER 5, 10, 15 & 20 CYCLES

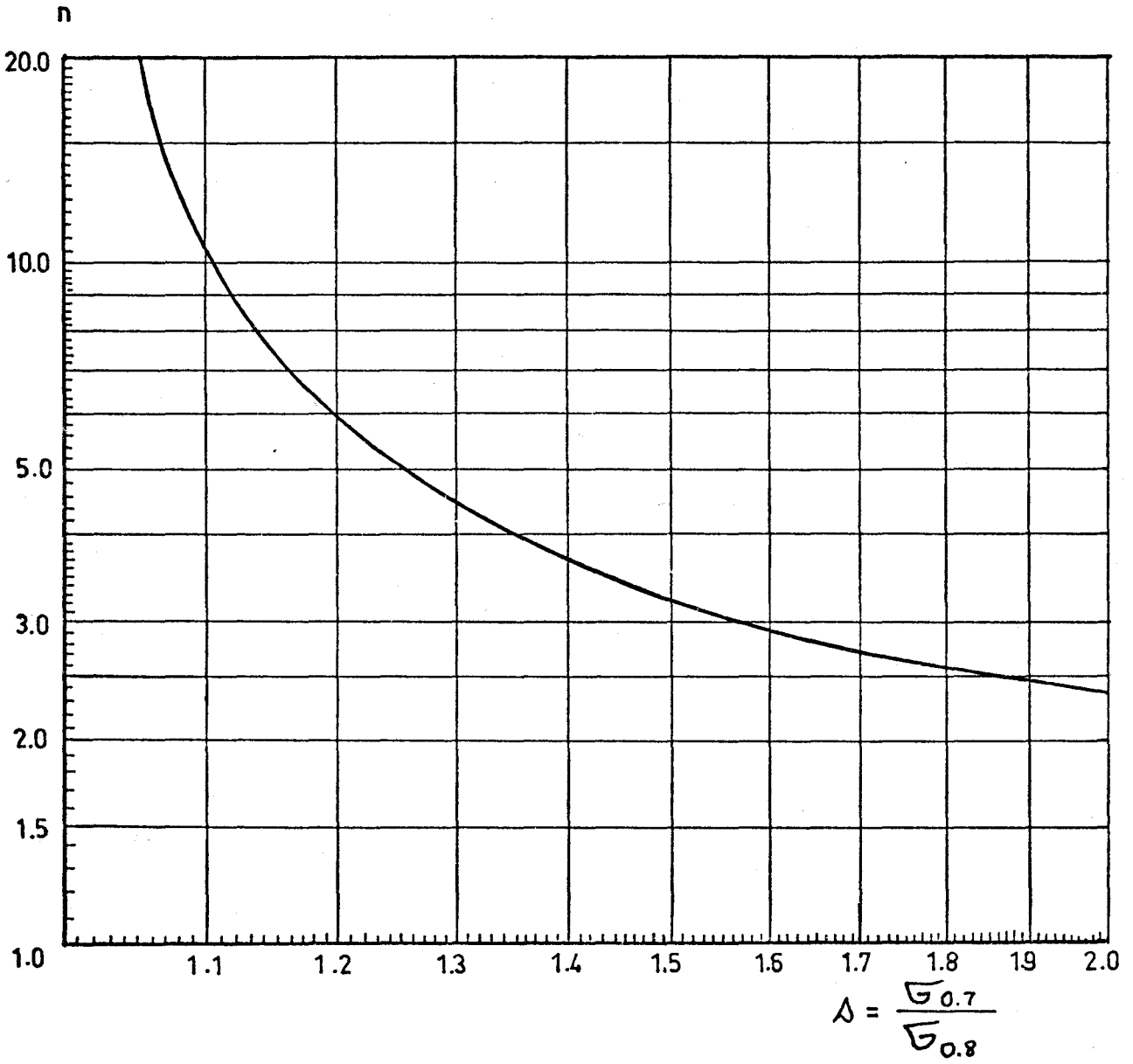

FIG. 3.5 RELATION BETWEEN "n" and "Δ"
NACA TECHNICAL NOTE № 902

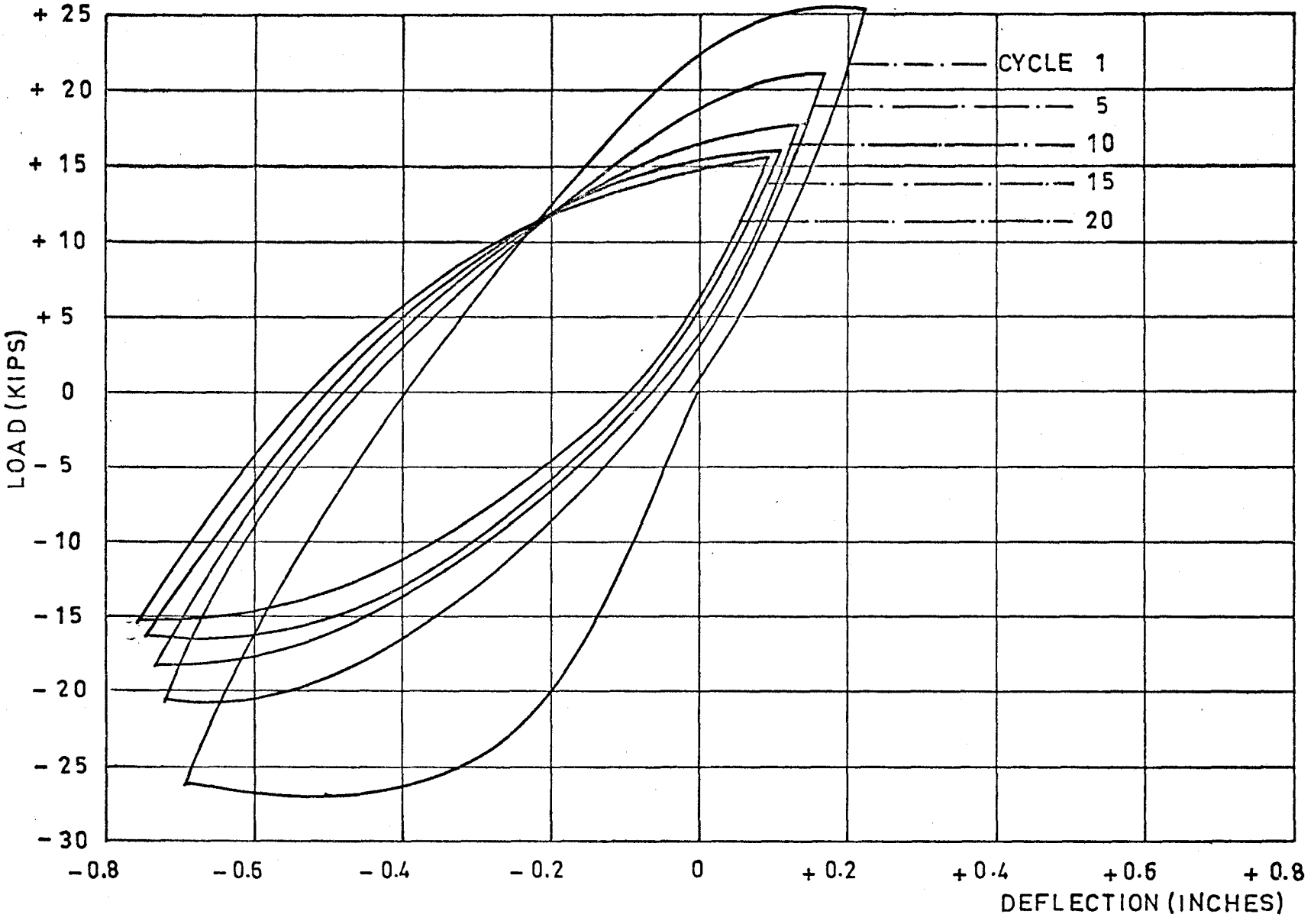

FIG. 3.6-a P_Δ LOOPS FOR T1

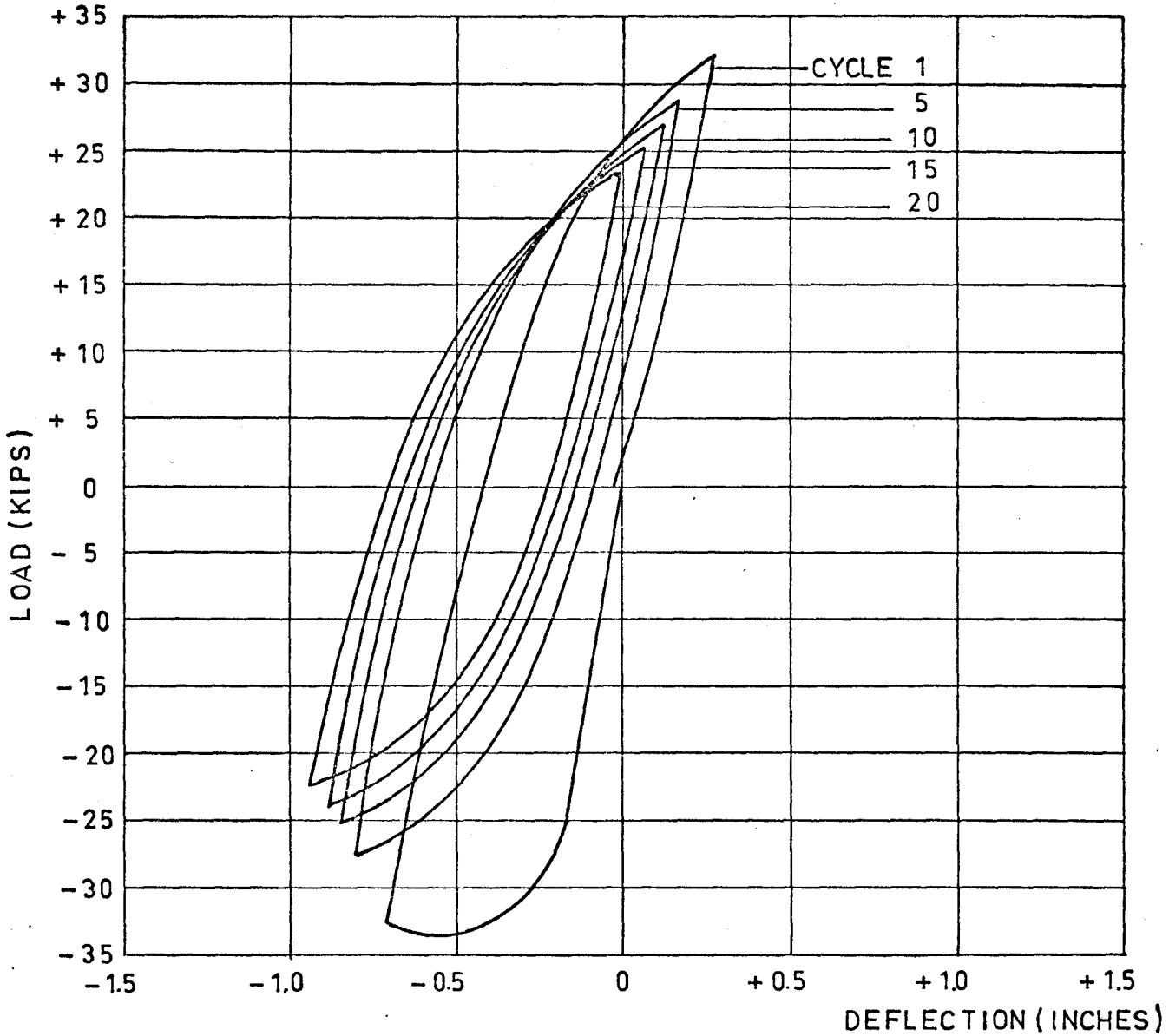

FIG. 3.6-b P_Δ LOOPS FOR T2

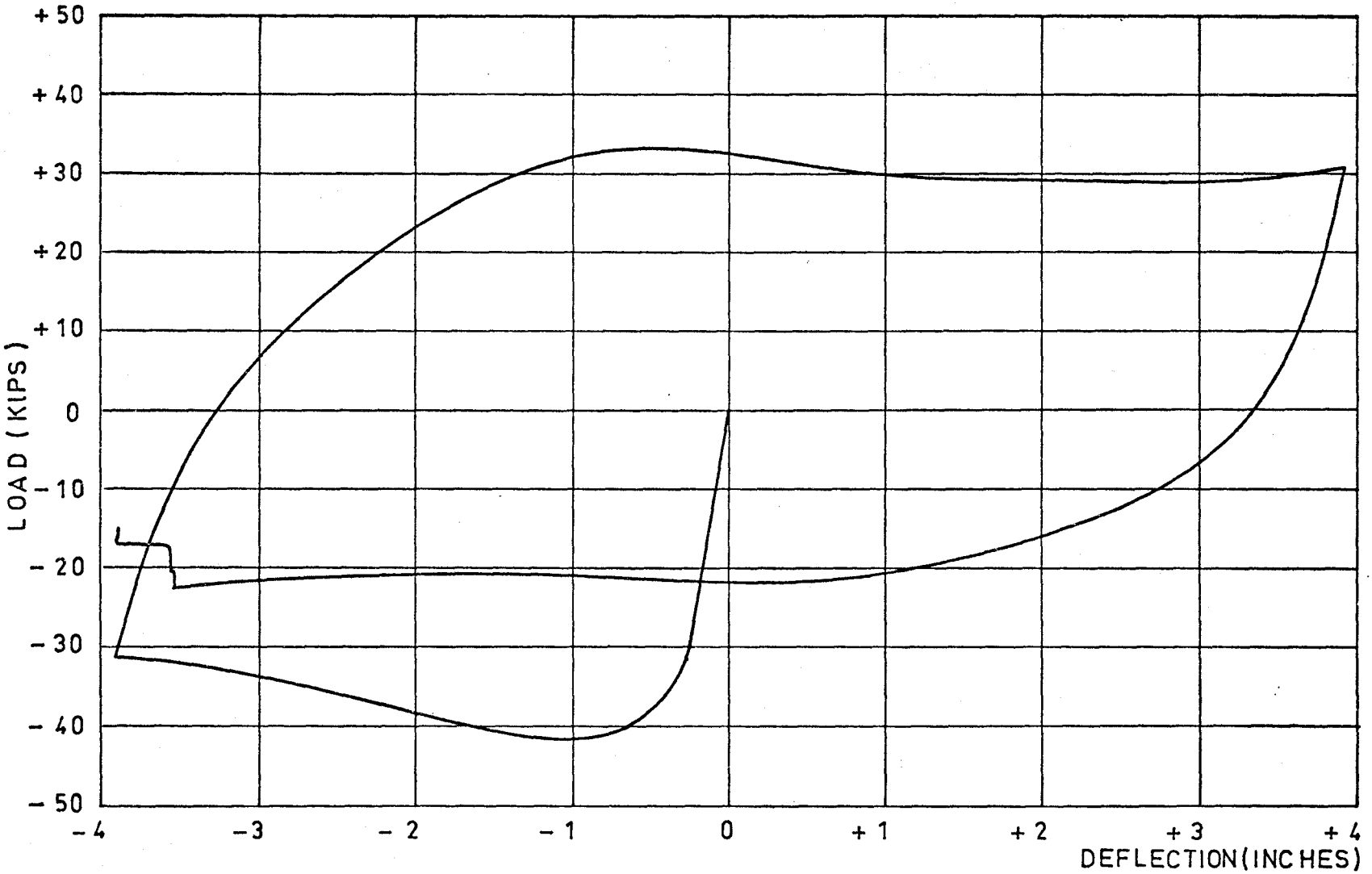

FIG. 3.6-c P_Δ LOOPS FOR T3 $\Delta = 17\,\Delta_p$

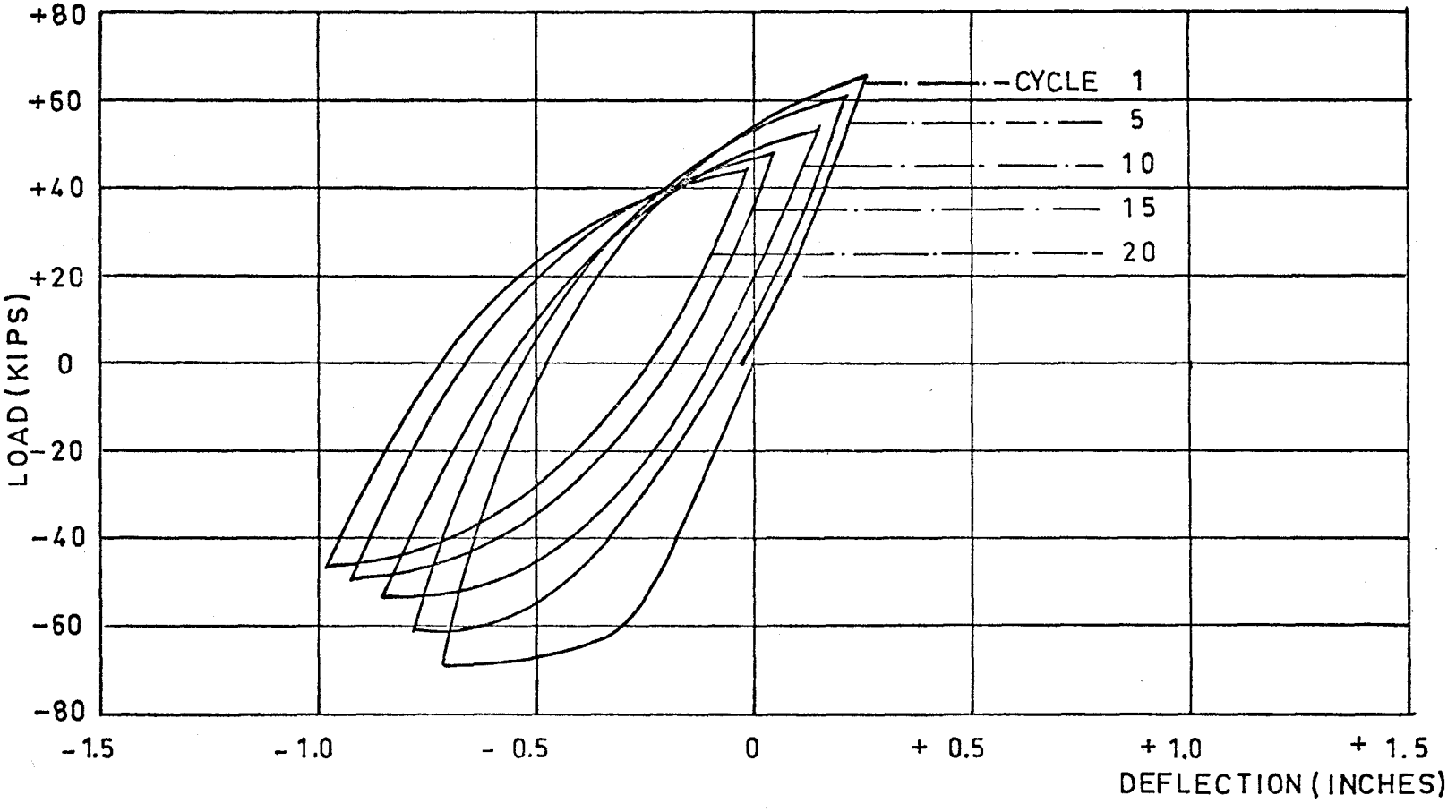

FIG. 3.6-d P_Δ LOOPS FOR T4

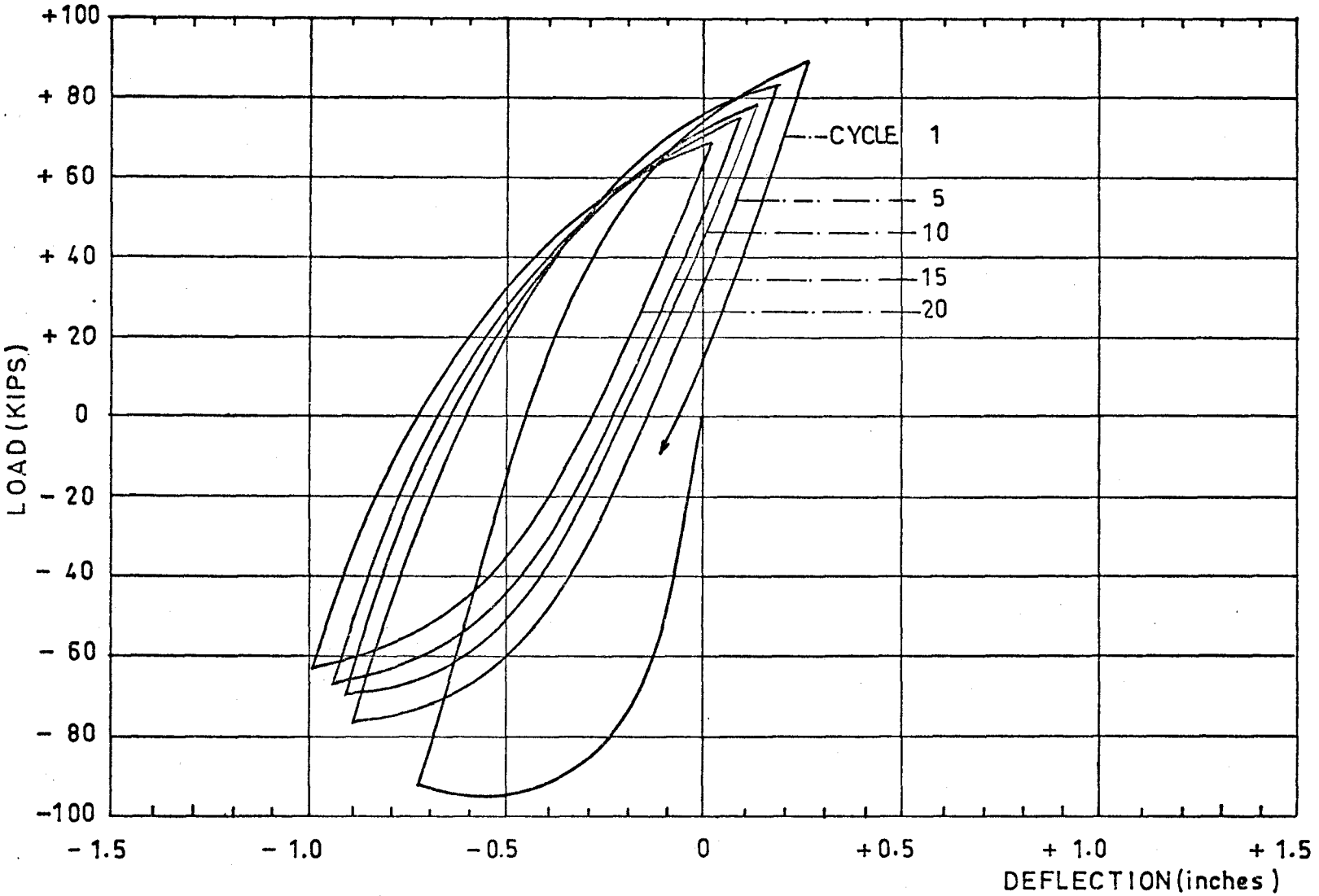

FIG. 3.6-e P-Δ LOOPS FOR T5

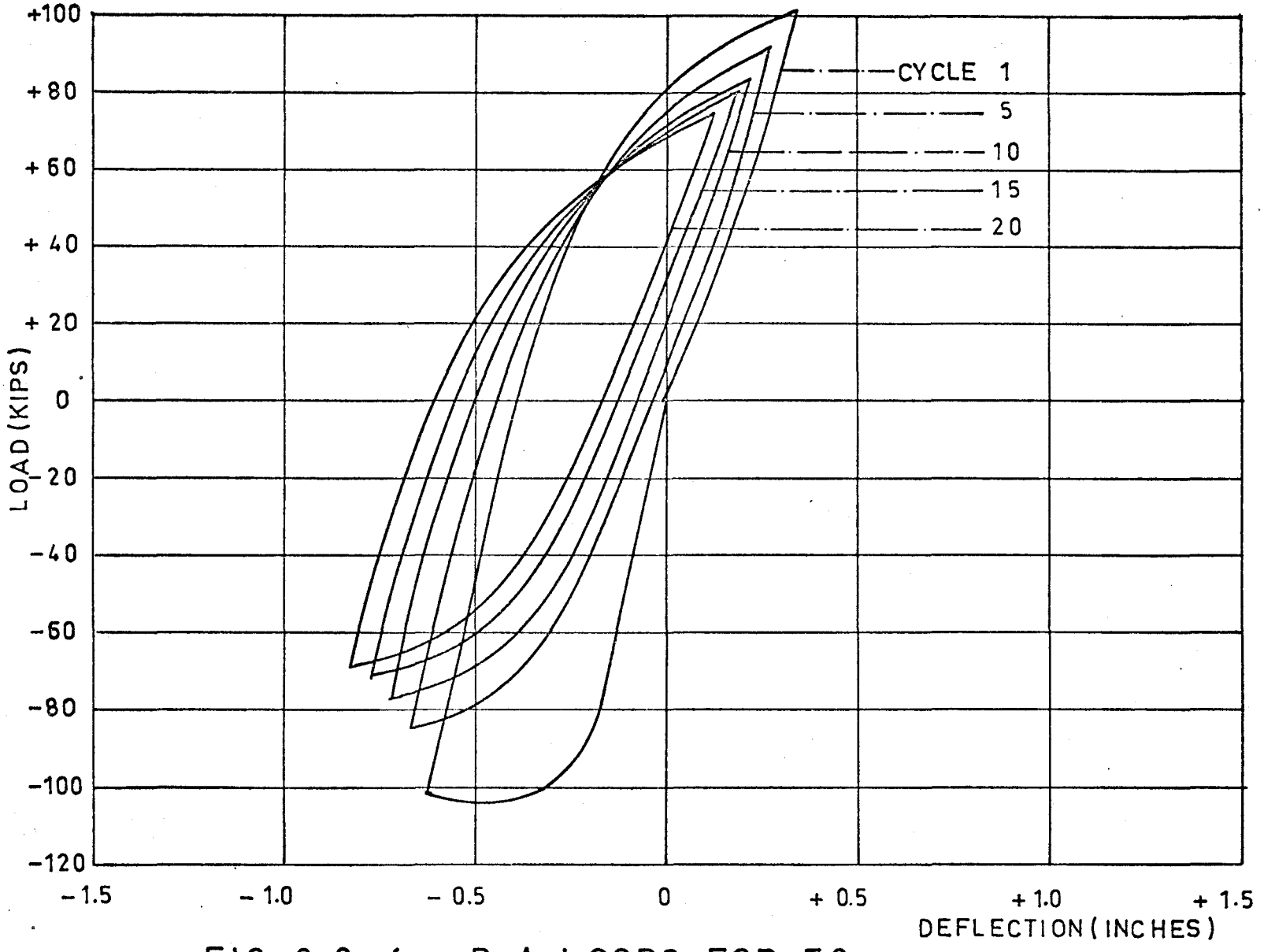

FIG. 3.6-f P_Δ LOOPS FOR T6

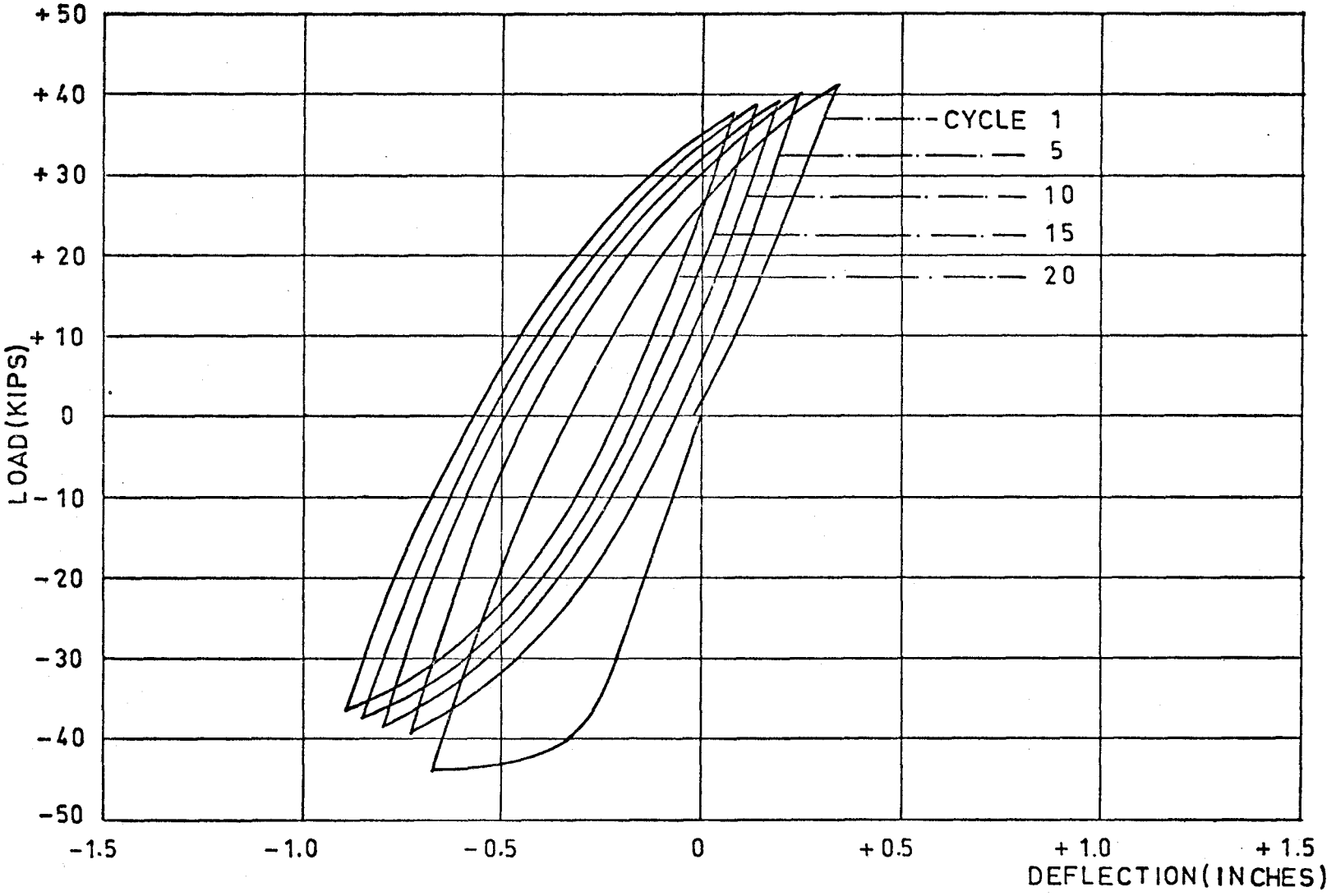

FIG. 3.6-g P_Δ LOOPS FOR T7 ($\Delta = 2.82\,\Delta_p$)

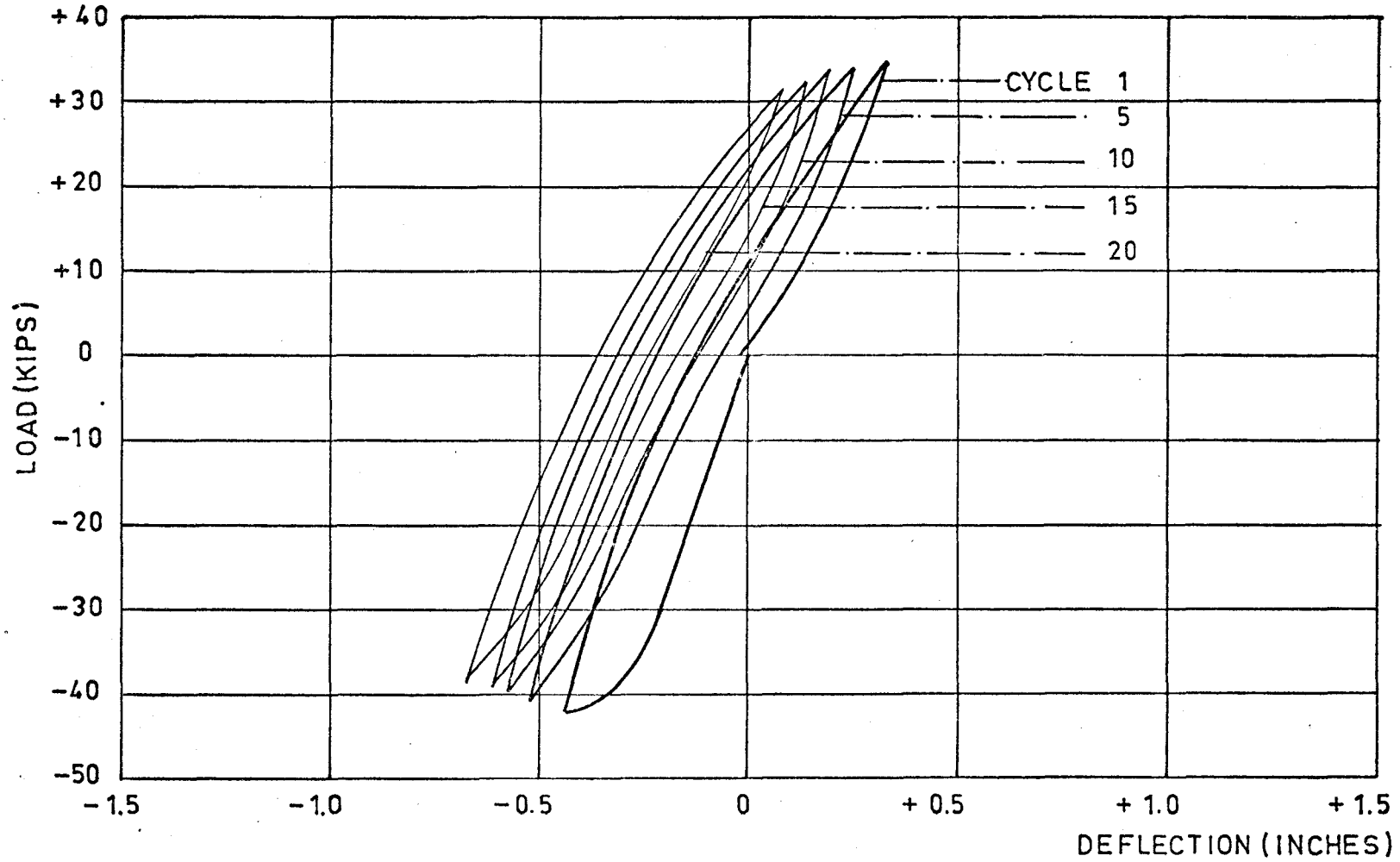

FIG. 3.6-h P_Δ LOOPS FOR T8 ($\Delta = 1.85\,\Delta_p$)

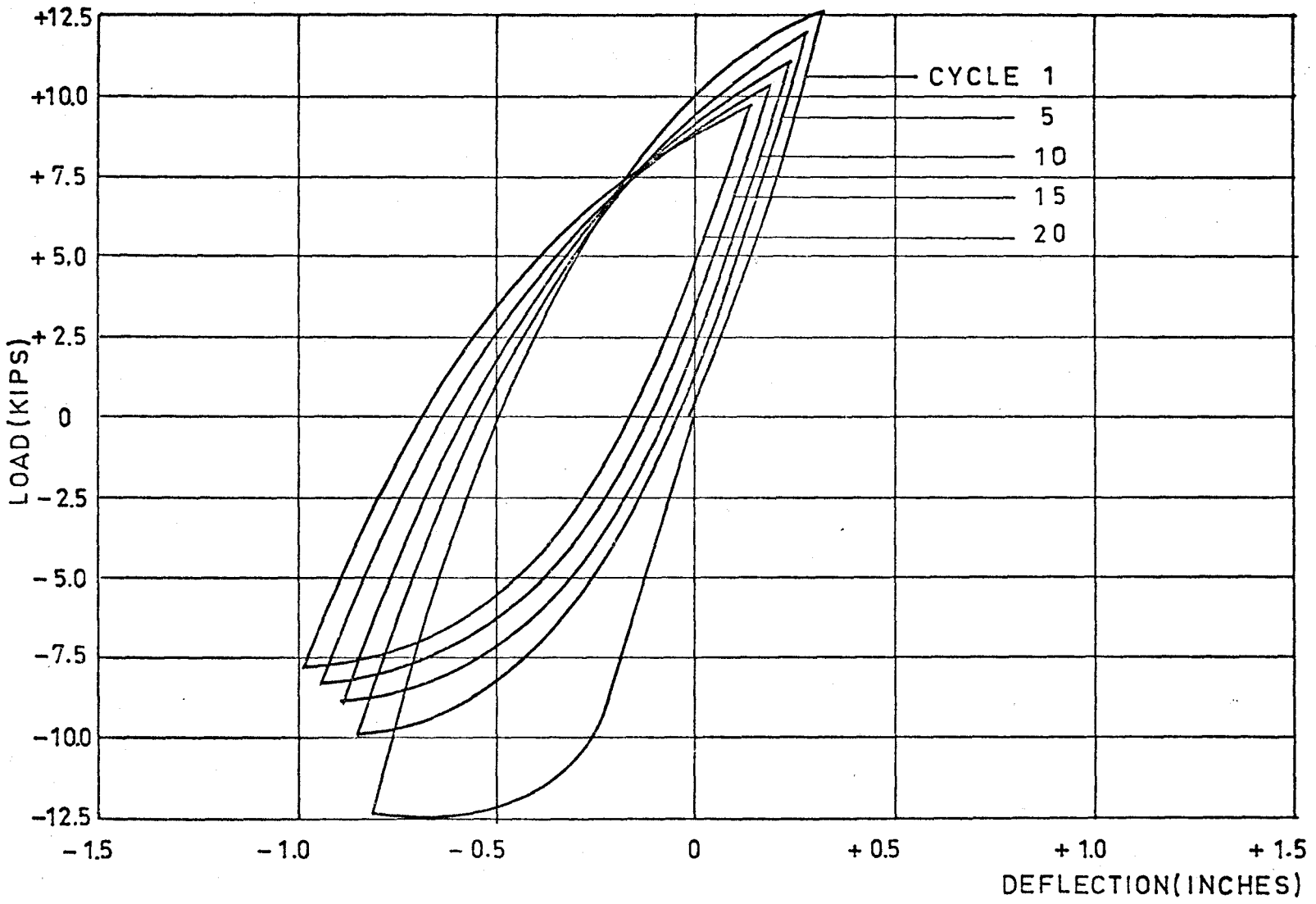

FIG. 3.6-i P_Δ LOOPS FOR T9

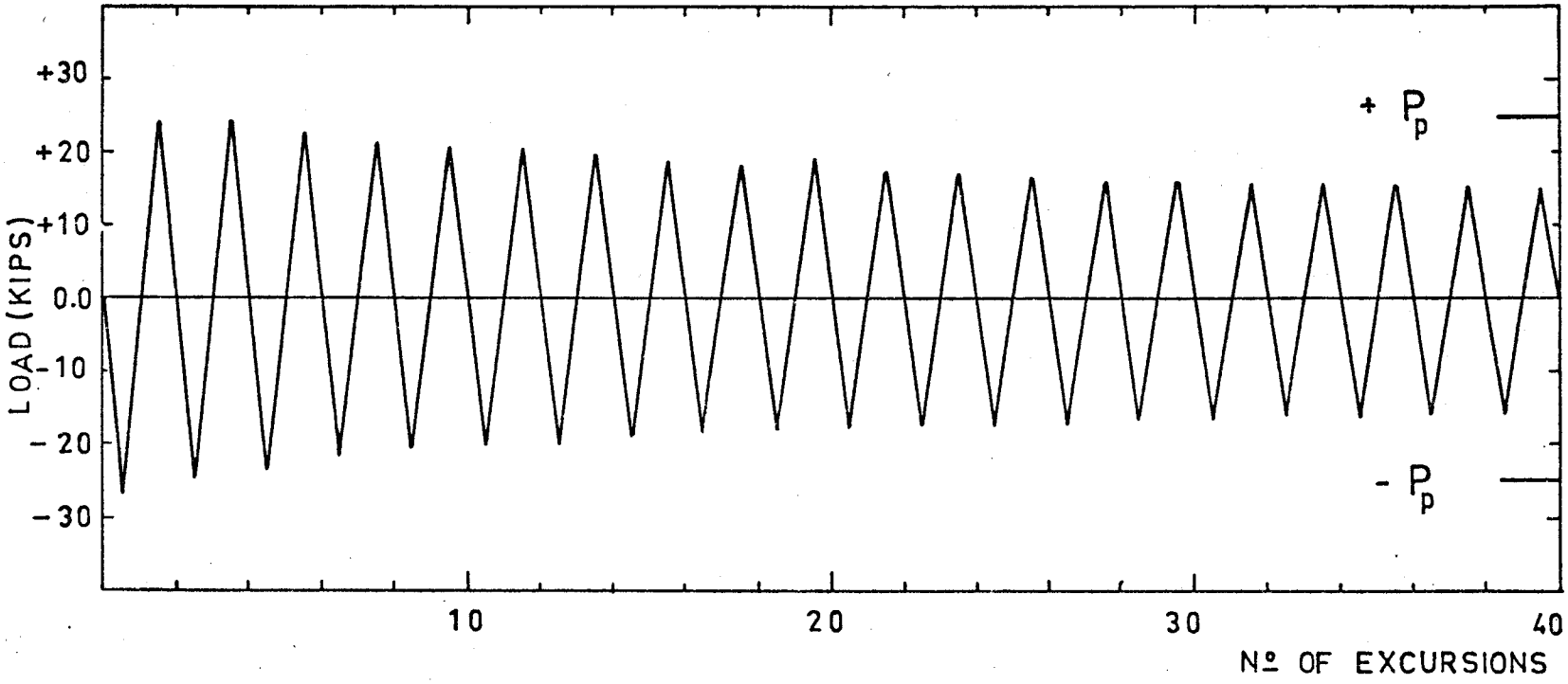

FIG. 3.7-a LOAD Vs. Nº OF EXCURSIONS FOR T1

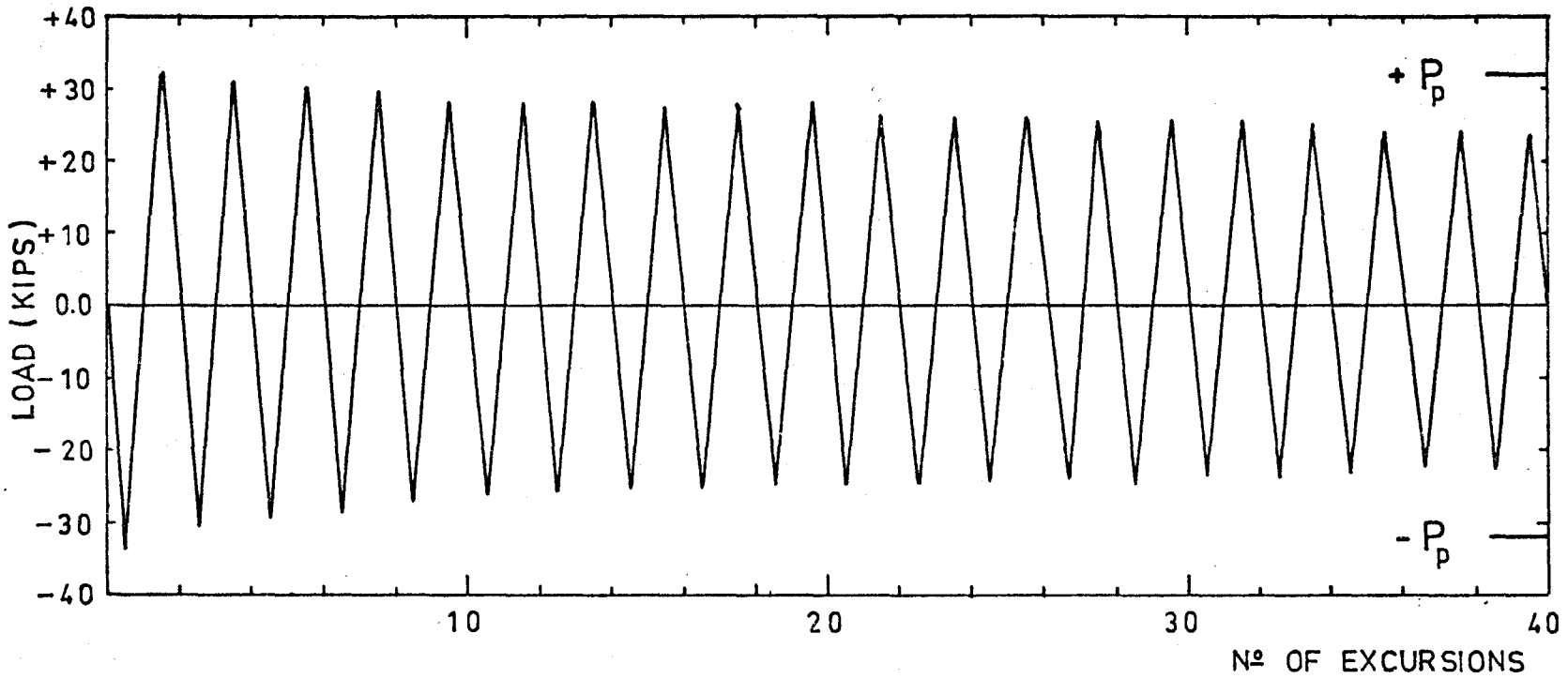

FIG. 3.7-b LOAD Vs. Nº OF EXCURSIONS FOR T2

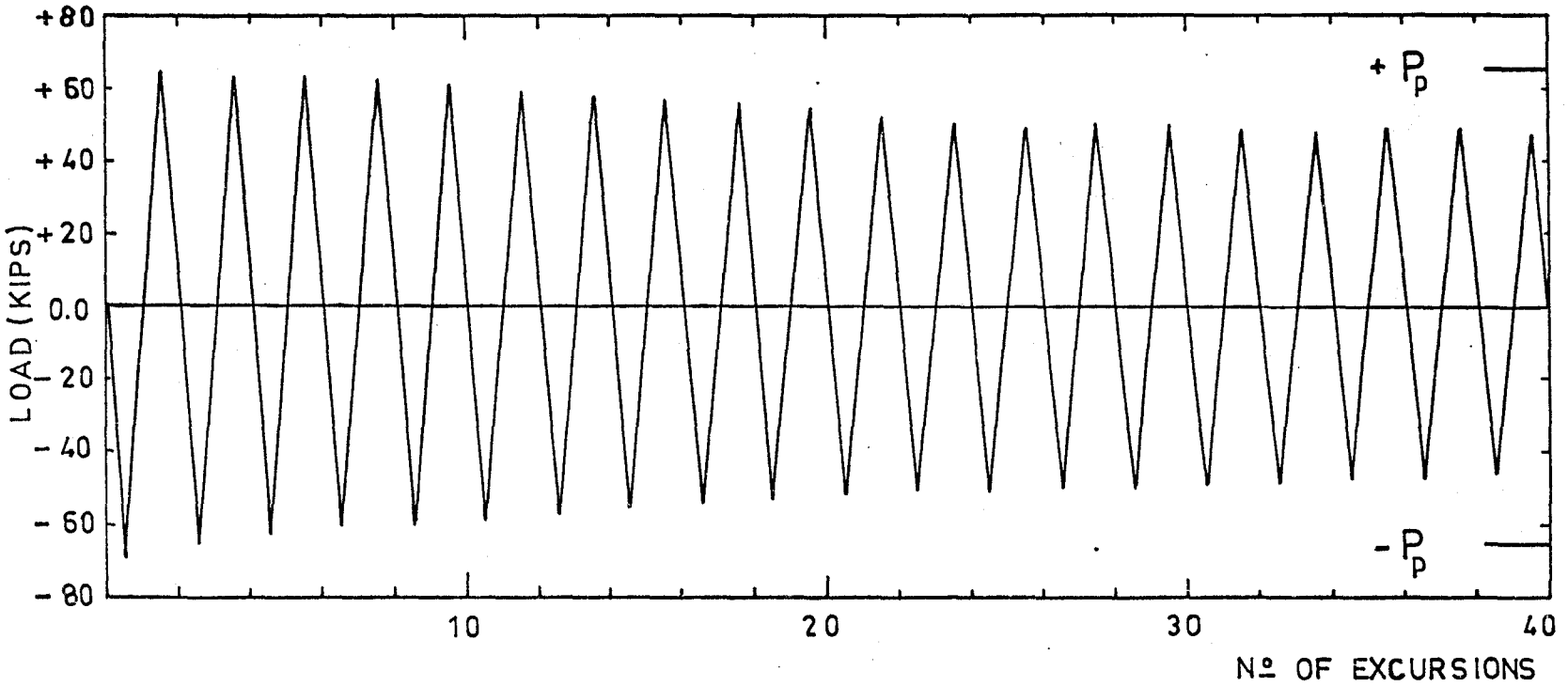

FIG. 3.7-c LOAD Vs. Nº OF EXCURSIONS FOR T4

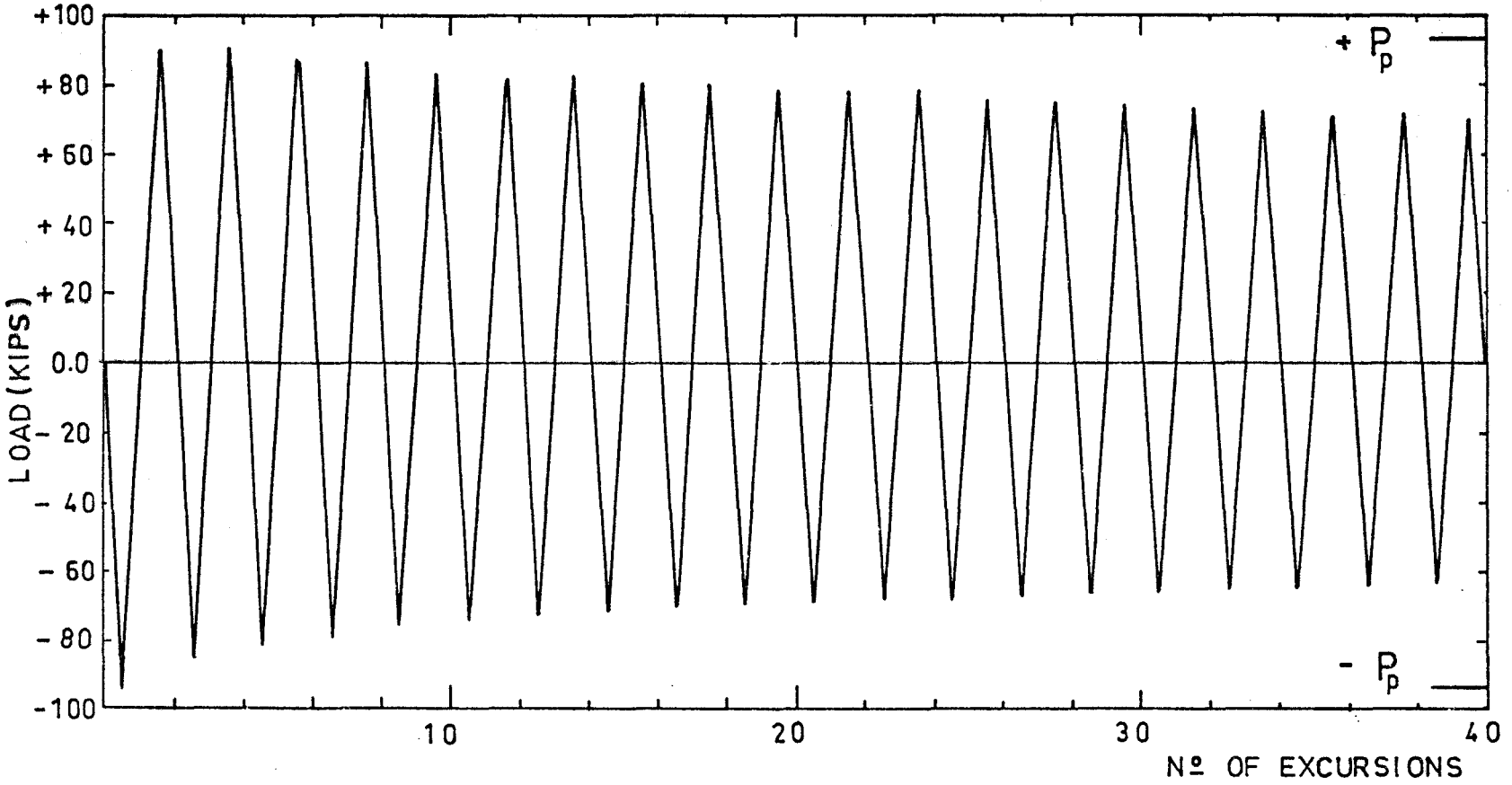

FIG. 3.7-d LOAD Vs. Nº OF EXCURSIONS FOR T 5

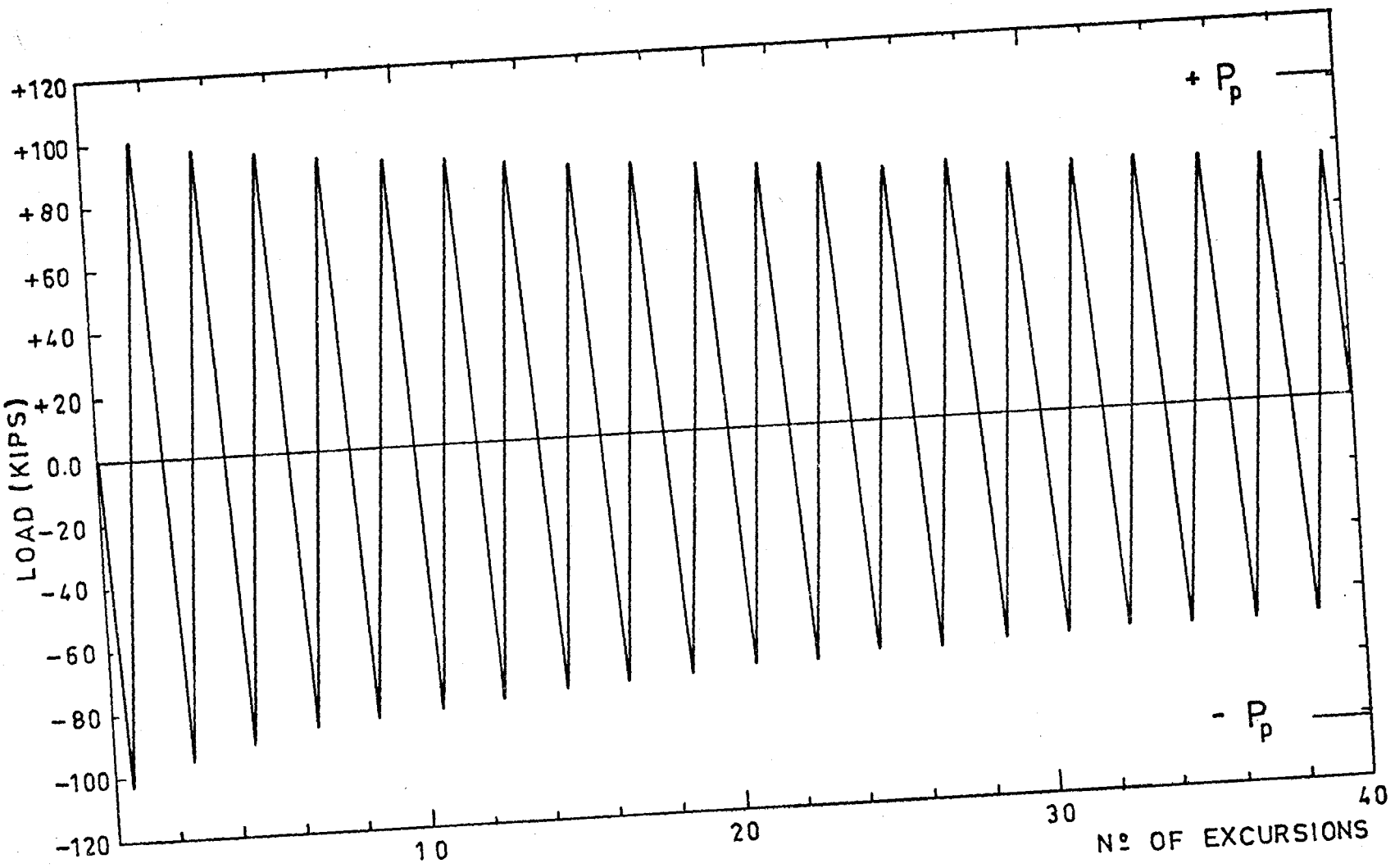

FIG. 3.7 - e LOAD Vs. Nº OF EXCURSIONS FOR T 6

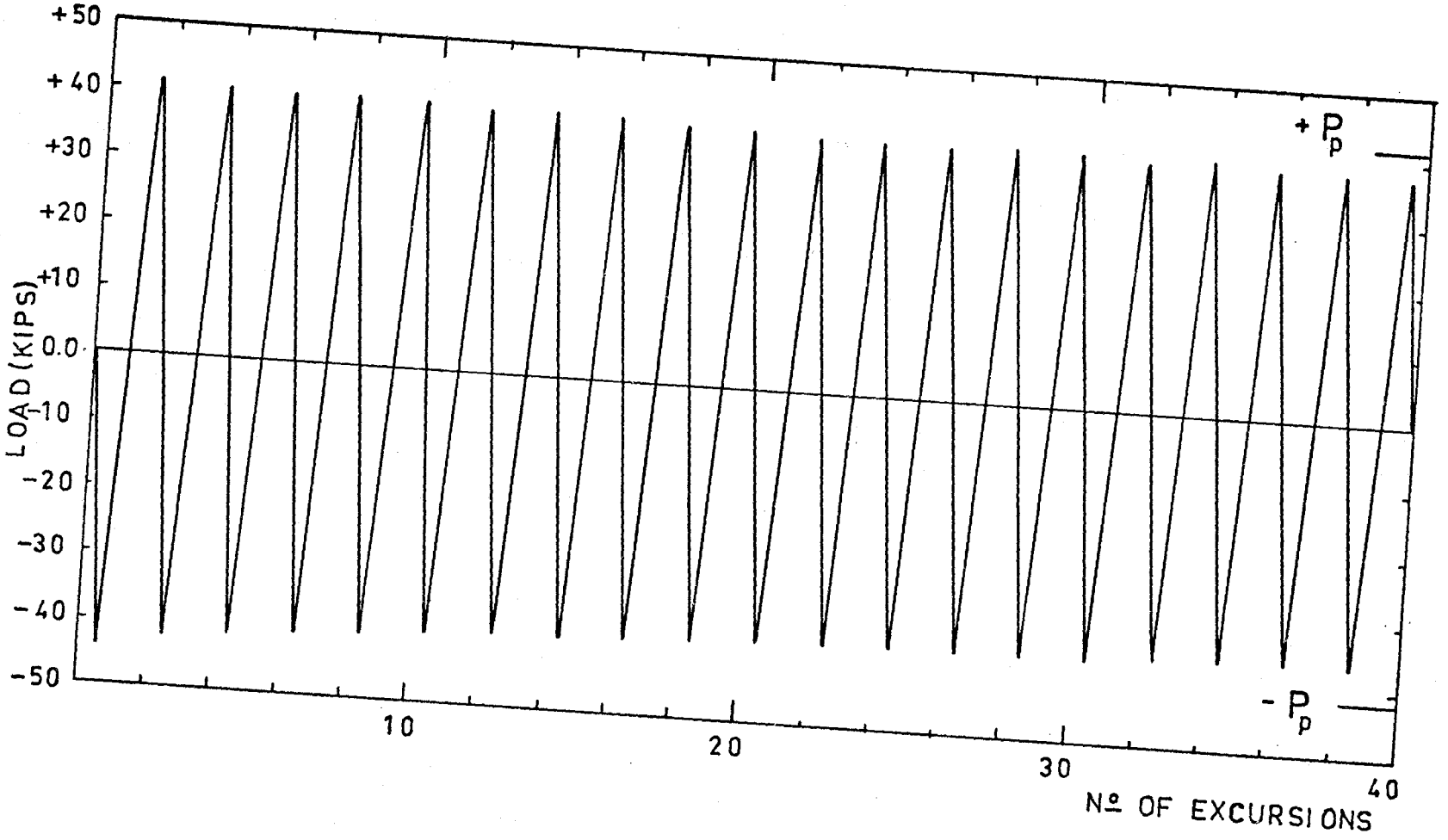

FIG. 3.7-f LOAD Vs. Nº OF EXCURSIONS FOR T7

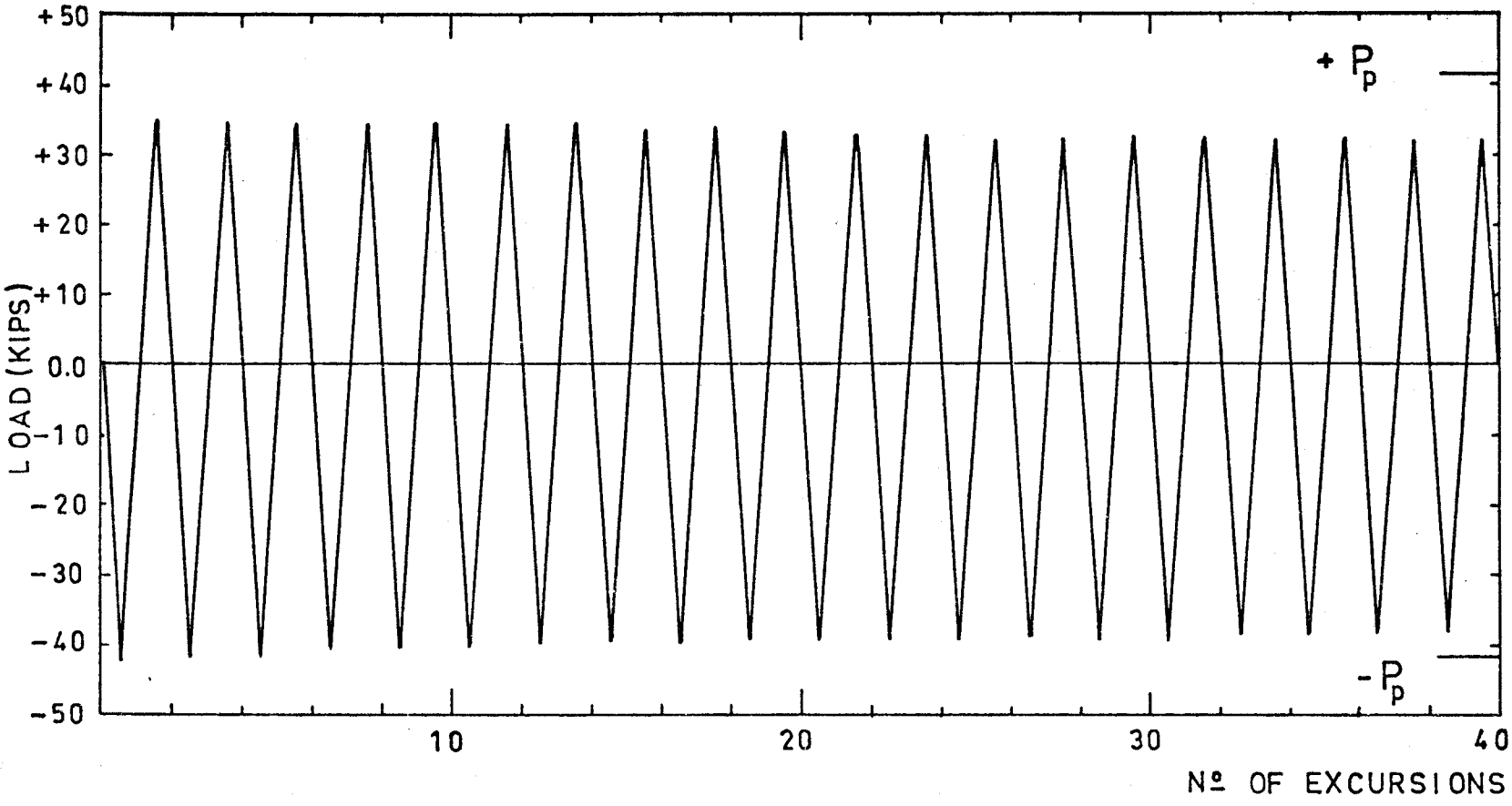

FIG. 3.7-g LOAD Vs. Nº OF EXCURSIONS FOR T 8

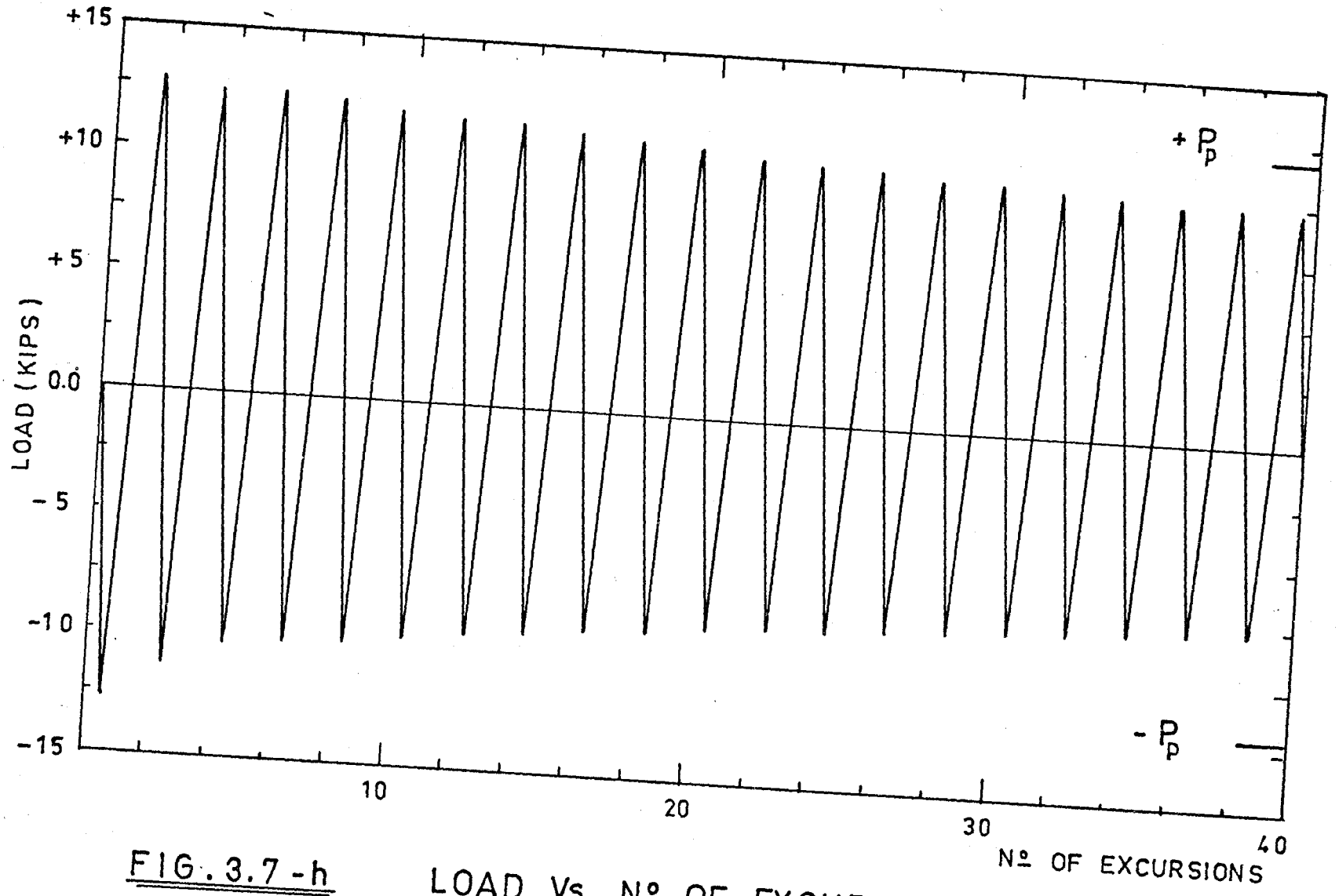

FIG. 3.7-h LOAD Vs. Nº OF EXCURSIONS FOR T9

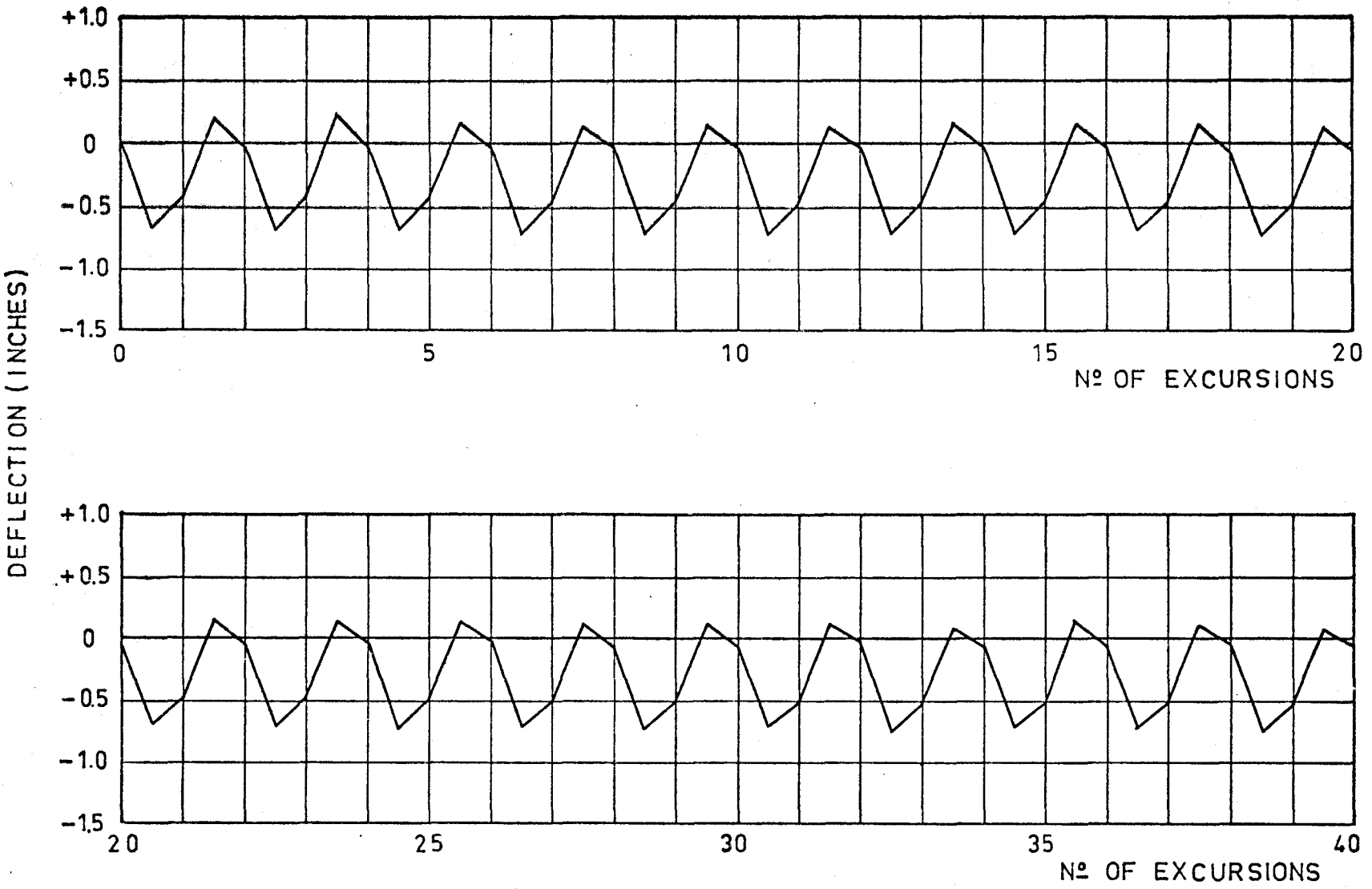

FIG. 3.8-a DEFLECTION Vs. Nº of EXCURSIONS FOR T1

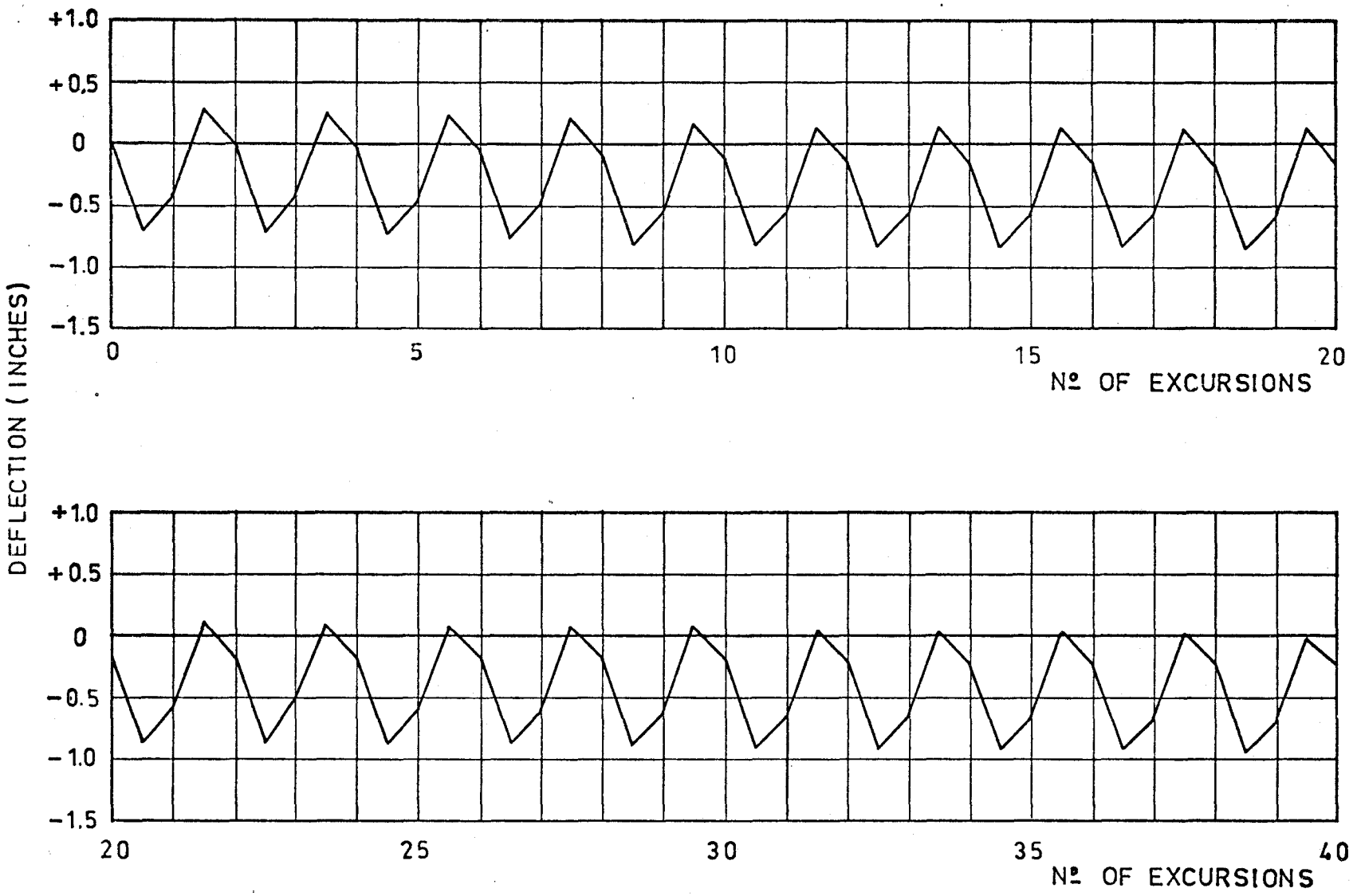

FIG. 3.8-b DEFLECTION Vs. Nº of EXCURSIONS FOR T2

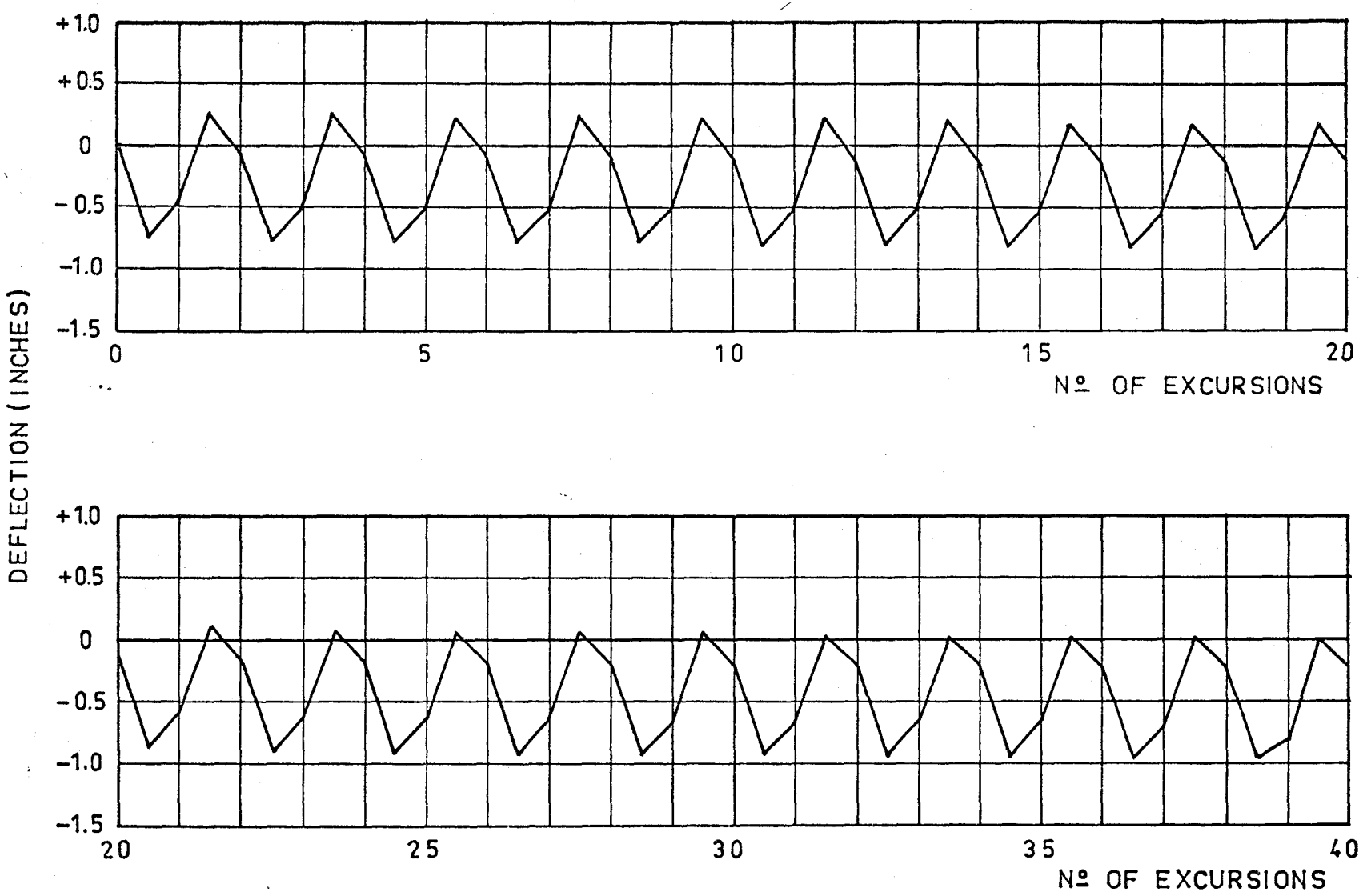

FIG. 3.8-c DEFLECTION Vs. Nº of EXCURSIONS FOR T4

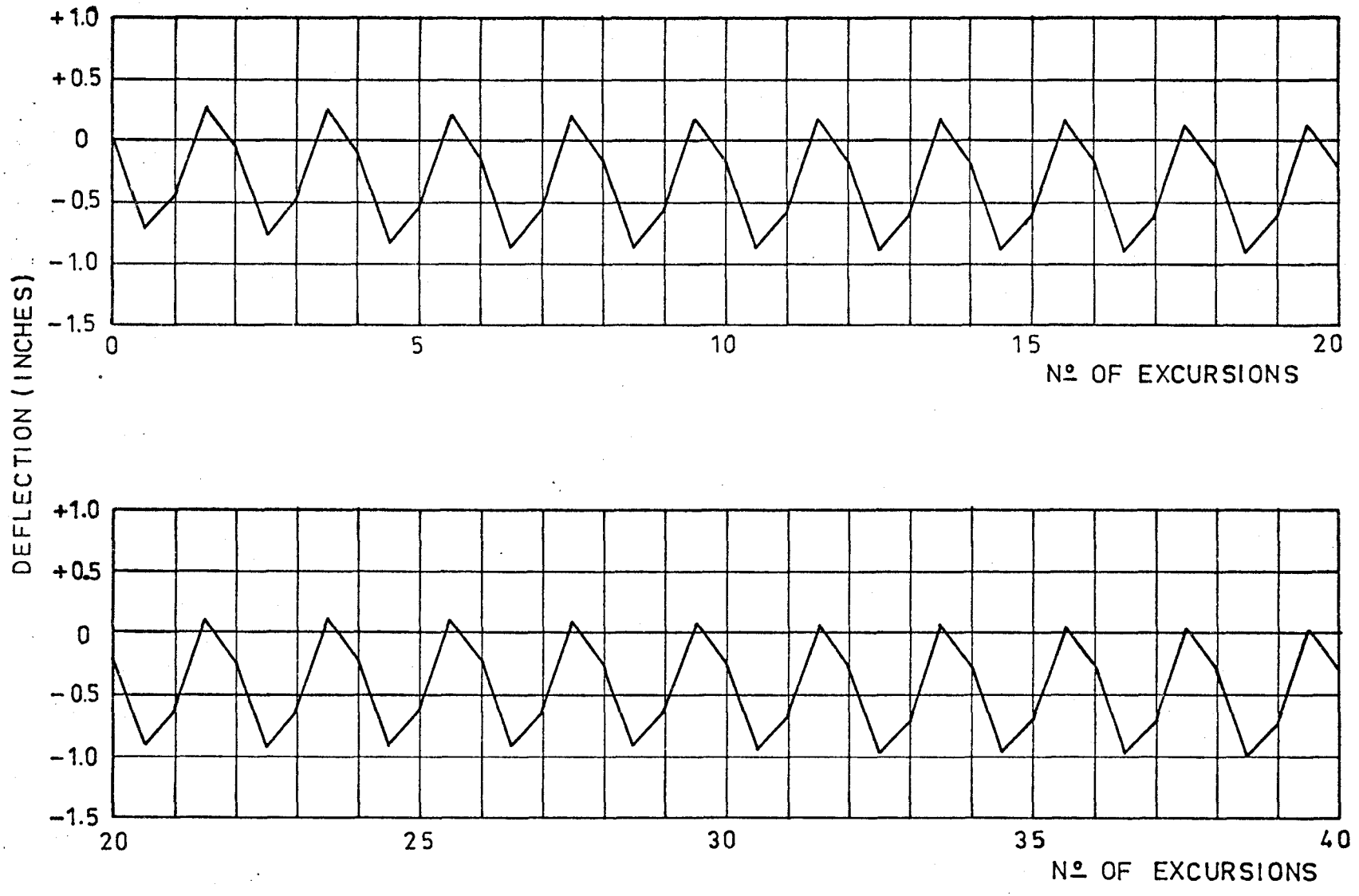

FIG. 3.8-d DEFLECTION Vs. Nº of EXCURSIONS FOR T5

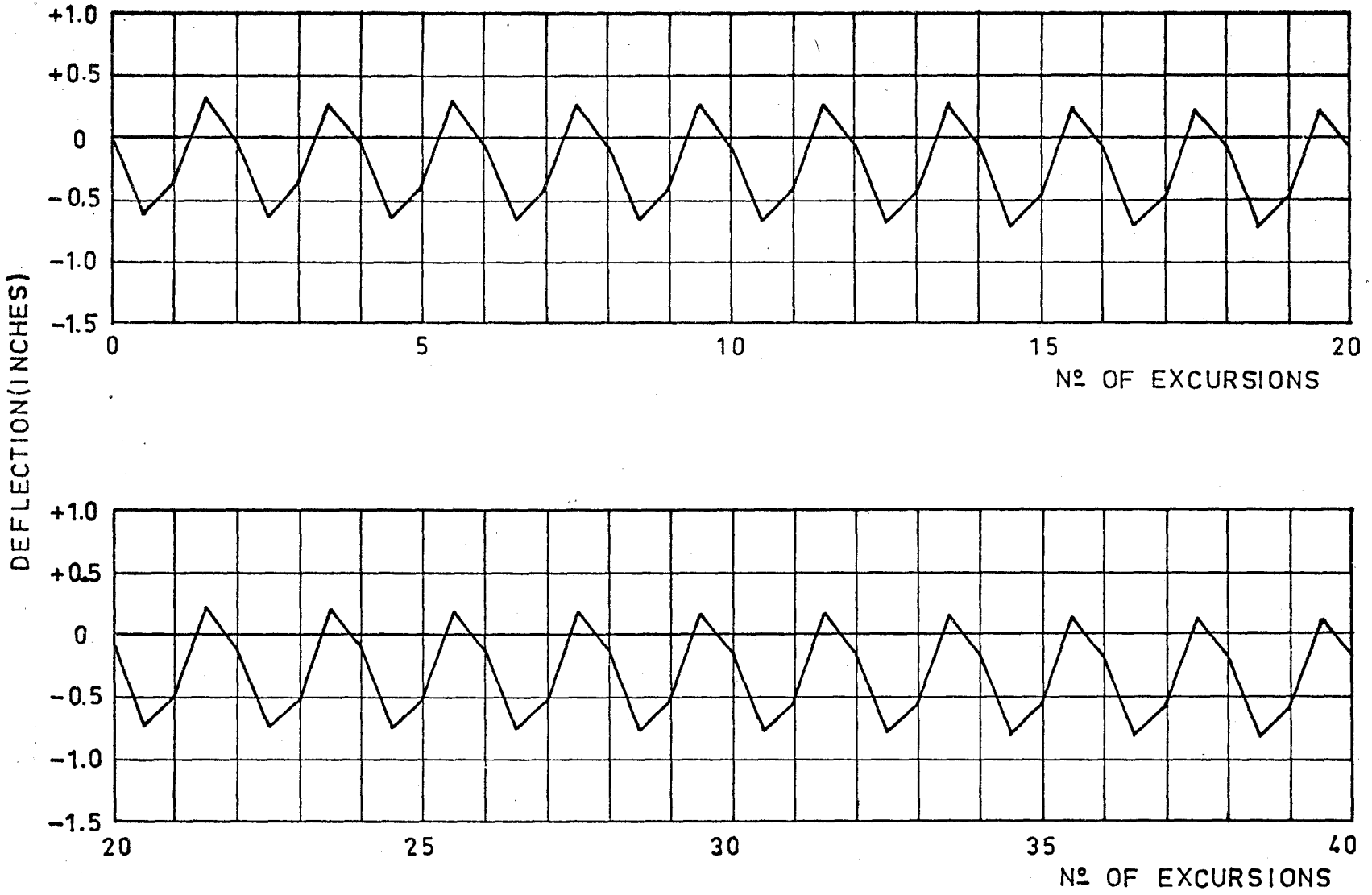

FIG. 3.8-e DEFLECTION Vs. Nº of EXCURSIONS FOR T6

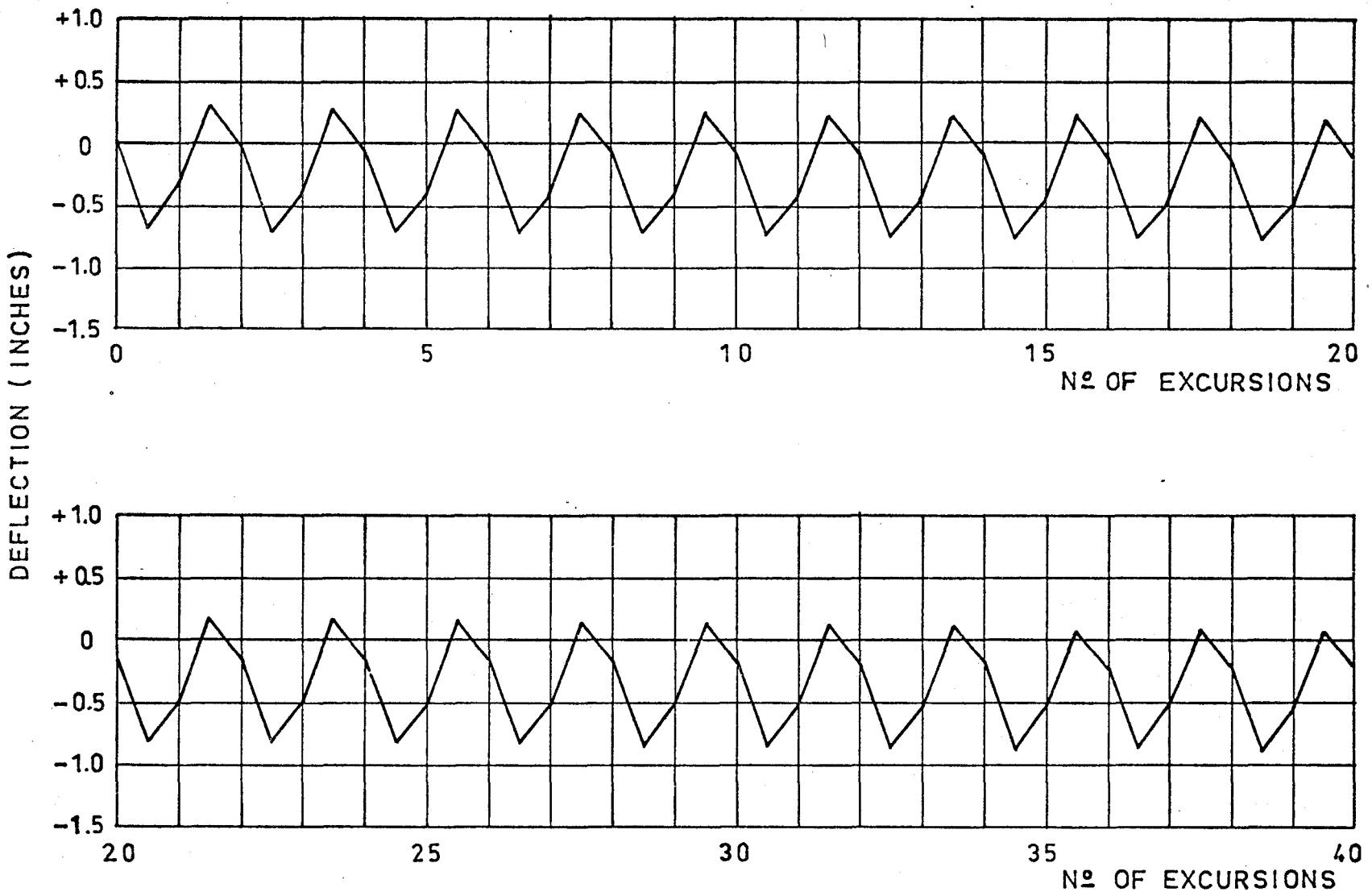

FIG.3.8-f DEFLECTION Vs. Nº of EXCURSIONS FOR T7

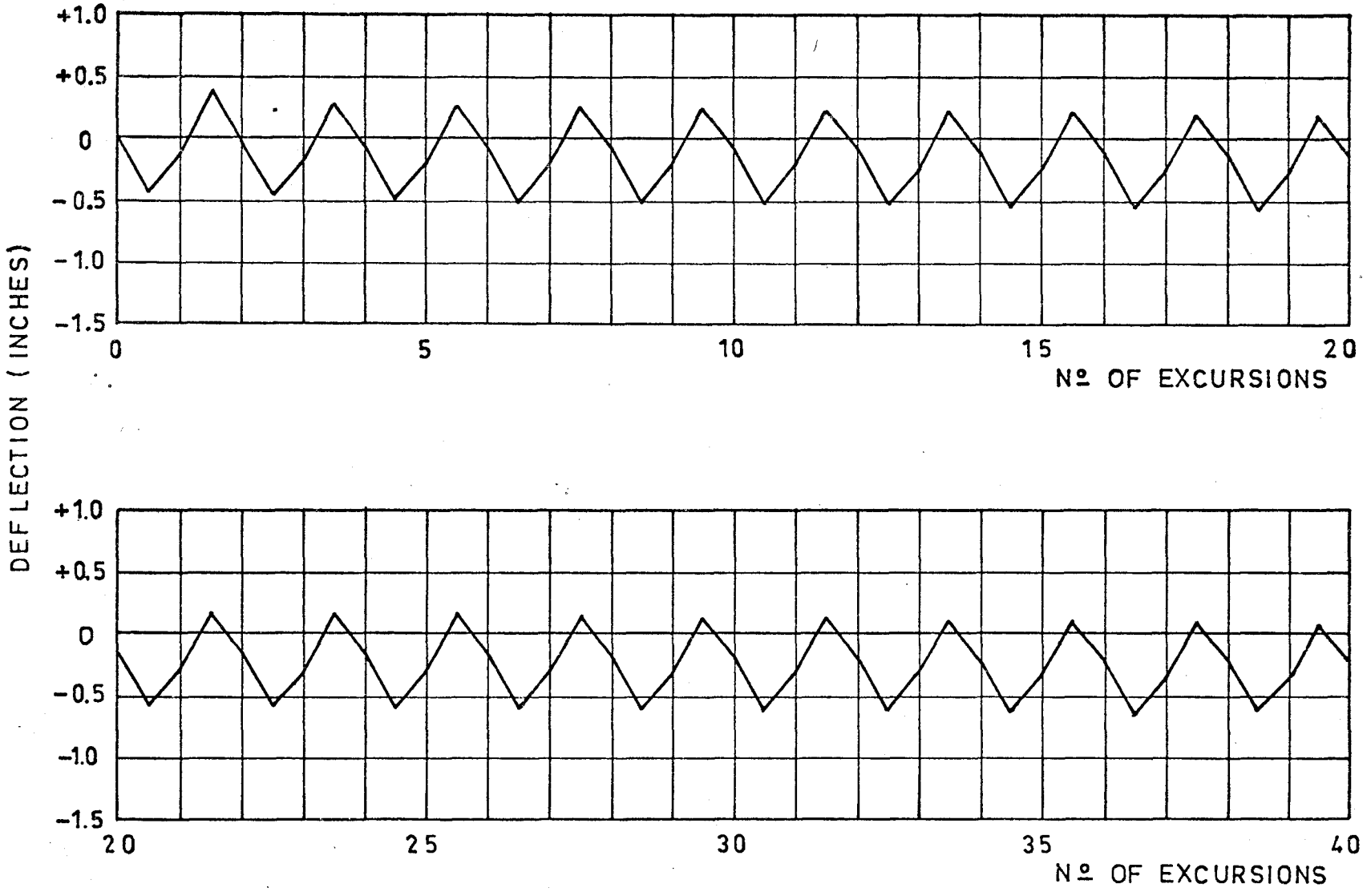

FIG. 3.8-g DEFLECTION Vs. Nº of EXCURSIONS FOR T 8

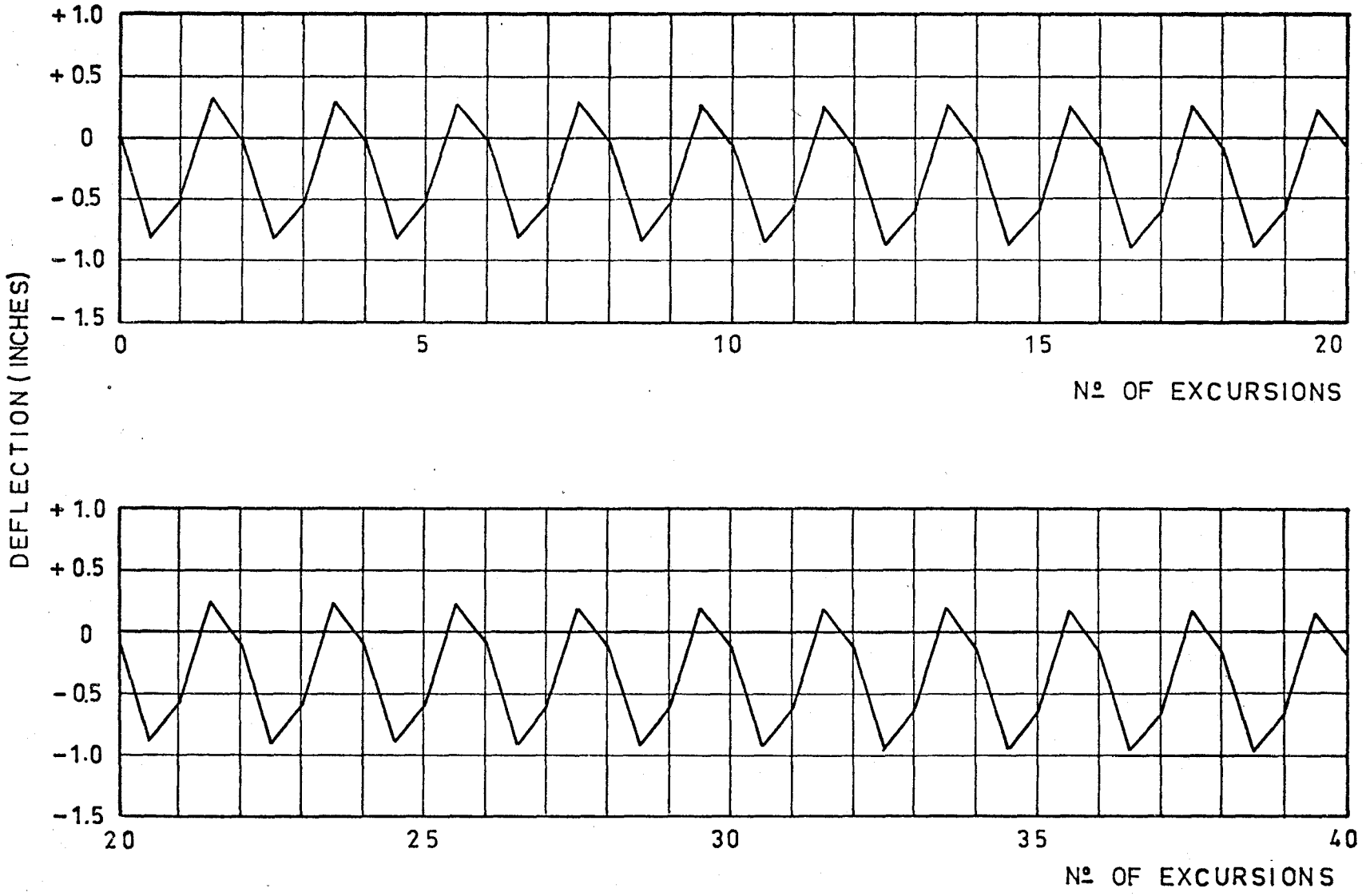

FIG. 3.8-h DEFLECTION Vs. Nº of EXCURSIONS FOR T9

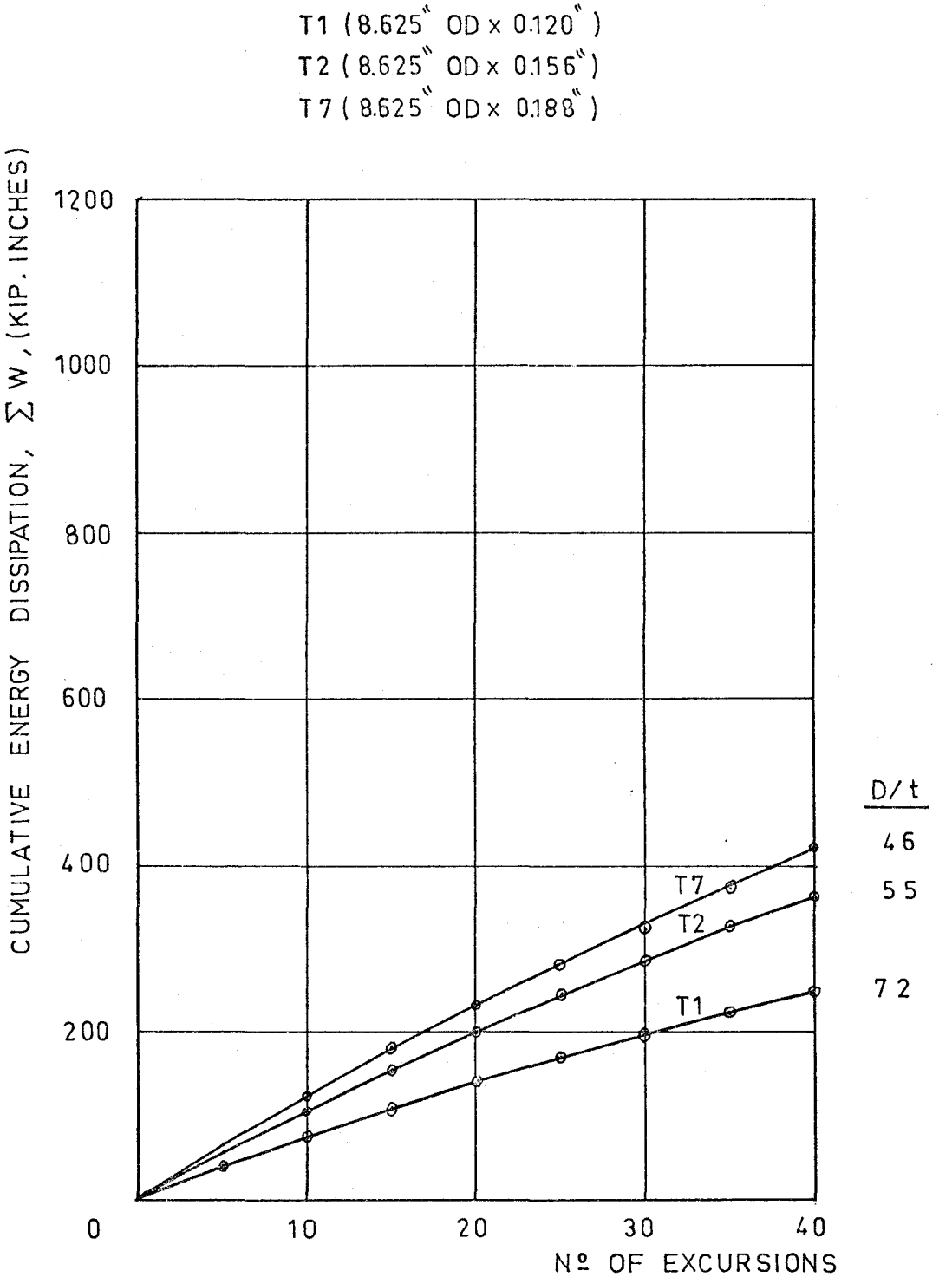

FIG.3.9-a ΣW Vs. Nº of EXCURSIONS

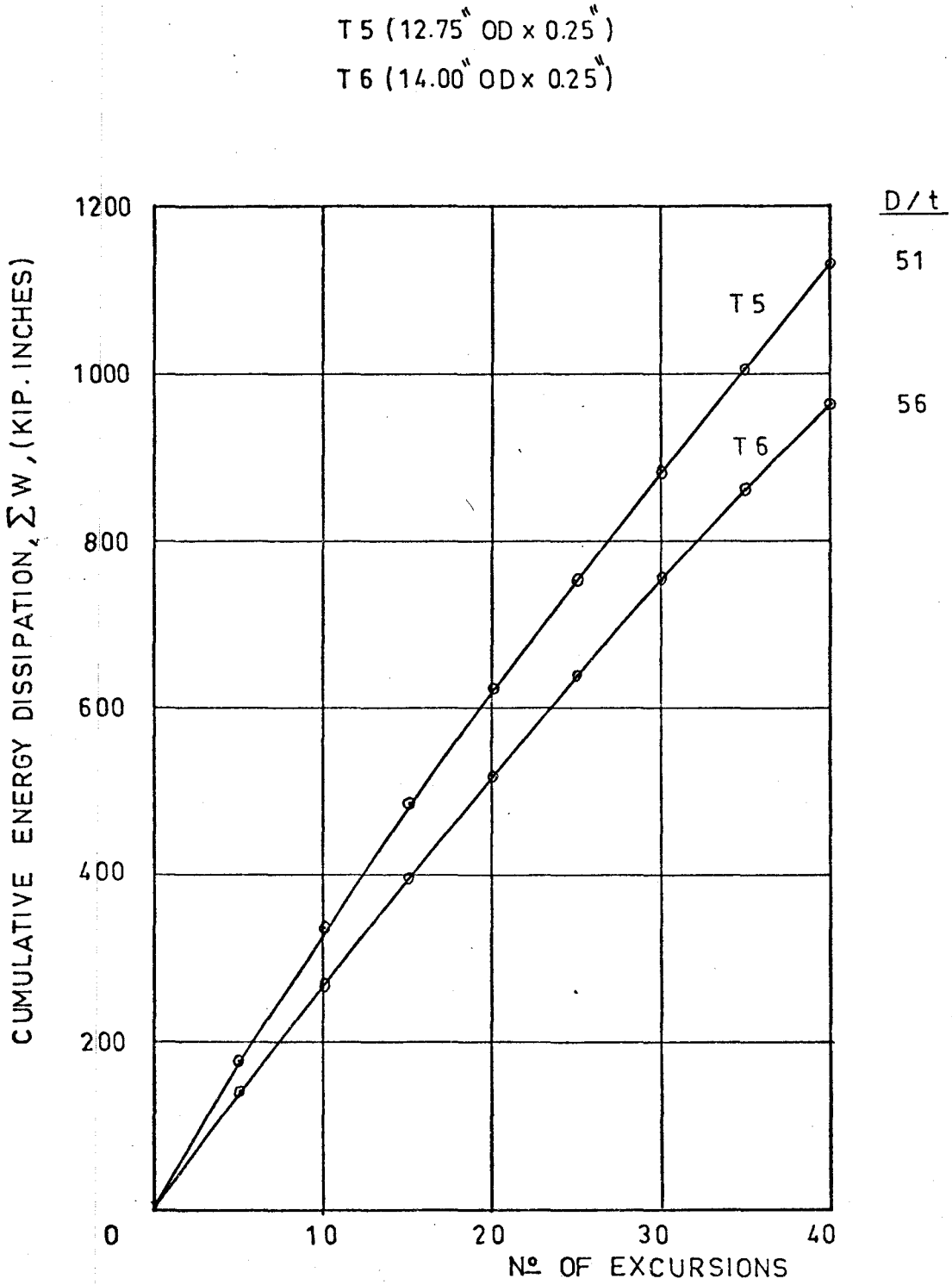

FIG.3.9-b ΣW Vs. № of EXCURSIONS

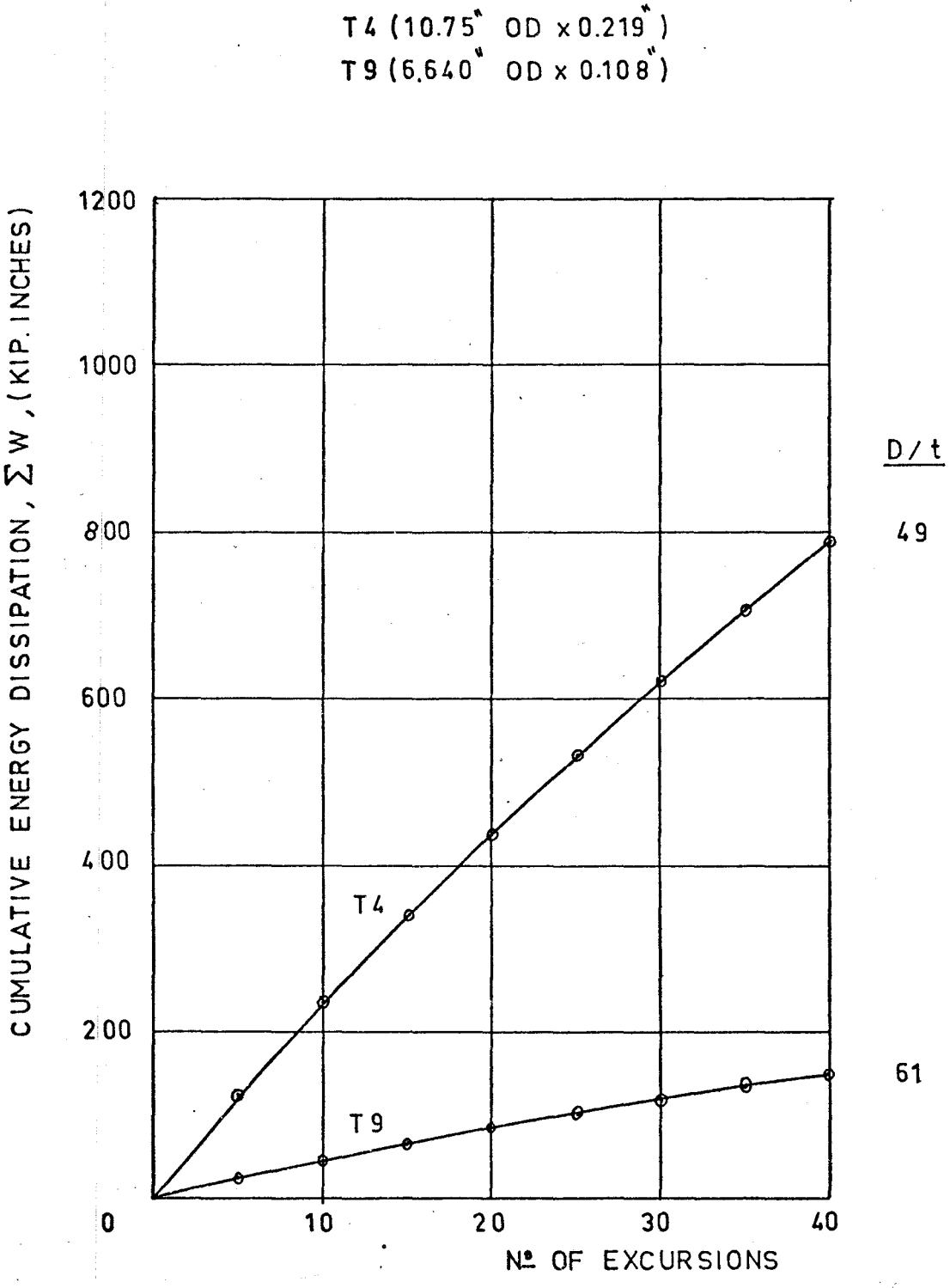

FIG. 3.9-c ΣW Vs. Nº of EXCURSIONS

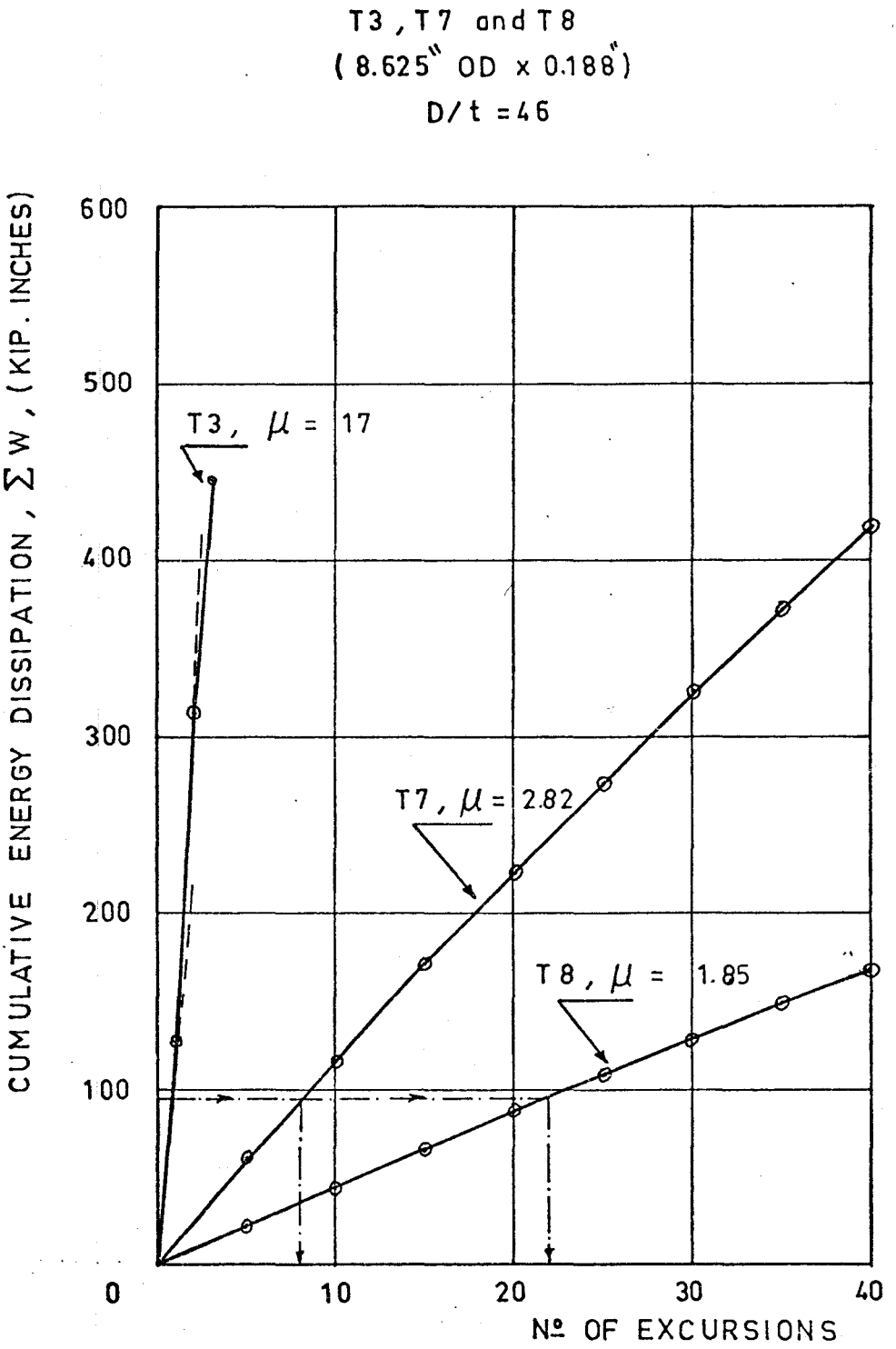

FIG. 3.9-d ΣW Vs. Nº of EXCURSIONS

FIG.3.10 ENERGY DISSIPATION on BASIS of 20 CYCLES

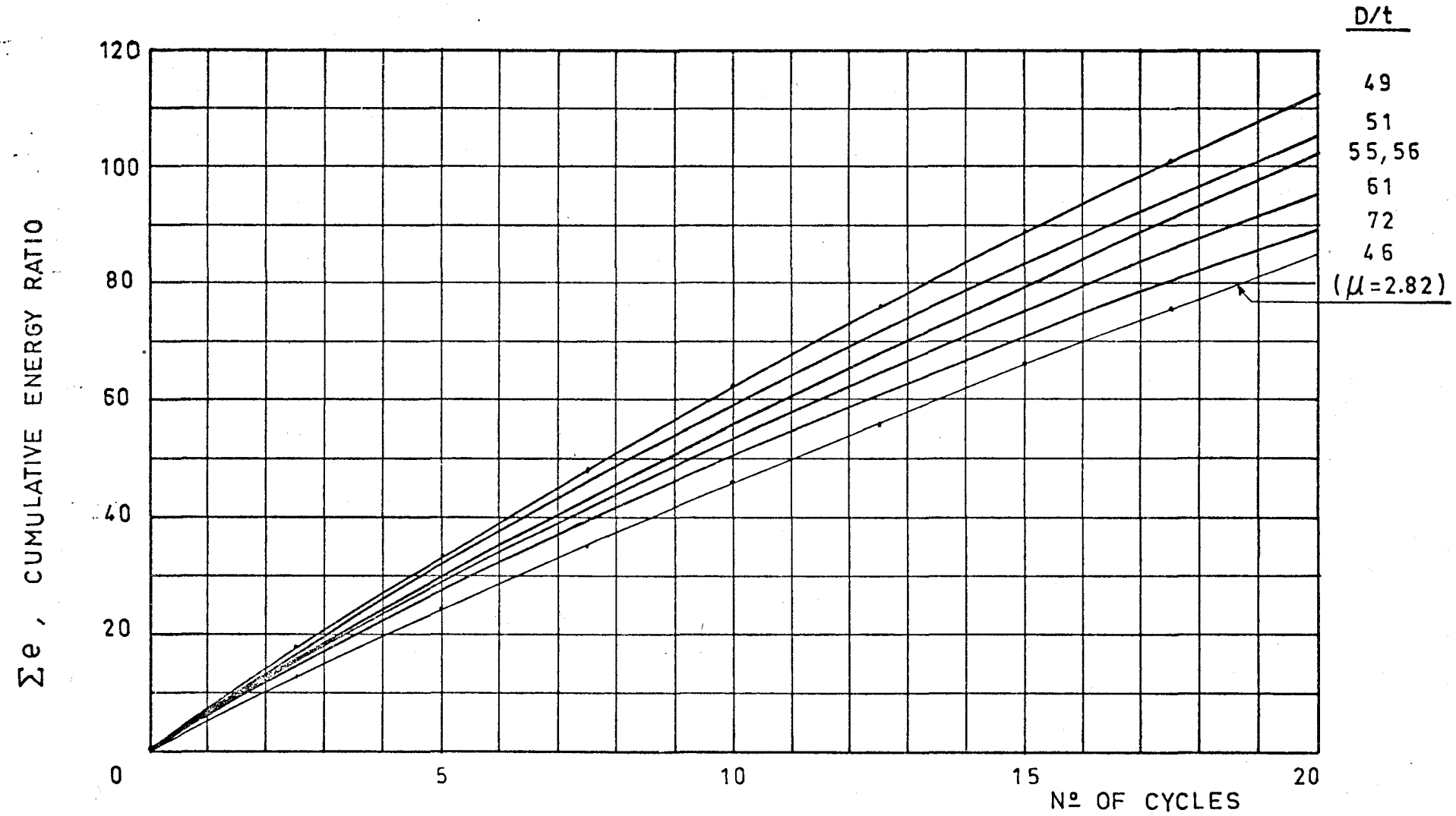

FIG. 3.11 Σe Vs. Nº of CYCLES FOR μ = 3.0 (except as noted)

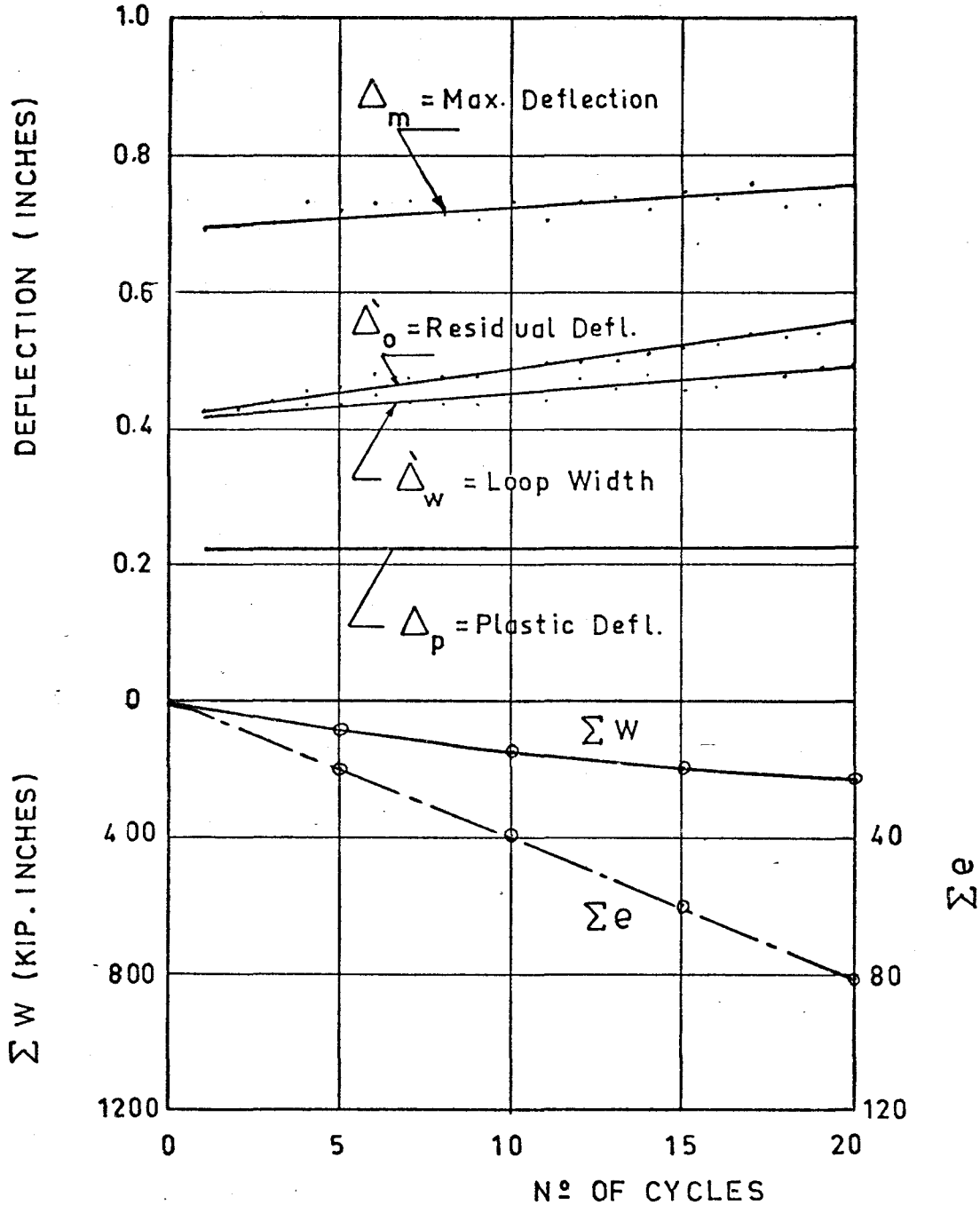

FIG. 3.12-a DEFLECTIONS, Σ W and Σ e Vs. Nº of CYCLES FOR T1

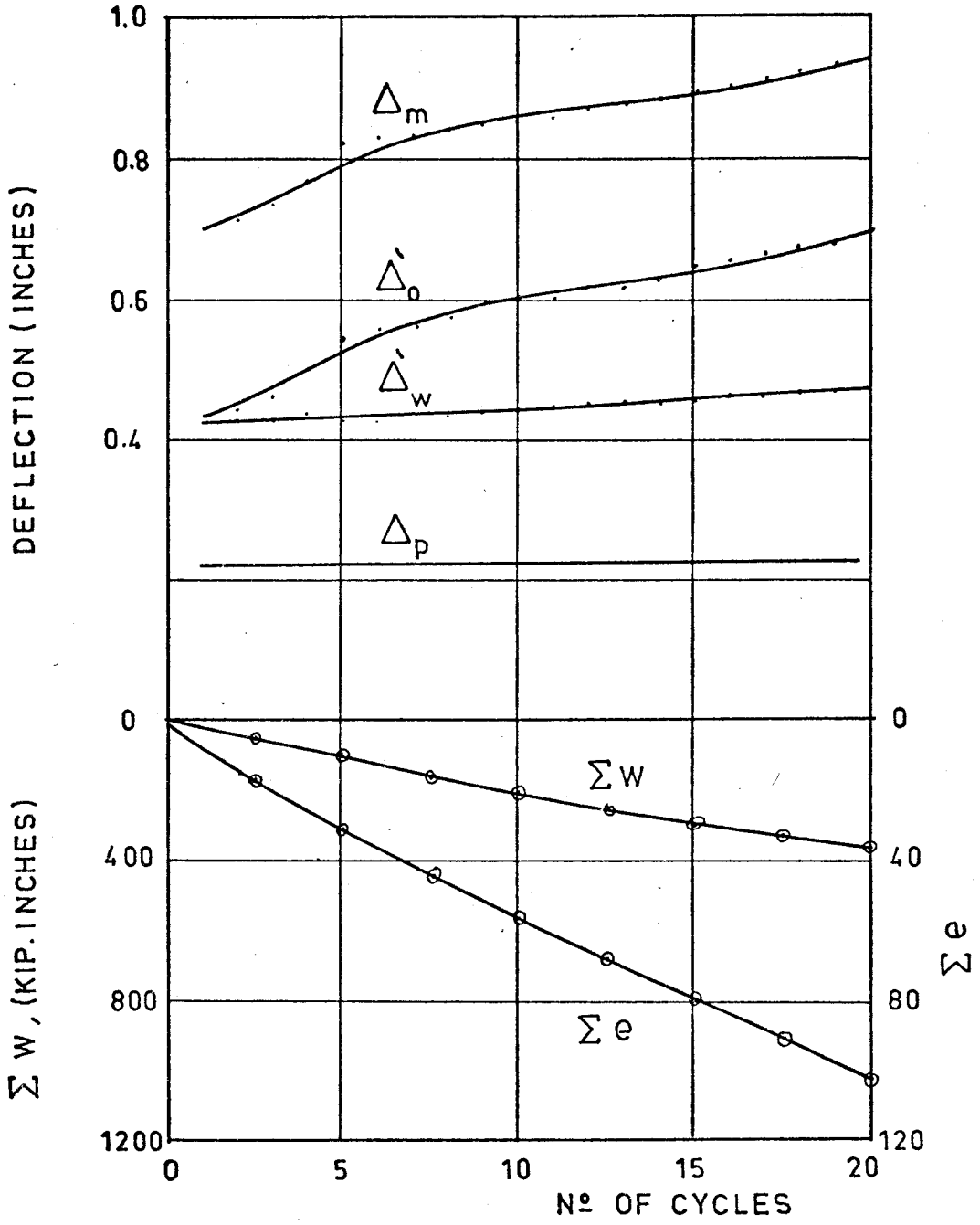

FIG. 3.12-b DEFLECTIONS, Σ W and Σ e Vs. Nº of CYCLES FOR T 2

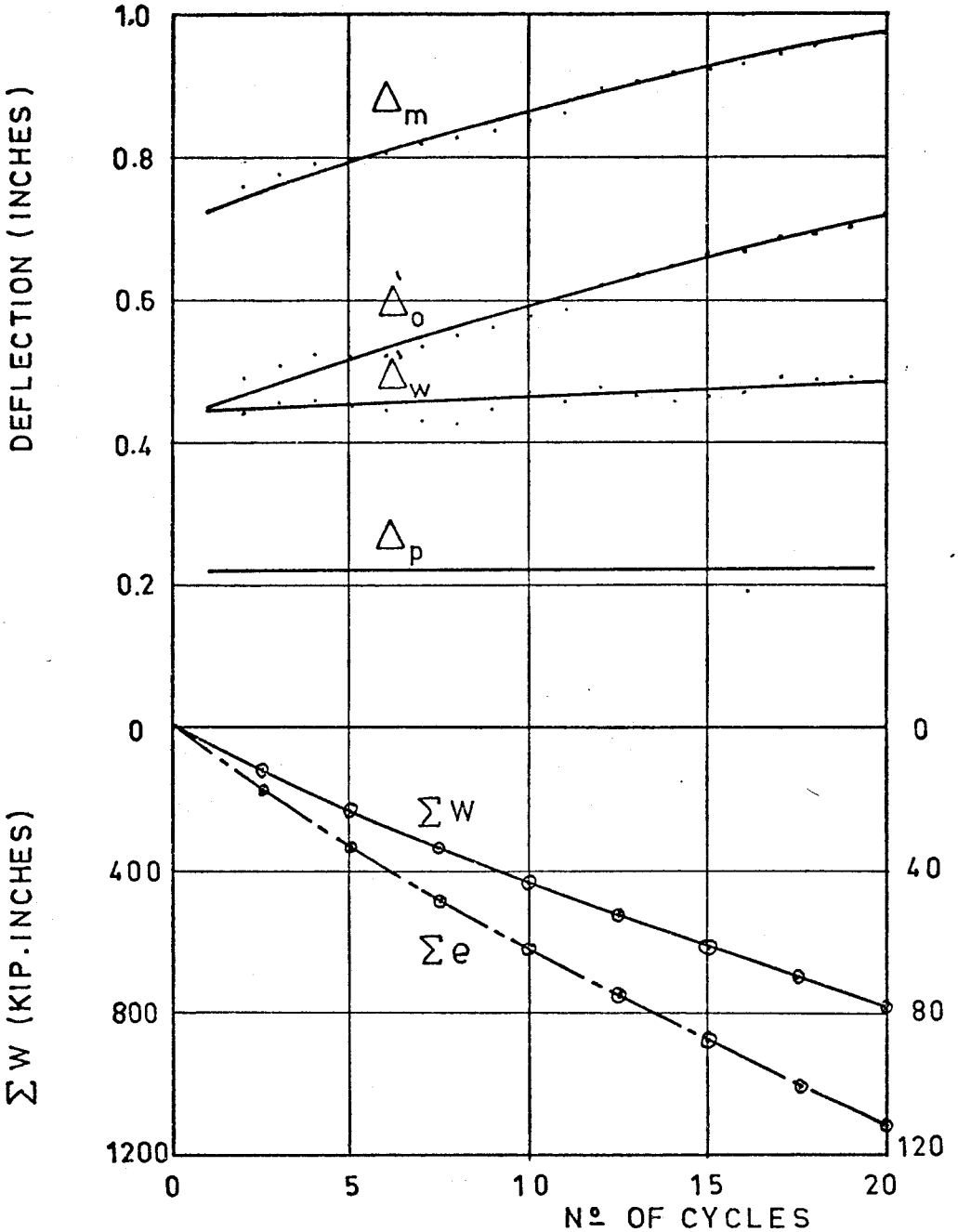

FIG. 3. 12-c DEFLECTIONS, ΣW and Σe Vs. Nº of CYCLES FOR T4

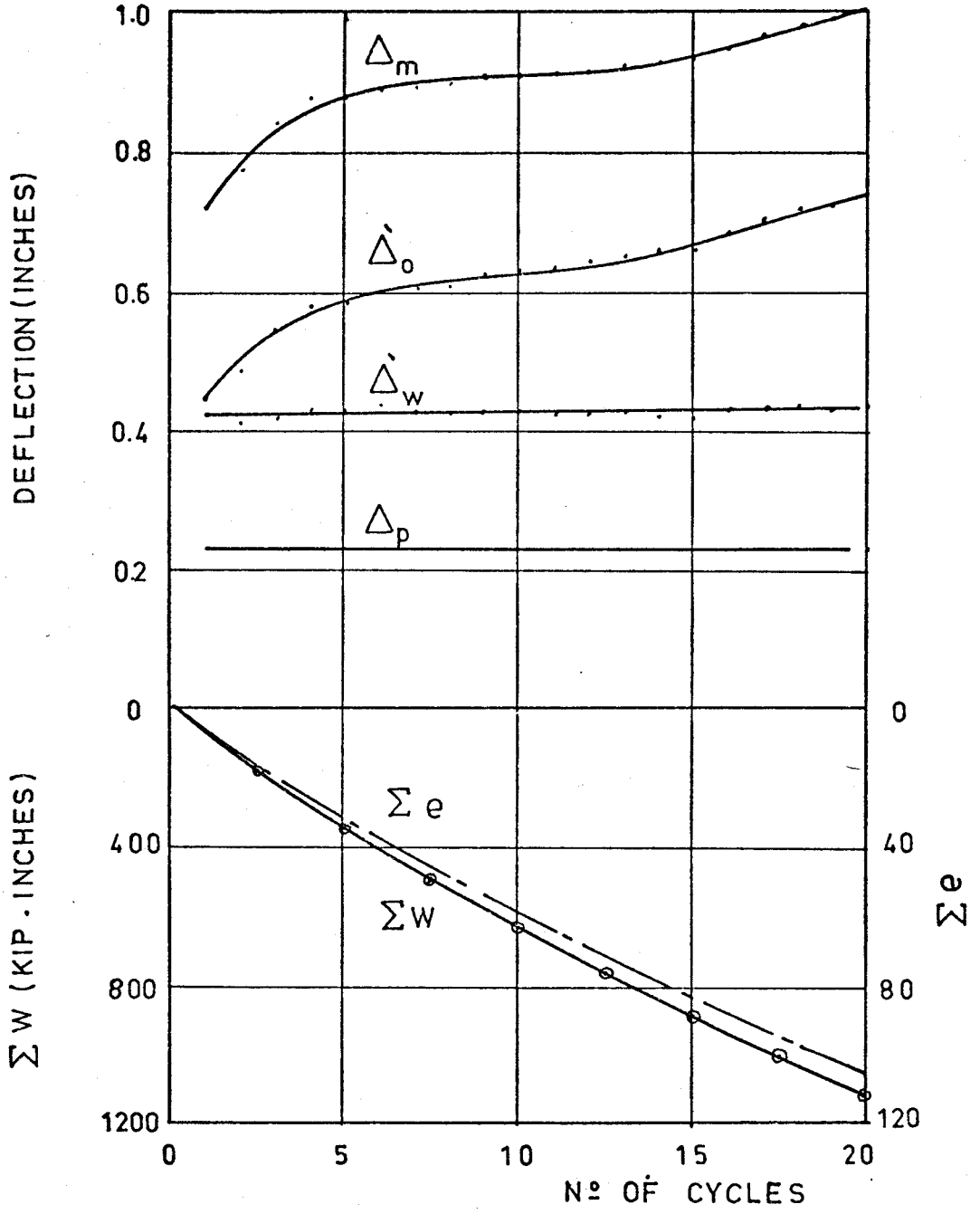

FIG. 3.12-d DEFLECTIONS, ΣW and Σe Vs. Nº of CYCLES FOR T 5

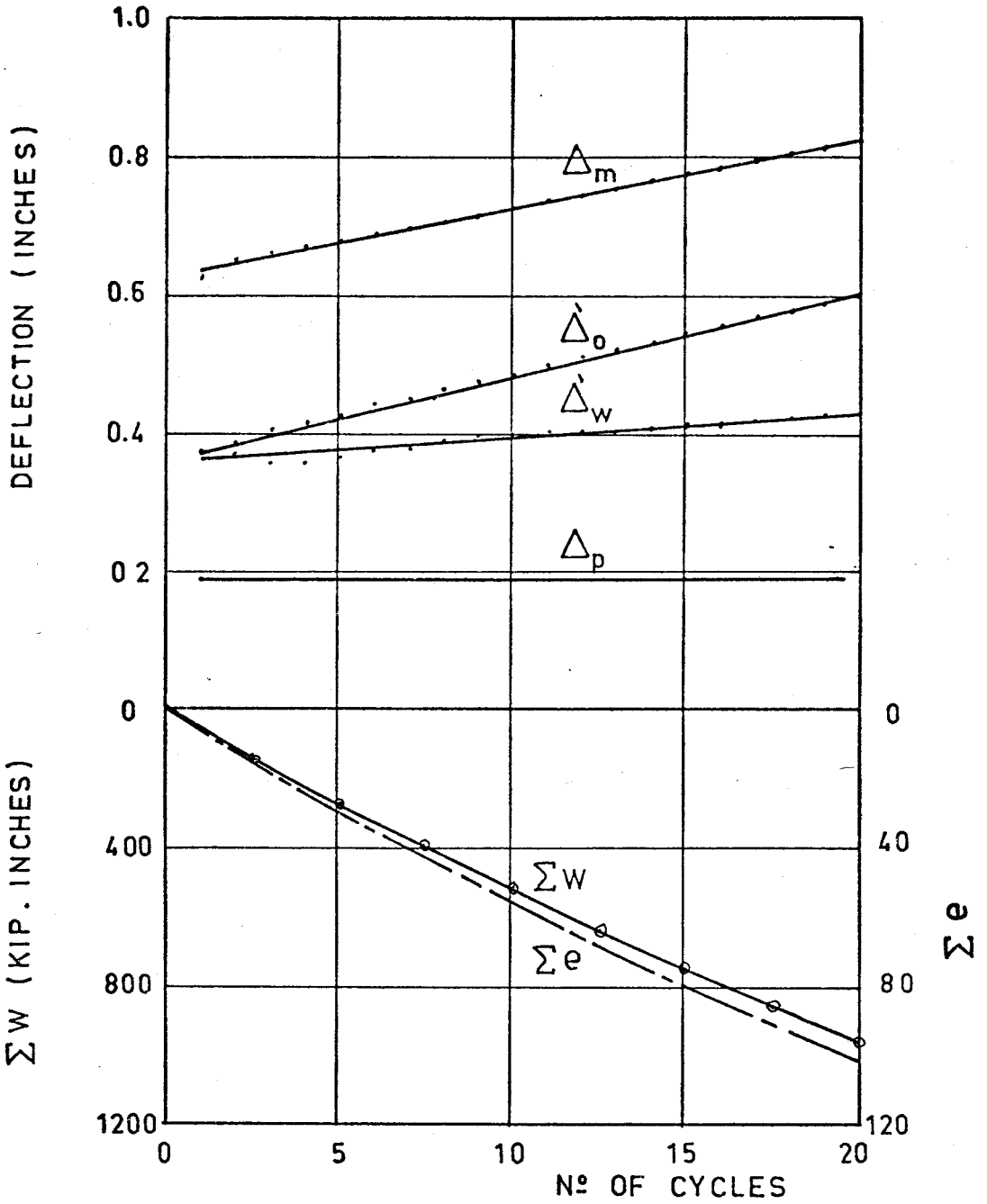

FIG. 3.12-e DEFLECTIONS, Σ W and Σ e Vs. Nº of CYCLES FOR T 6

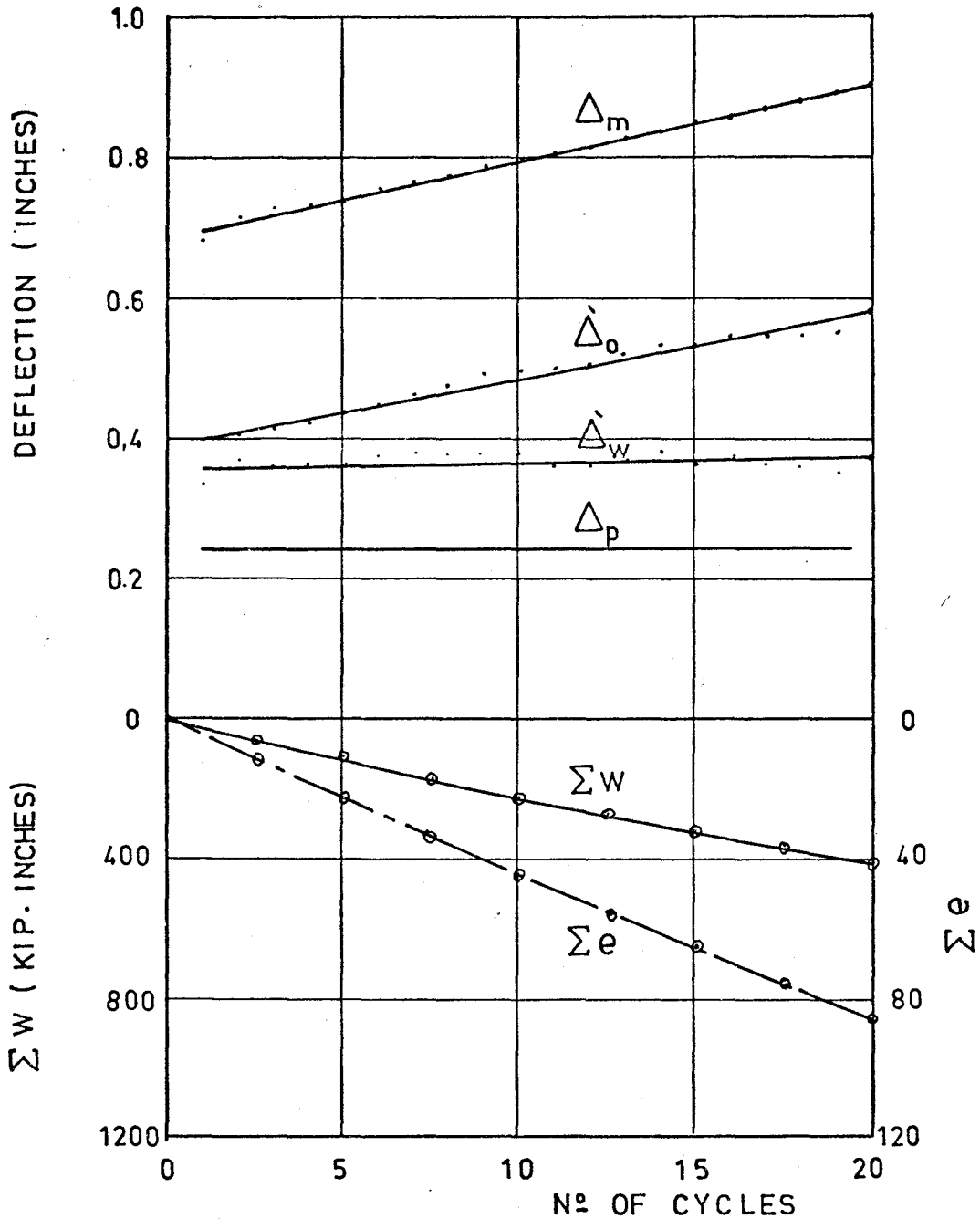

FIG. 3.12-f DEFLECTIONS, ΣW and Σe Vs. Nº of CYCLES FOR T7

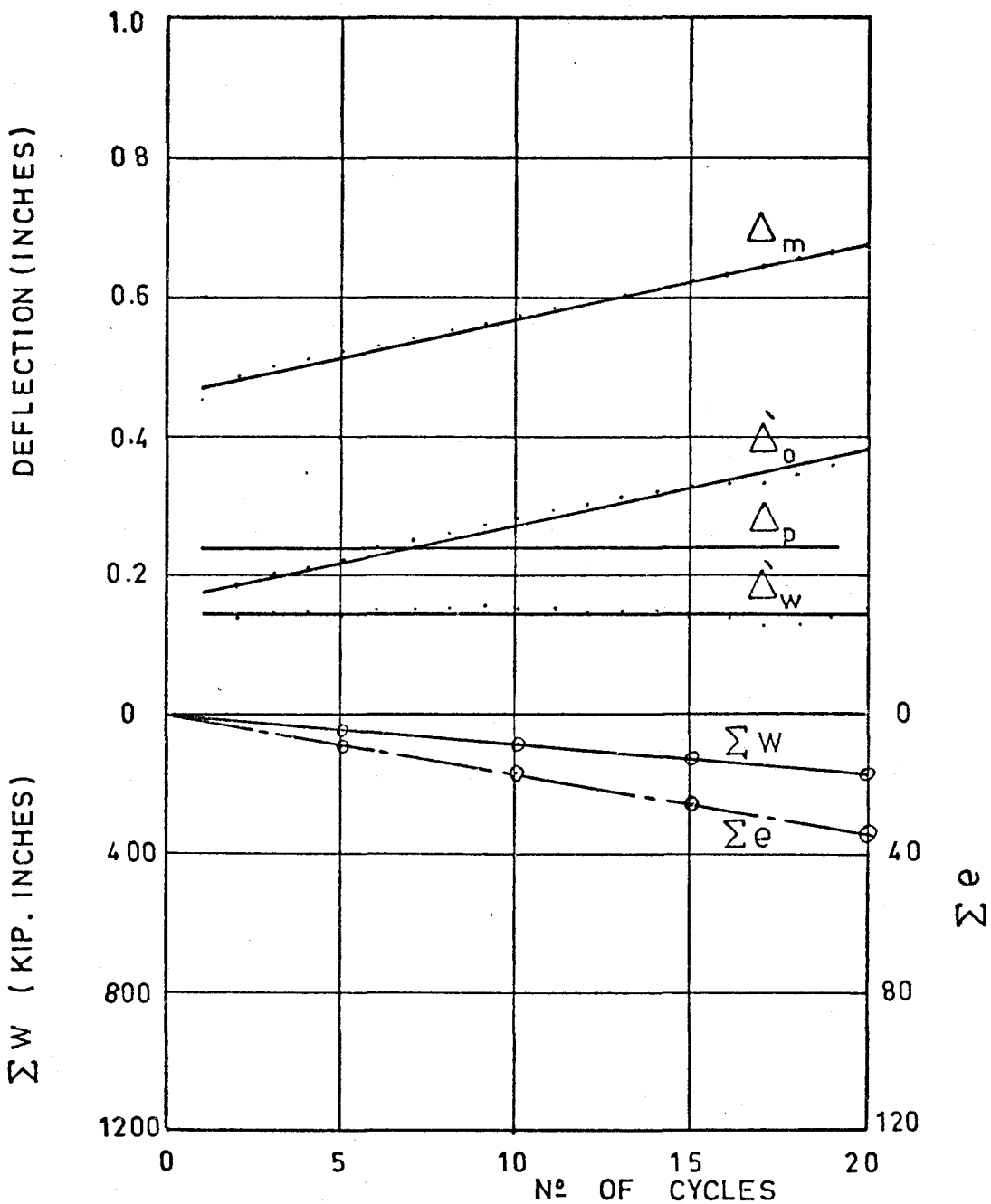

FIG. 3.12-g DEFLECTIONS, ΣW and Σe Vs. Nº of CYCLES FOR T 8

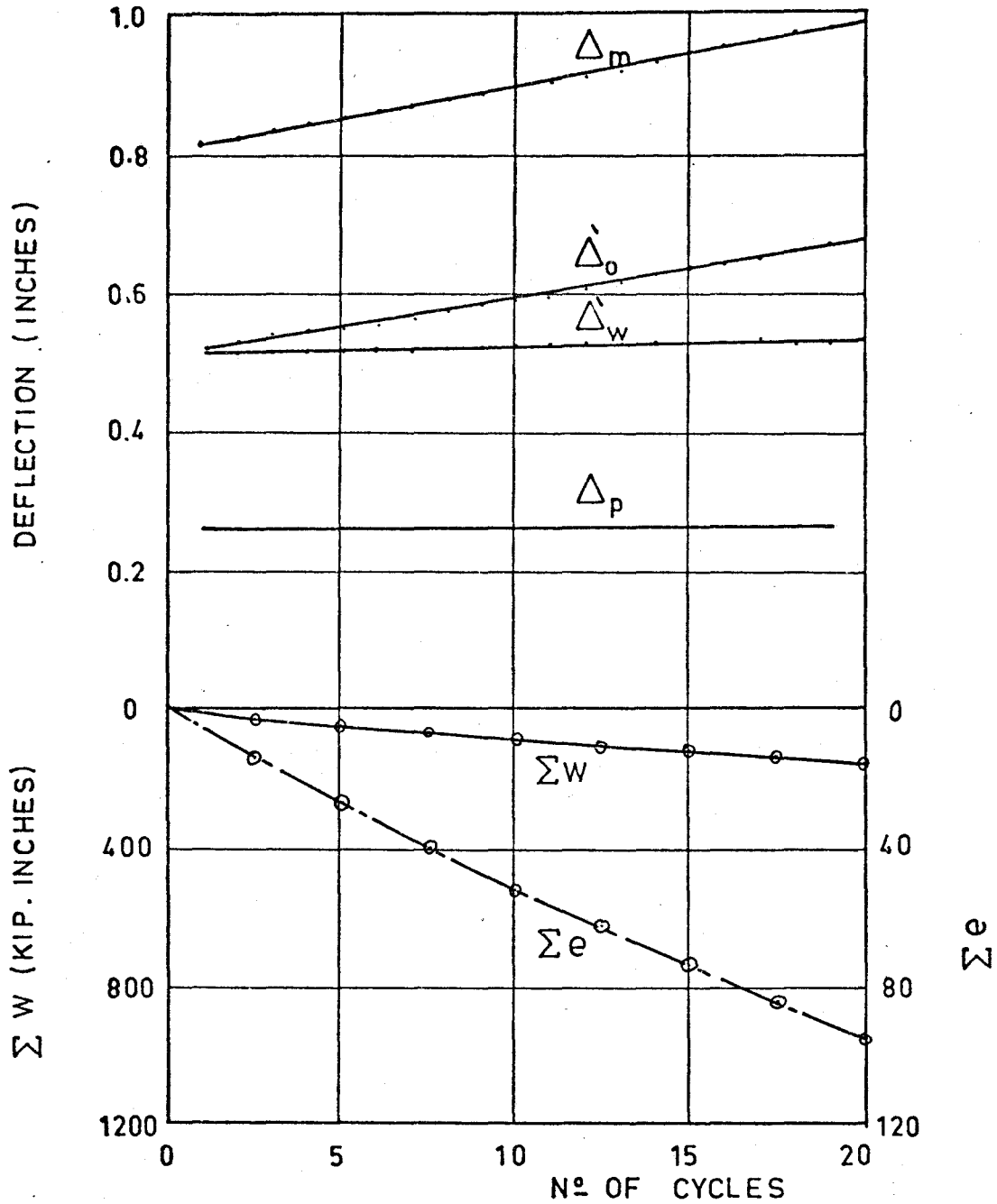

FIG. 3.12-h DEFLECTIONS, ΣW and Σe Vs. Nº of CYCLES FOR T9

T 1 (8.625" OD x 0.120")
T 2 (8.625" OD x 0.156")
T 7 (8.625" OD x 0.188")
T 9 (6.640" OD x 0.108")

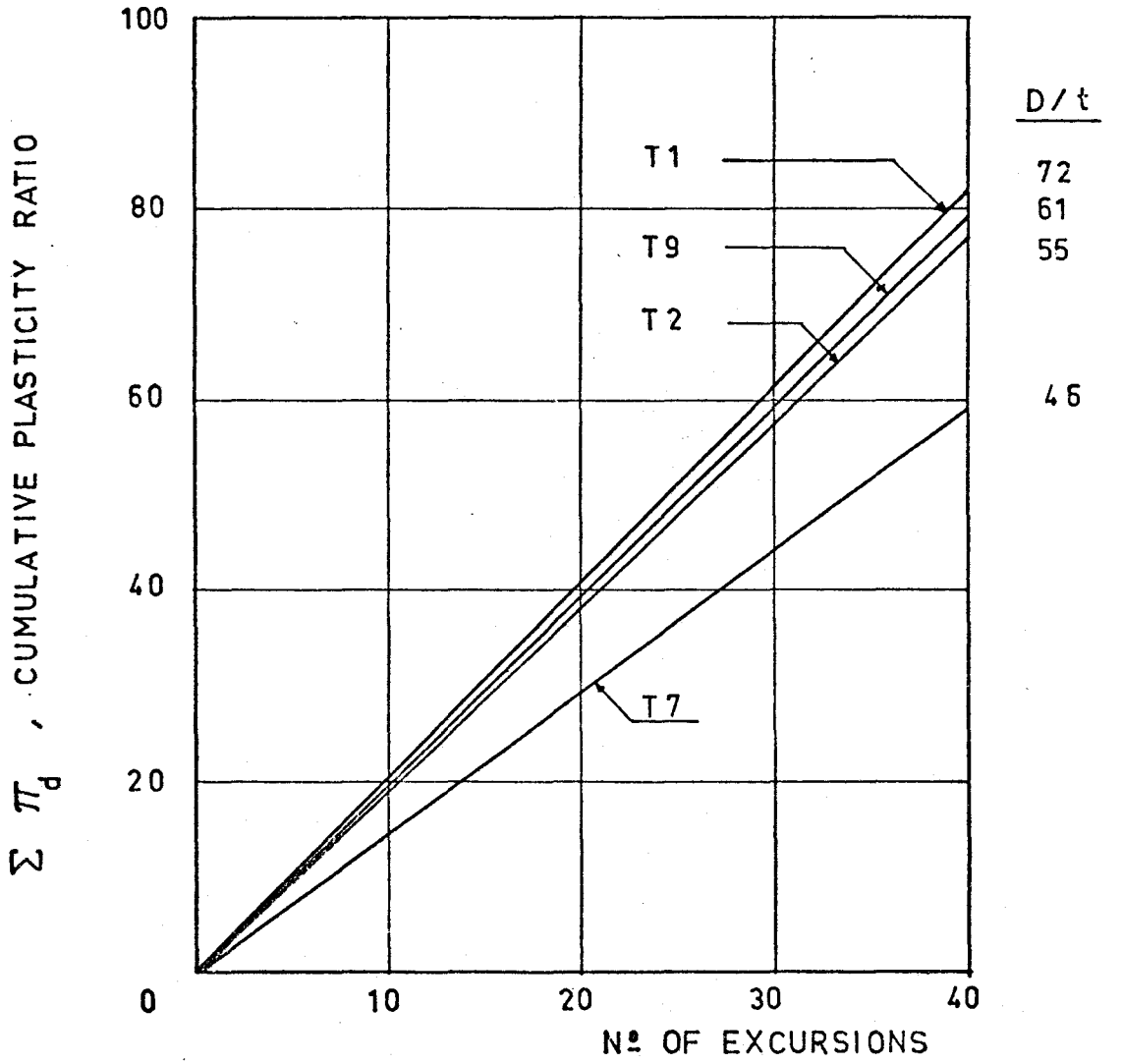

FIG. 3.13-a $\Sigma \pi_d$ Vs. Nº of EXCURSIONS

T5 (12.75" OD x 0.25")

T6 (14.00" OD x 0.25")

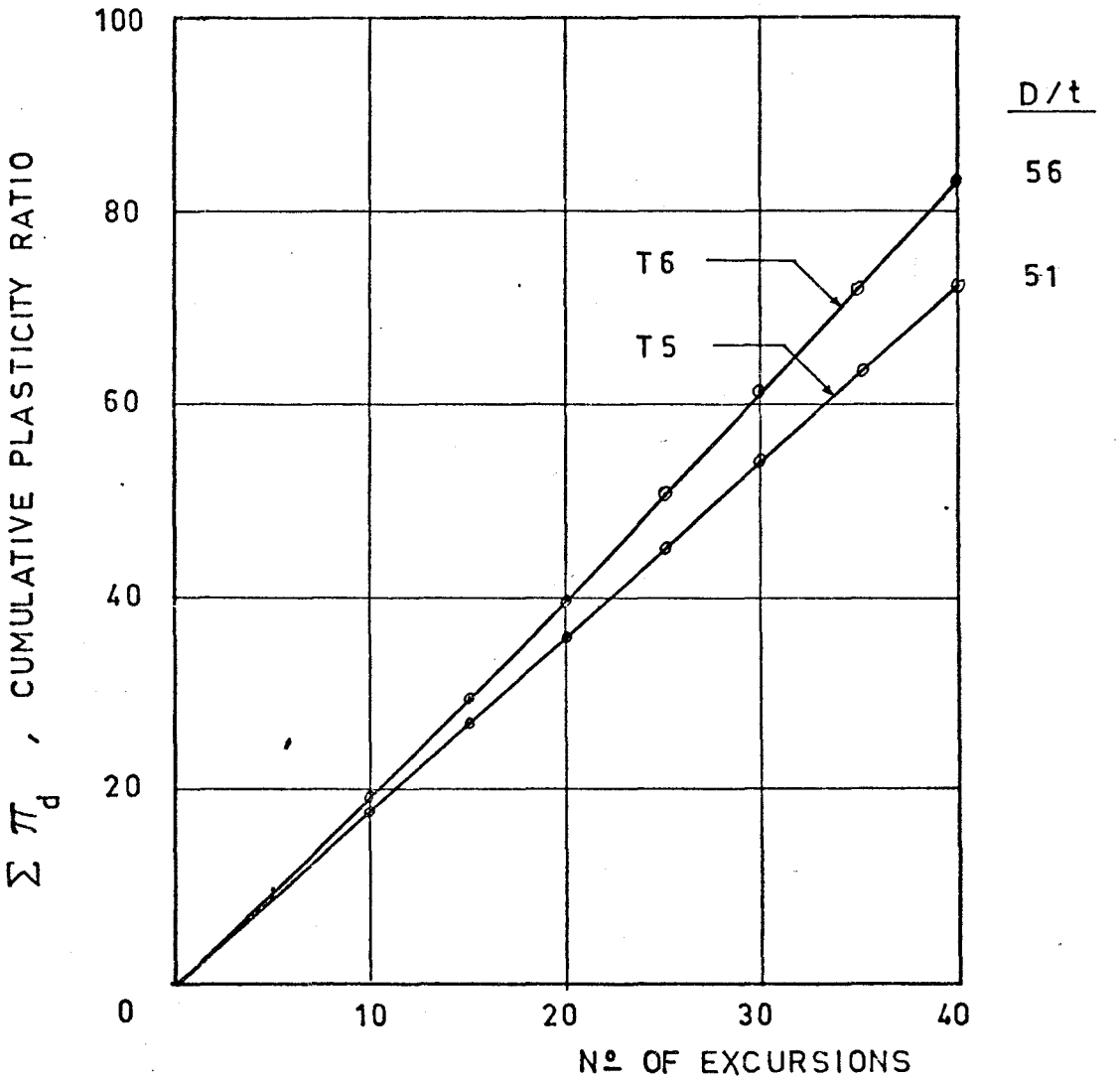

FIG. 3.13 - b $\Sigma \pi_d$ Vs. Nº of EXCURSIONS

T 4 (10.75" OD x 0.219")

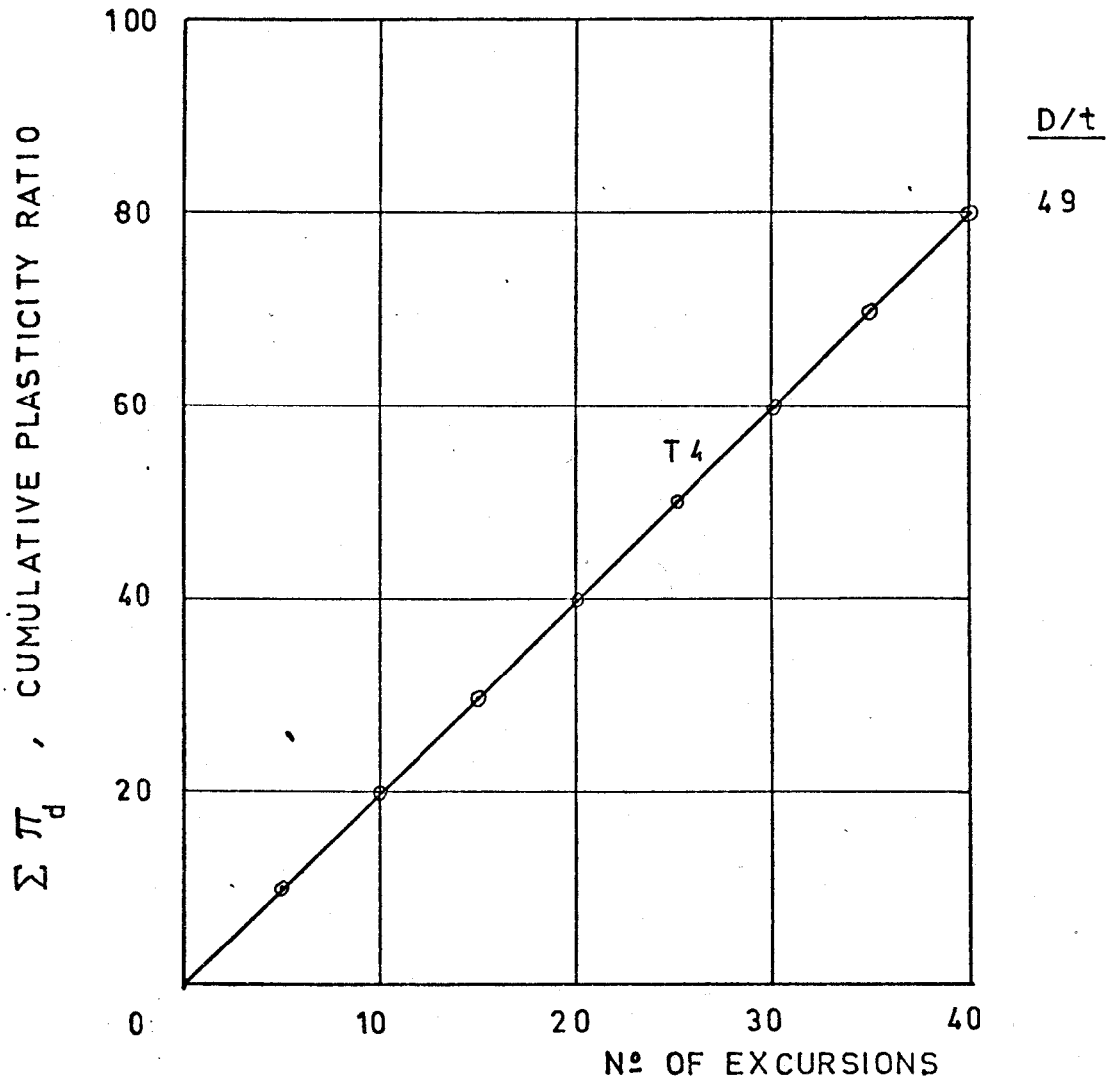

FIG. 3.13-c $\Sigma \pi_d$ Vs. Nº of EXCURSIONS

D/t = 46
FOR
T3, T7 and T8
(8.625" OD x 0.188")

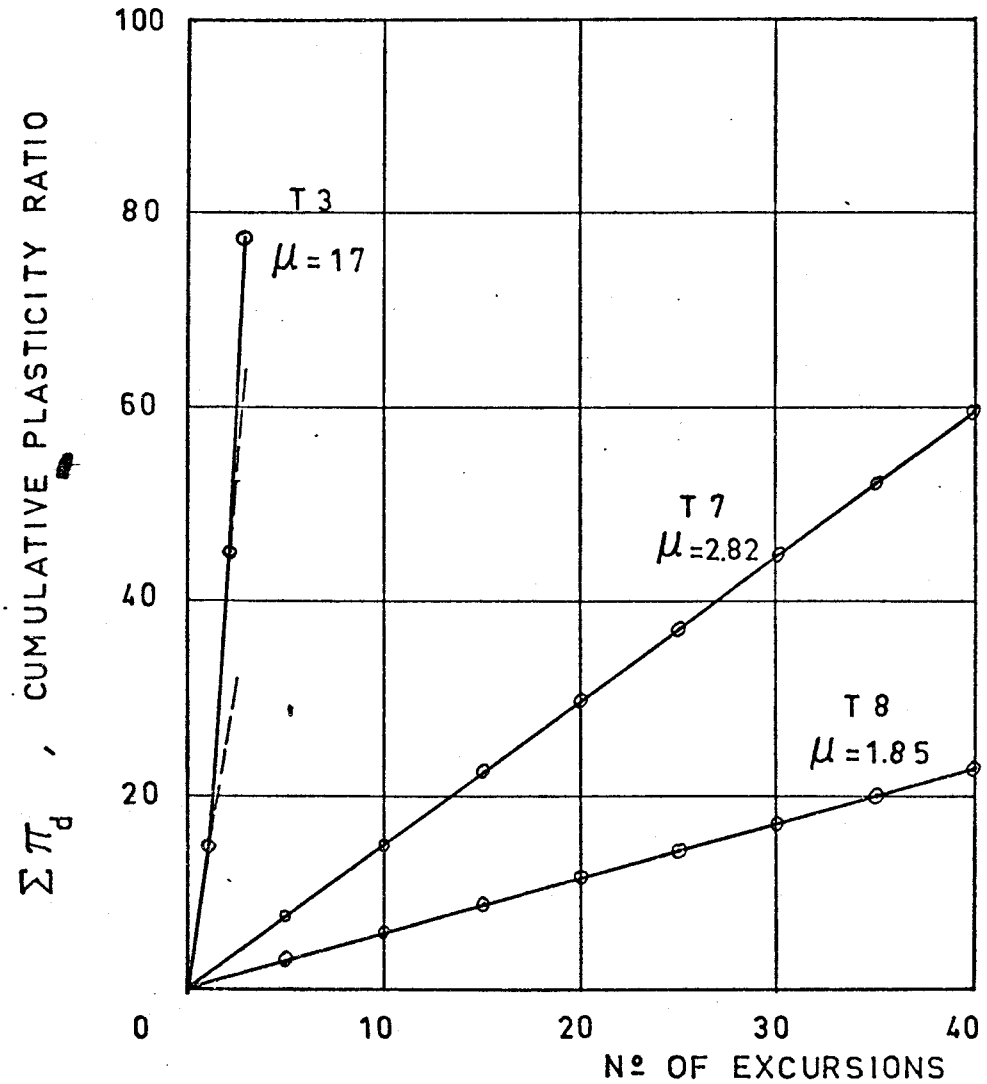

FIG.3.13-d $\Sigma \pi_d$ Vs. Nº of EXCURSIONS

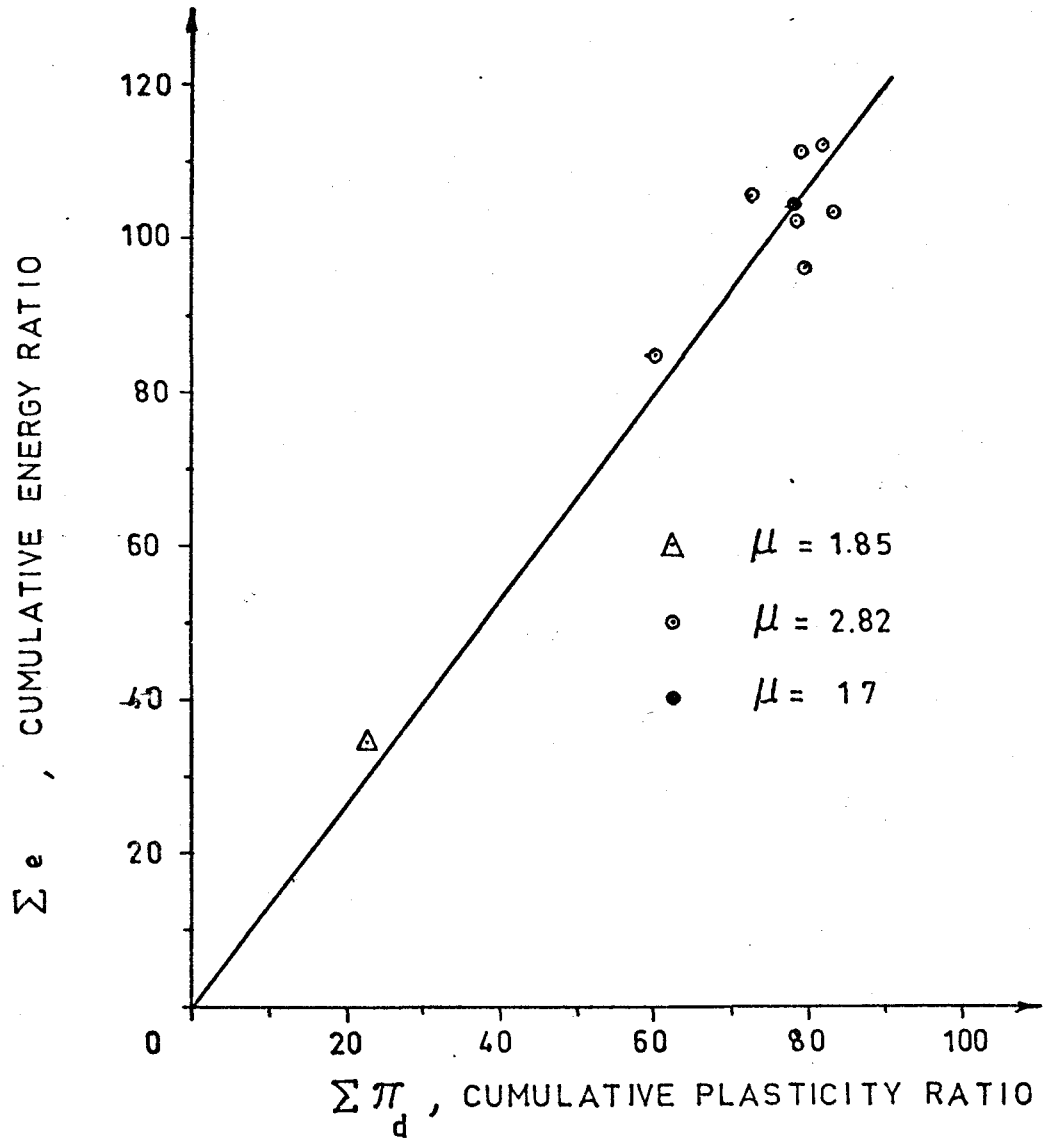

FIG. 3.14 Σe Vs. $\Sigma \pi_d$

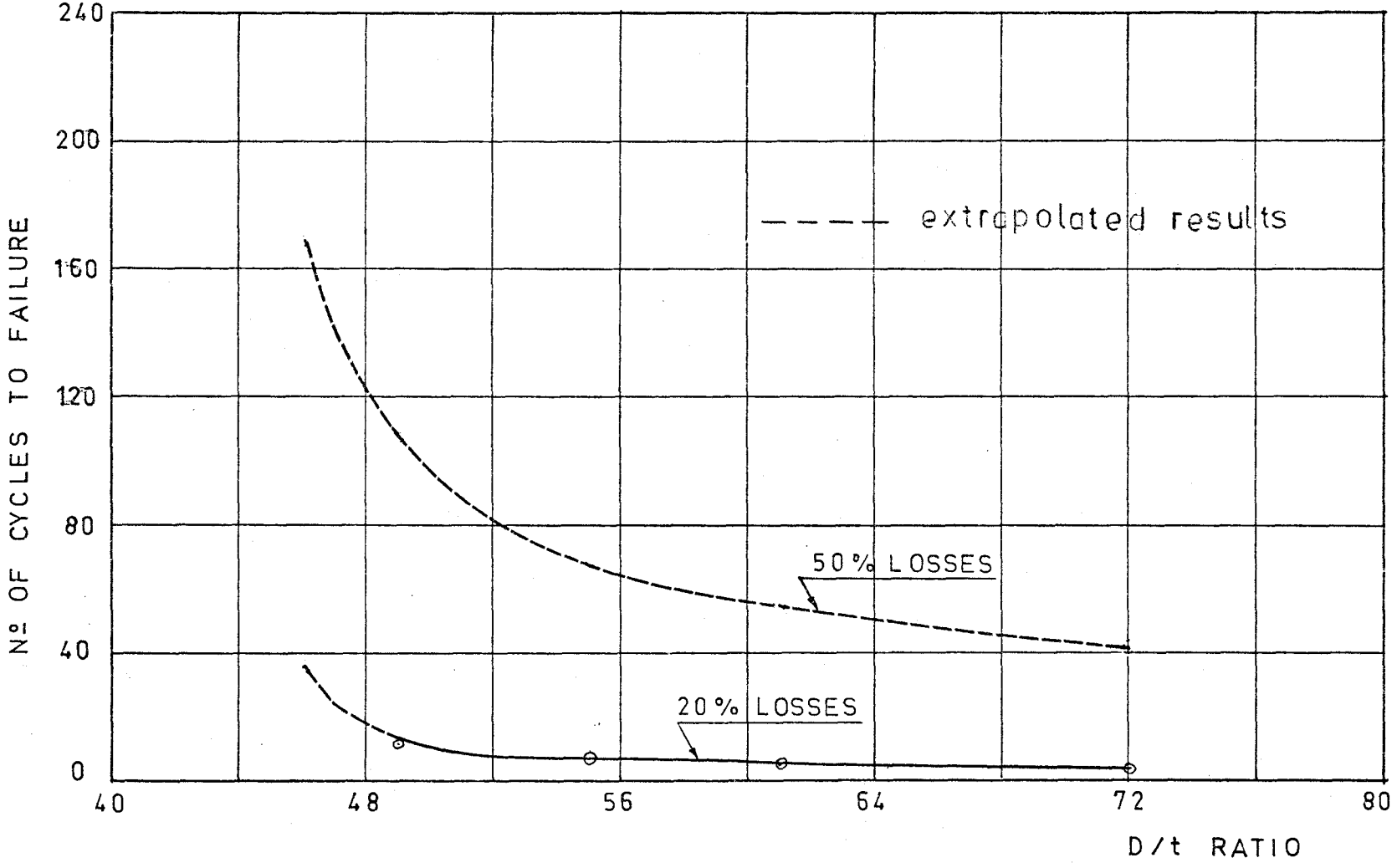

FIG. 3.15 NUMBER of CYCLES Vs. D/t RATIO for 20 & 50% LOSSES

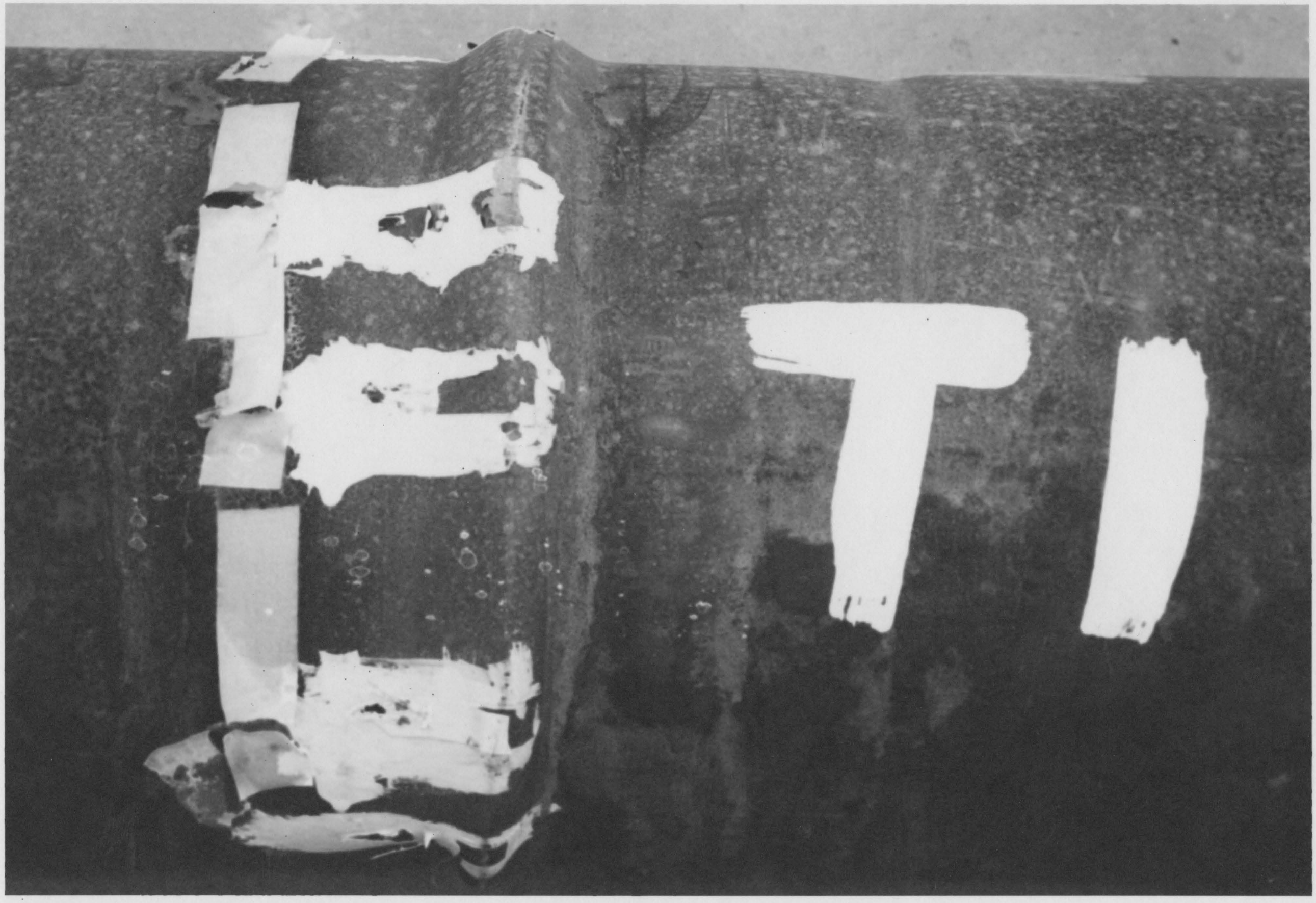

FIGURE 3.16-a Top Buckle Shape of Tube T1.

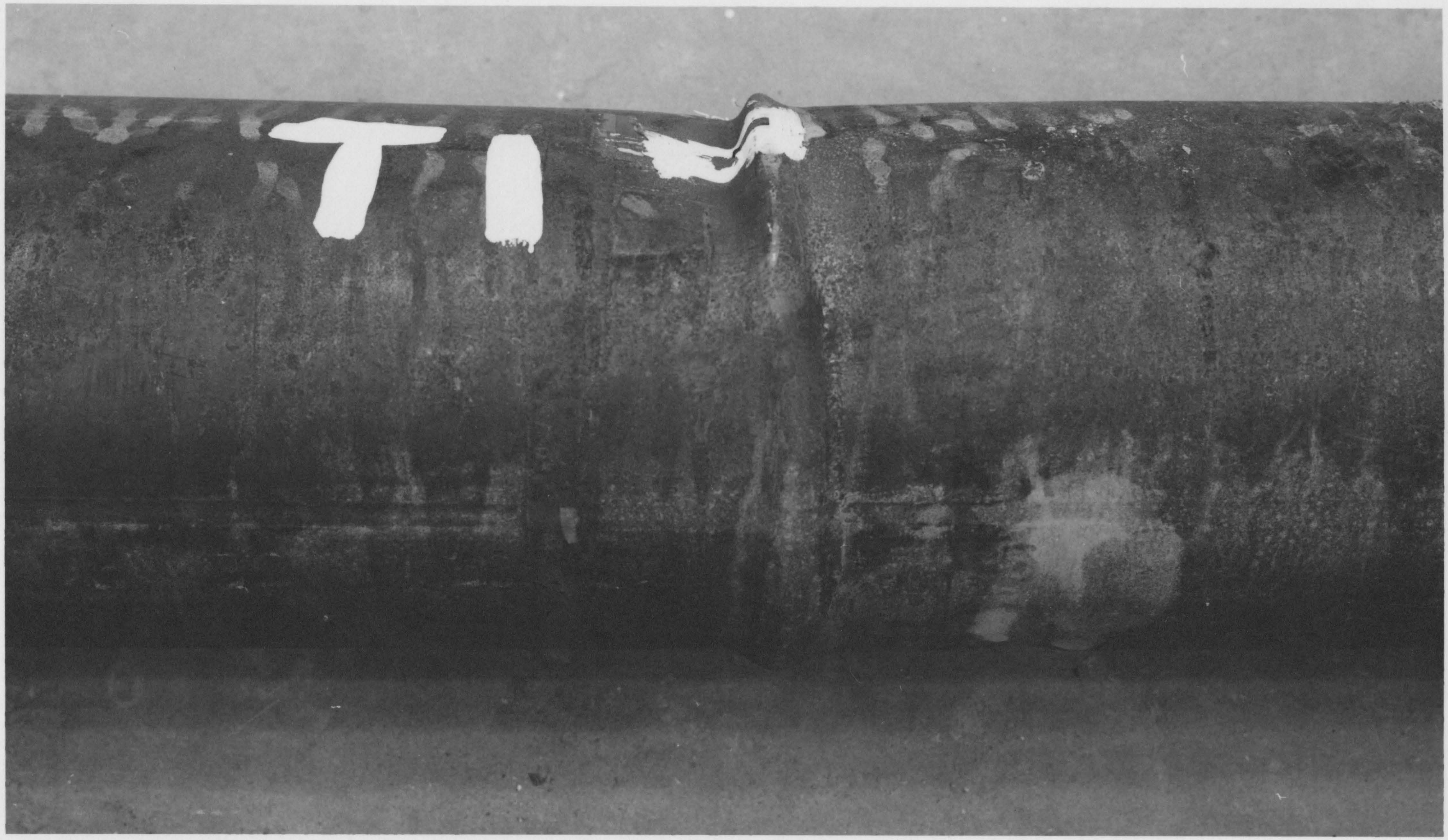

FIGURE 3.16-b Bottom Buckle Shape of Tube T1.

FIGURE 3.17 Crack of Tube T2 Occurred at the Middle of the Top Buckle.

FIGURE 3.18-a Top Crack of Tube T3 Occurred Outside the Buckle Zone.

FIGURE 3.18-b Bottom Crack of T3 During Loading.

FIGURE 3.18-c Bottom Crack of T3 After Removing the Tube.

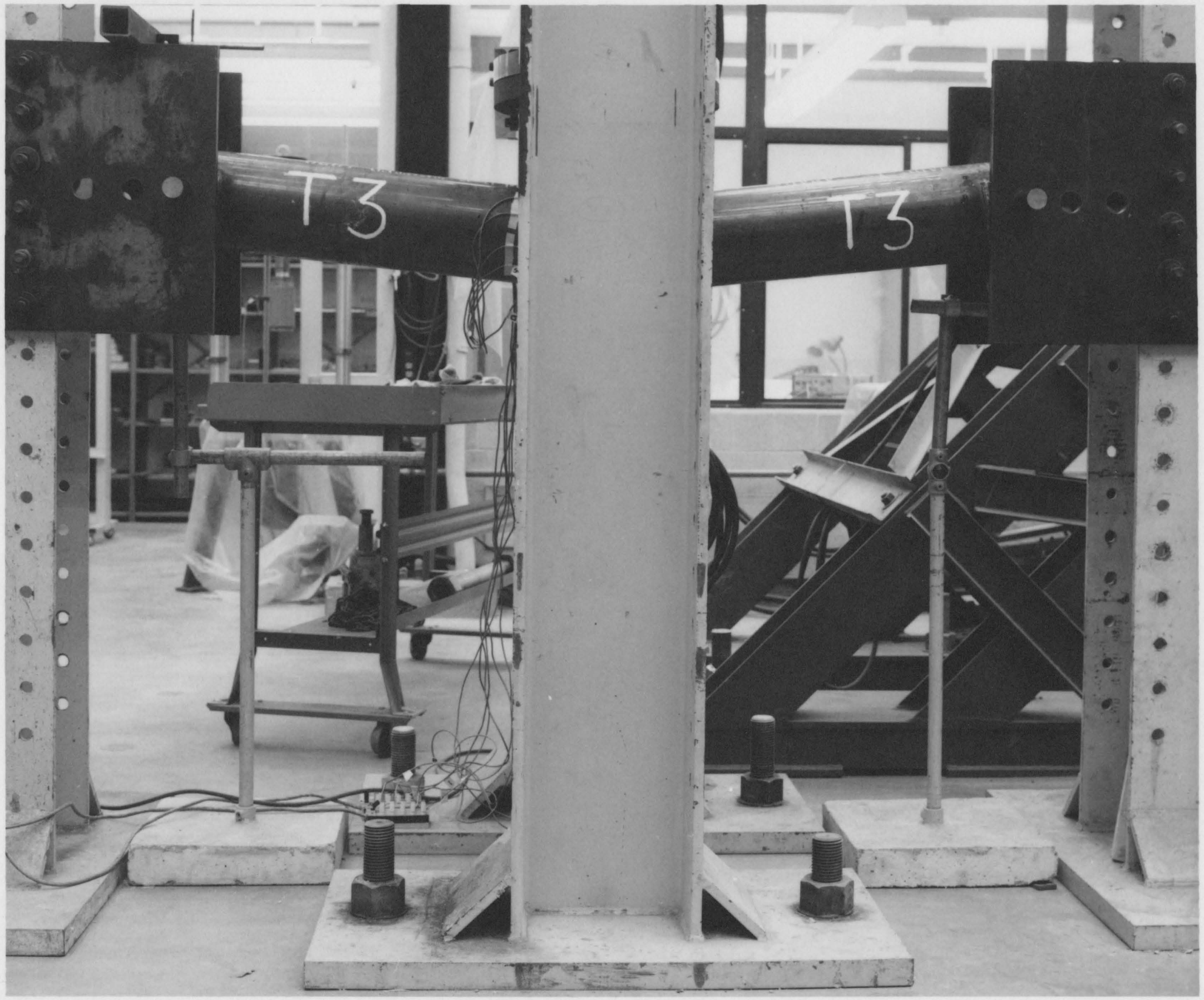

FIGURE 3.18-d Residual Deflection of Tube T3.

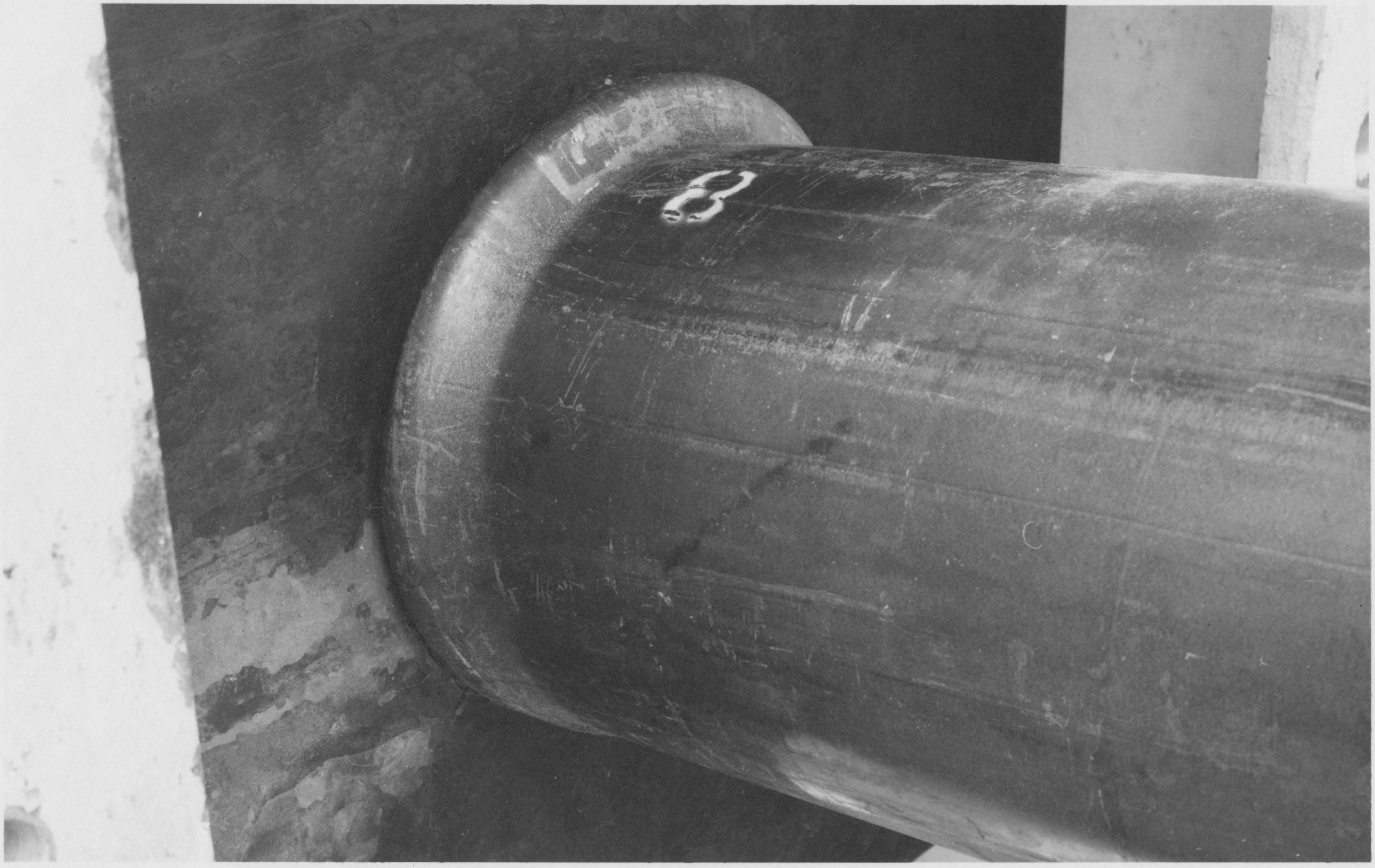

FIGURE 3.18-c Large Top Buckle of Tube T3 During Operation.

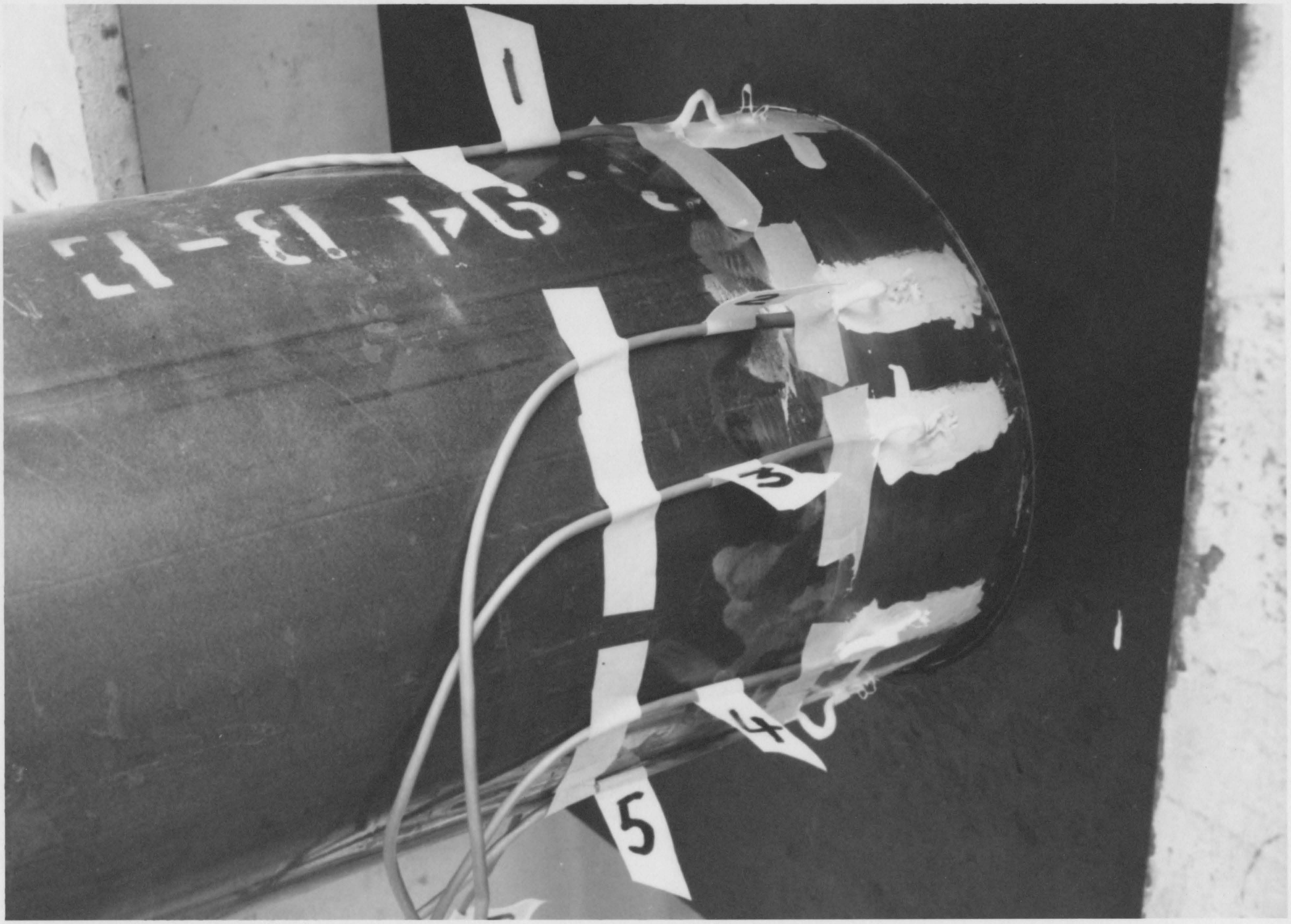

FIGURE 3.18-f Tiny Buckle Occurred Where the Strain Gauges Were Mounted.

FIGURE 3.19 No Cracks Occurred for Tube T4.

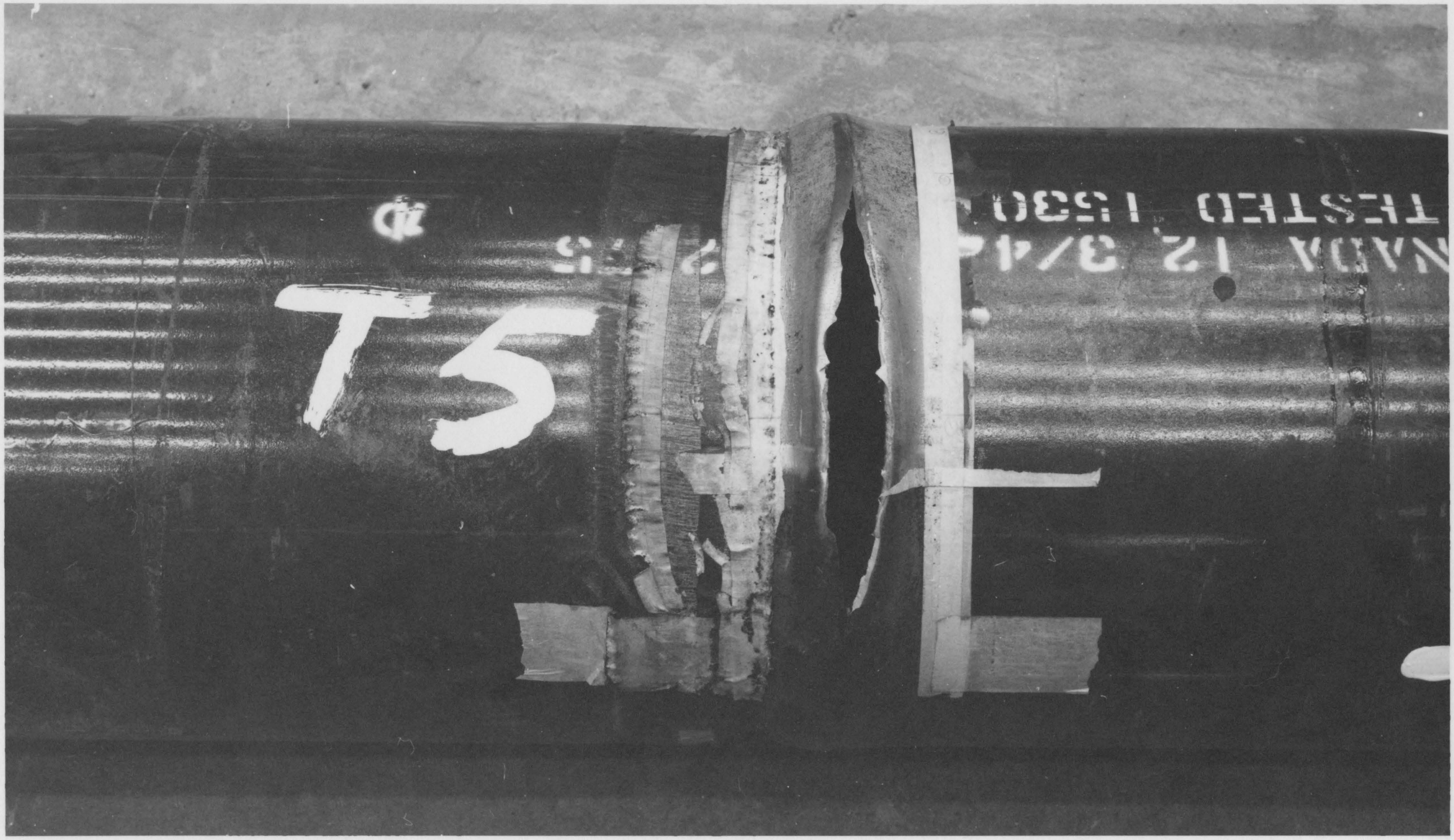

FIGURE 3.20 Crack of Tube T5 Occurred at the Middle of the Top Buckle.

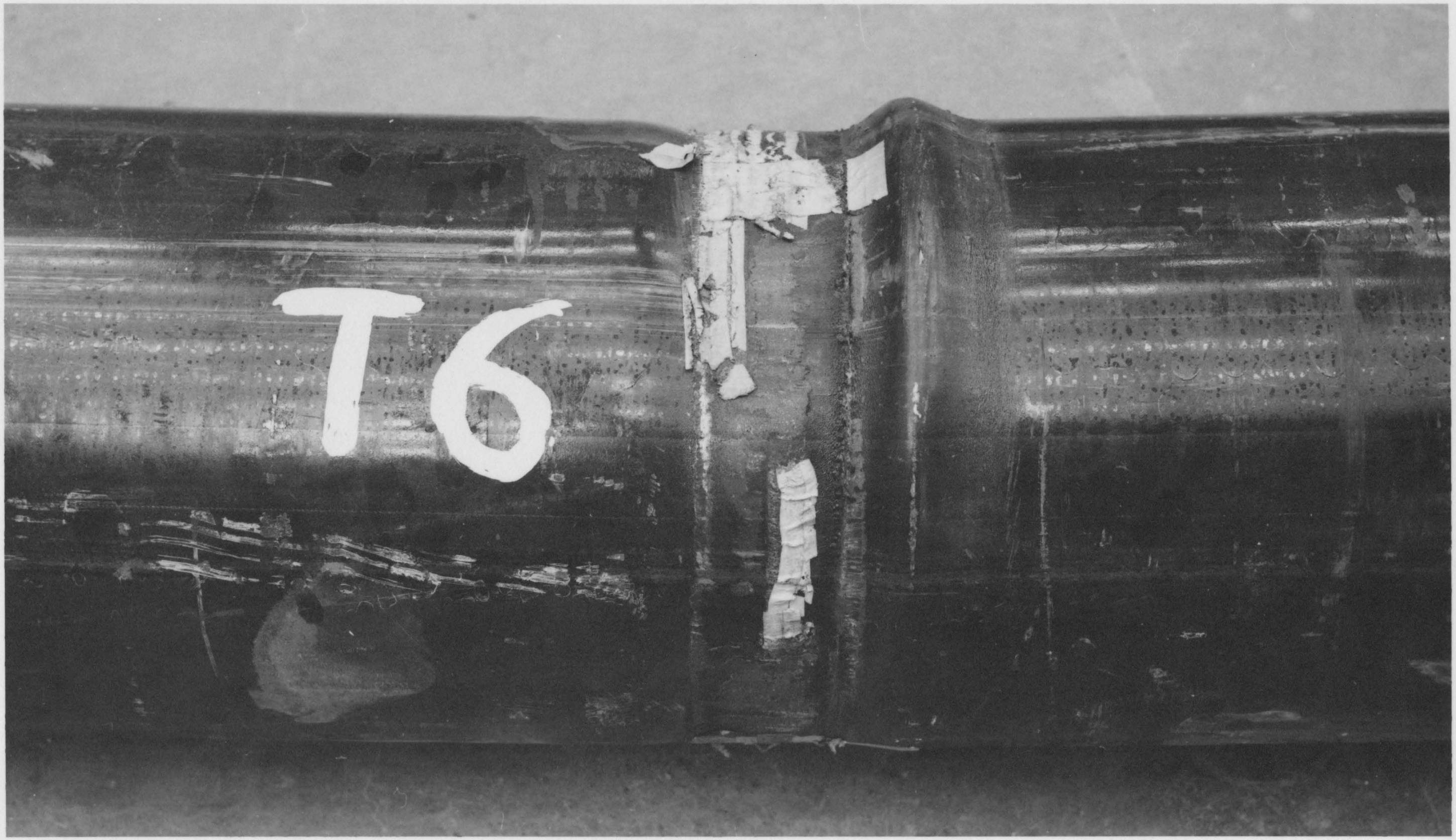

FIGURE 3.21 No Cracks Occurred in Tube T6.

FIGURE 3.22 Buckle Shapes for Tubes T7 and T8 After 20 Cycles.

FIGURE 3.23 No Cracks Occurred for Tube T9.

CHAPTER 4

CONCLUSIONS AND SUGGESTIONS FOR FURTHER RESEARCH

4.1 Conclusions

The behaviour of Round HSS subjected to cyclic loading in the inelastic zone was investigated by the author. The following conclusions are drawn for the range of D/t tested (46 to 72) based on a limited number of specimens:

1. About fifty percent of the losses at the end of the cyclic loading programme occurred after five cycles for all the beams cycled to a limiting deflection equal to $3\Delta_p$. Hence, cycling Round HSS within the range tested for 5 cycles, would provide a good indication of the losses after 20 cycles.

2. For D/t $\geqslant$ 49, the loss in load capacity was larger than 30% and increases linearly with an increase of D/t for $\Delta \simeq 3\Delta_p$. For D/t = 46, the loss was considerably smaller and in the acceptable range i.e. $\leqslant$20%.

3. A sudden change in behaviour occurred between D/t = 46 and 49. Only one test point was investigated for D/t $<$ 49, hence more test data is necessary to accurately define the behaviour of the transition zone. However with proviso that the altered behaviour shown in Fig. 3.2 is based on one test, the following result was established:

   a) For D/t = 46, local buckling appeared in the first half cycle, but after 20 cycles the loss in load capacity was 16.4%. Hence, it seems that for stocky sections local buckling is not a condition of failure since significant load capacity can be maintained after 20 cycles.

   b) A tube of D/t about 46 has a satisfatory level of performance after 20 cycles at $\Delta = 2.82\Delta_p$. The response is characterized by:

      i- stability of the hysteresis loops (same shape, same area and no rotation)

      ii- a percentage of loss $<$ 20% in load capacity

      iii- smaller buckle size in comparison with the other tubes with larger D/t.

4. The accumulated energy dissipation $\sum e$, increases as a function of D/t. Any decrease in the D/t ratio will increase the value of $\sum e$.

5. Cycling of a Round HSS (D/t = 46) to two different limiting deflections ($\Delta = 2.82\Delta_p$ and $1.85\Delta_p$ respectively), produced a ratio of 2.75 between the number of cycles required to reach the same amount of energy dissipated. Therefore it may be possible to develop a relationship between the limiting deflection and the number of cycles for energy dissipation.

6. When a Round HSS (D/t = 46) was cycled to three different limiting delfections (1.85, 2.82 and $17.4\Delta_p$ respectively), it was found that the accumulated energy dissipation $\sum e$, was proportional to the cumulative plasticity ratio in the form $\sum e \simeq 1.33 \sum \pi_d$.

7. Cracks did not occur in any of the sections during the twenty cycle programme at a limiting deflection equal to $3\Delta_p$. Hence, it appears that even when the elastic limit is exceeded slightly, a large number of cycles can be tolerated prior to failure.

8. During cyclic loading, compressive forces will alternate with tensile forces at the buckled zone. If the induced strains or stresses are large enough, the effect of the force will be greater in magnitude over the weakened cross-section, hence crack generation may be expected. This situation occurred to tubes T2

and T5 when they were cycled to the maximum stroke of the jack ($\Delta \simeq 17\Delta_p$) after 20 cycles.

9. Local buckling, kinking action and fatigue will be the reason for the occurrence of any fracture. Hence, it is difficult to relate these three factors together to predict the remaining life of any section. A common but arbitrary assumption is that at a 20% loss in load capacity, any Round HSS will be considered to have structurally failed. A curve for the number of cycles to failure versus D/t was drawn in Fig. 3.15.

10. Based on a single comparison of two tubes having the same D/t ratio (but from different thicknesses and diameters), a scale effect does not seem to have a major effect on the behaviour of Round HSS under cyclic loading. These included:
    a) the same loss in load capacity
    b) the same accumulated energy dissipation $\sum e$
    c) the same cumulative plasticity ratio $\sum \pi_d$.

11. Comparing the behaviour of simulated cantilevers of Round and Square HSS it was observed that for the limiting slenderness ratio prescribed by the code, Round sections perform better than Square sections, in that there is:

a) a smaller loss in load capacity

b) higher accumulated energy dissipated $\sum e$

c) the effect of local buckling leading to deterioration is less in severity

The use of values suggested in the text for various limitations for D/t relationships are limited because of the need for further experimental verification. However despite this cautioning, it is hoped that these results provide a worthwhile first step in establishing useful design criteria for the use of Round HSS in situations of plastic reversed loadings. In addition this study has helped to define the region where additional work should be concentrated. This will be discussed in the next section.

4.2 Suggestions for Further Research

It will be useful to complete this series of tests for a range of D/t smaller than 46 and concentrate further research on tubes having a value of D/t falling between 40 and 50. Hence, the superior performance of the transition zone may be confirmed.

To obtain reasonable strain readings, the author suggests that strain gauges must be mounted on both sides of the collar, so that if the buckle occurred at the right hand side of the collar, the gauges located at the left hand side will give reasonable readings. Strain gauges must be mounted at a distance greater than 2 inches from midspan.

A cyclic loading program like the one done by Bertero and Popov (1), will be helpful for the Round HSS. A certain value of D/t is chosen, and a series of cyclic loading tests may be done on this section by using a different limiting deflection for every test. Hence a curve relating the limiting deflection and the number of cycles to fracture for a certain value of D/t may be obtained, similar to Bertero and Popov's (1) curve. Refer to Fig. 4.1.

The work done by the author must be followed by an investigation on connections between Round HSS subjected to cyclic loading.

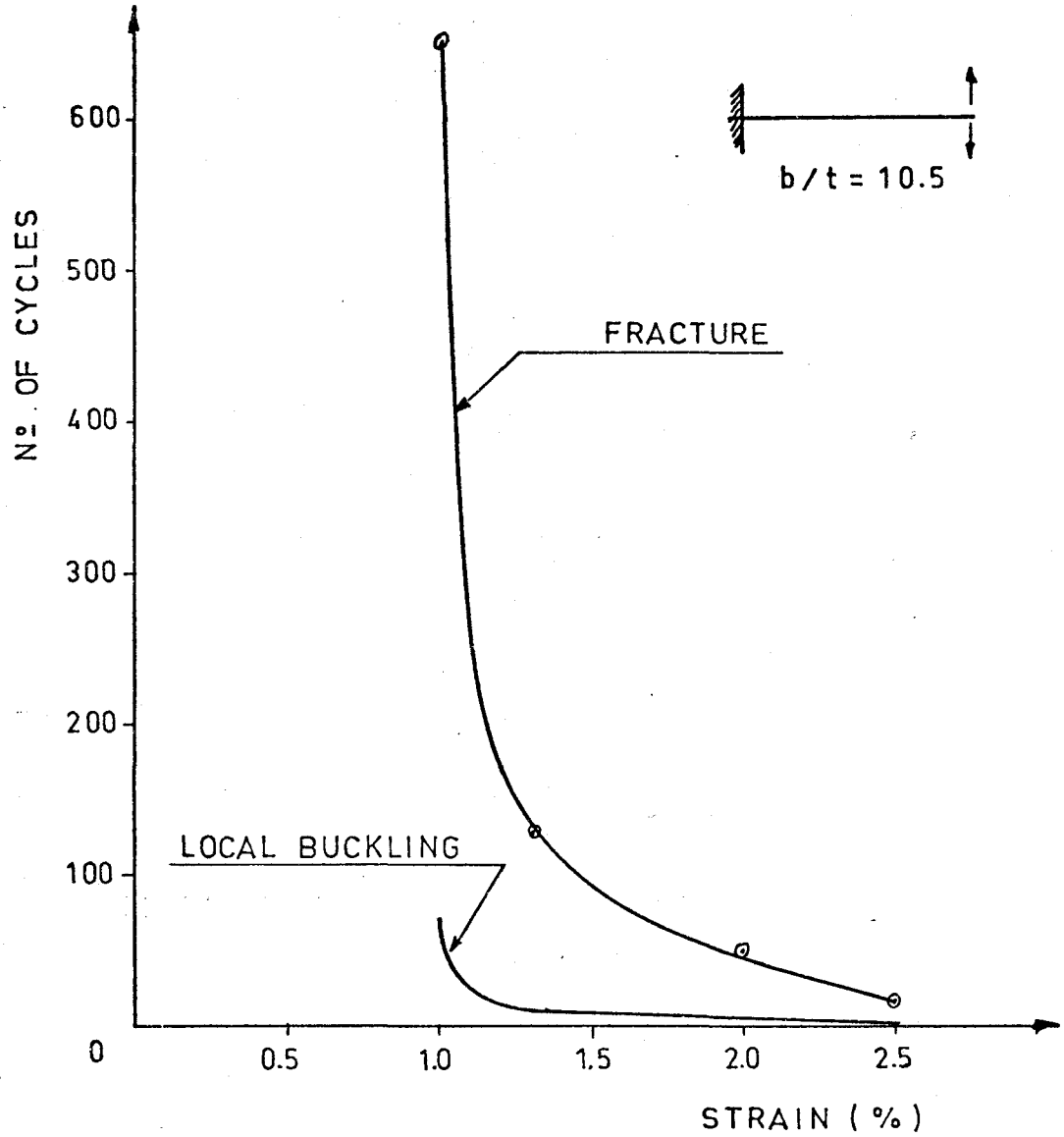

FIG. 4.1 NUMBER OF CYCLES TO FRACTURE Vs. CYCLIC STRAIN

APPENDIX 1

Description of the Equations Used by Prasad in his Computer Program

For theoritical purposes the round HSS were approximated by thin-walled cylindrical shells. The stability criterion was determined by an approach similar to that of Seide and Weingarten (24) taking into account the inelastic behaviour of the material for a thin circular cylinder with simply supported ends and subjected to constant bending moments at the ends. Stress concentrations and residual stresses were neglected.

Seide and Weingarten's approach made use of the small deflection theory (Donnell's theory modified by Batdorf (25)) in the elastic range in which the stability criterion ultimately resulted in the solutions of an eighth-order differential equation. A typical small wave type of deflection function was assumed and solved by the approximate method of Galerkin satisfying the stability criterion

The basic equation used by Prasad for the evaluation of buckling load was:

$$
\begin{aligned}
Q(w) = {} & \alpha_1 \frac{\partial^8 w}{\partial x^8} + \frac{\alpha_2}{R^2} \frac{\partial^8 w}{\partial x^6 \partial \theta^2} + \frac{\alpha_3}{R^4} \frac{\partial^8 w}{\partial x^4 \partial \theta^4} + \frac{\alpha_4}{R^6} \frac{\partial^8 w}{\partial x^2 \partial \theta^6} \\
& + \frac{\alpha_5}{R^8} \frac{\partial^8 w}{\partial \theta^8} + \frac{\alpha_6}{R} \frac{\partial^7 w}{\partial x^6 \partial \theta} + \frac{\alpha_7}{R^3} \frac{\partial^7 w}{\partial x^4 \partial \theta^3} + \frac{\alpha_8}{R^5} \frac{\partial^7 w}{\partial x^2 \partial \theta^5} \\
& + \frac{\alpha_9}{R^7} \frac{\partial^7 w}{\partial \theta^7} + \alpha_{10} \frac{\partial^6 w}{\partial x^6} + \frac{\alpha_{11}}{R^2} \frac{\partial^6 w}{\partial x^4 \partial \theta^2} \\
& + \frac{\alpha_{12}}{R^4} \frac{\partial^6 w}{\partial x^2 \partial \theta^4} + \frac{\alpha_{13}}{R^6} \frac{\partial^6 w}{\partial \theta^6} + \frac{\alpha_{14}}{R} \frac{\partial^5 w}{\partial x^4 \partial \theta} \\
& + \frac{\alpha_{15}}{R^3} \frac{\partial^5 w}{\partial x^2 \partial \theta^3} + \alpha_{16} \frac{\partial^4 w}{\partial x^4} + \frac{\alpha_{17}}{R^2} \frac{\partial^4 w}{\partial x^2 \partial \theta^2} \\
& + \frac{\alpha_{18}}{R} \frac{\partial^3 w}{\partial x^2 \partial \theta} + \alpha_{19} \frac{\partial^2 w}{\partial x^2} = 0
\end{aligned}
\tag{11}
$$

where α_1, α_2, ..., α_{19} are variable coefficients involving the geometrical parameters and material properties of the cylinder. The values of all the above coefficients are given by Prasad (6).

For the elastic case, Donnell's stability criterion as modified by Batdorf was:

$$
D_e \nabla^4 w + \frac{Et}{R^2} \nabla^{-4} \frac{\partial^4 w}{\partial x^4} + t(\sigma_{cb} \cos\theta) \frac{\partial^2 w}{\partial x^2} = 0 \tag{13}
$$

A suitable solution for the deflection function 'w' to satisfy the stability criterion which fulfills the conditions appropriate to simple support of the ends with bulkheads rigid in their own plane but free to warp out of their plane was assumed as follows:

$$w = \sin \frac{m\pi x}{L} \sum_{n=0}^{\infty} a_n \cos n\theta \tag{15}$$

In practice, the number of terms used in the deflection function is limited. Therefore, it was assumed that only 'p' terms need to be considered, that is,

$$w = \sin \frac{m\pi x}{L} \sum_{n=0}^{(p-1)} a_n \cos n\theta \tag{16}$$

Coefficients a_0 , a_1 , ..., a_{p-2} , a_{p-1} were calculated from:

$$\int_0^{2\pi} \int_0^{L} Q'(w) \sin \frac{m\pi x}{L} \cos q\theta \, dx d\theta = 0 \tag{17}$$

$$q = 0, 1, 2, \ldots, (p-1)$$

where Q'(w) represents the stability criterion, equation (11),

after substituting the assumed deflection function w in equation (15).

since $\int_0^L \sin^2 \frac{m\pi x}{L}\, dx = \frac{L}{2}$.

equation (17) may be reduced to the form:

$$\int_0^{2\pi} Q''(w) \cos q\theta \, d\theta = 0 \qquad q = 0, 1, 2, \ldots, (p-1) \tag{18}$$

where $Q''(w) = \frac{Q'(w)}{\sin(m\pi x/L)} = \Omega$

and where Ω is purely a function of θ.

Equation (18) reduces to the form:

$$\sum_{j=1}^{19} \int_0^{2\pi} \alpha_j q_j \cos q\theta \, d\theta = 0 \qquad q = 0, 1, 2, \ldots, (p-1). \tag{19}$$

All the values of coefficient q_j are given by Prasad (6). The system of equations obtained by integration of

equation (19) is a homogeneous system of 'p' equation in 'p' unknowns, a_o, a_1, ..., a_{p-2}, a_{p-1}, etc, as follows

$$
\begin{aligned}
& a_0 \beta_{11} + a_1 \beta_{12} + - - - - + a_{p-1} \beta_{1p} = 0 \\
& a_0 \beta_{21} + a_1 \beta_{22} + a_2 \beta_{23} + - - - - + a_{p-1} \beta_{2p} = 0 \\
& - \\
& - \\
& - \\
& a_0 \beta_{(p-1)} + a_1 \beta_{(p-1)2} + a_2 \beta_{(p-1)3} + - - - - \\
& \quad + a_{p-1} \beta_{(p-1)p} = 0 \\
& a_0 \beta_{p1} + a_1 \beta_{p2} + a_2 \beta_{p3} + - - - - + a_{p-1} \beta_{pp} = 0
\end{aligned}
\tag{21}
$$

Such a system of homogeneous equations has a non-trival solution in the case when the determinant formed by the coefficients of a_o, a_1, ..., a_{p-2}, a_{p-1} vanishes , that is,

$$\Delta = \begin{vmatrix} \beta_{11} & \beta_{12} & \cdots & \beta_{1(p-1)} & \beta_{1p} \\ \beta_{21} & \beta_{22} & \cdots & \cdots & \cdots \\ \cdots & \cdots & \cdots & \cdots & \cdots \\ \cdots & \cdots & \cdots & \cdots & \cdots \\ \cdots & \cdots & \cdots & \cdots & \cdots \\ \cdots & \cdots & \cdots & \cdots & \cdots \\ \beta_{p1} & \beta_{p2} & \cdots & \beta_{p(p-1)} & \beta_{pp} \end{vmatrix} = 0 \qquad (22)$$

Equation (22) is of pth degree of a certain function of the stress-strain relationship and would give p values of the critical buckling strain ϵ_c for a particular longitudinal buckle wave-length, if the cylinder behaved elastically. However, because of non-linear nature of equation (22), a solution was obtained by assuming a value of ϵ_c, t and the half buckle wave-length yielding the value of D/t required.

APPENDIX 2

NOMENCLATURE

A	Cross-sectional area of Round HSS.
b	Width of Square HSS or width of Wide Flange Sections.
D	Diameter of Round HSS = OD.
D_c	Hole diameter of the collar.
e	Dimensionless energy ratio.
$\sum e$	Accumulated energy ratio.
E	Modulus of elasticity.
$E_{ext.}$	Modulus of elasticity obtained by using extensometer.
$E_{s.g.}$	Modulus of elasticity obtained by using strain gauges.
HSS	Hollow structural sections.
I	Moment of inertia of Round HSS.
L	Half buckle wave-length.
L'	Span of simple beam.
m	Number of longitudinal half waves.
M_p	Plastic moment
M_y	Yield moment.
n	Parameter which controls the shape of the stress-

strain diagram.

N	Number of elements into which the circumference of the tube is divided, in Prasad computer program's.
$P_{fail.}$	Failure load for any tensile specimen.
$P_{max.}$	Maximum load sustained by a tensile specimen.
P_p	Plastic load.
P_y	Yield load.
R	Radius of Round HSS.
s	Shape factor for Round HSS
S	Section modulus for Round HSS.
t	Thickness.
W	Energy dissipated per single load excursion.
$\sum W$	Cumulative energy dissipation.
Z	Plastic section modulus for Round HSS.
Δ	Limiting cyclic deflection at midspan of beam.
Δ_m	Maximum deflection at midspan, measured from the original zero position.
Δ_p	Elastic deflection corresponding to the plastic load P_p.
Δ_y	Yield deflection.
Δ'_o	Residual deflection at midspan measured from the original zero position.
Δ'_w	Residual deflection which equals to the width of the hysteresis loop.
σ	Stress at any point.

σ_u	Ultimate stress.
σ_y	Yield stress.
$\sigma_{0.7}$	Stress value obtained by drawing a straight line through the origin of the stress-strain curve, at a selected slope of 0.7 E
$\sigma_{0.85}$	Stress value at 0.85 E.
ϵ	Corresponding strain to σ.
ϵ_c	Critical buckling strain.
π_d	Plasticity ratio = Δ'_w / Δ_p.
$\Sigma\pi_d$	Cumulative plasticity ratio.
μ	Ductility factor = Δ / Δ_p.
b/t	Width to thickness ratio for Wide Flange Sections and Square HSS.
D/t	Diameter to thickness ratio for Round HSS.
$m\pi R/L$	Buckle half wave-length parameter.
λ	$\sigma_{0.7} / \sigma_{0.85}$.
W_p	$\frac{1}{2} P_p \Delta_p$

APPENDIX 3

LIST OF REFERENCES

1. Bertero, V.V., and Popov, E.P.,
   "Effect of Large Alternating Strains of Steel Beams", Journal of the Structural Division, ASCE, Vol. 91, No. ST1, Proc. Paper 4217, Feb. 1965, pp. 1-12.
2. Benham, P.P., and Ford, H.,
   "Low Endurance Fatigue of a Mild Steel and Aluminum Alloy", Journal of Mechanical Engineering Science, Vol. 3, No. 2, June 1961, pp. 119-132.
3. ASCE and WRC,
   "Plastic Design in Steel - A Guide and Commentary", ASCE, Manuals and Reports on Engineering Practice, No. 41, 1971.
4. Popov, E.P., and Pinkney, R.B.,
   "Behaviour of Steel Building Connections Subjected to Inelastic Strain Reversals", University of California, Bulletin No. 13, American Iron and Steel Institute, November 1968, 150 East 42nd Street,

New York, N.Y. 10017.

5. Takanashi, K.,
"Inelastic Lateral Buckling of Steel Beams Subjected to Repeated and Reversed Loadings", Fifth World Conference on Earthquake Engineering, Rome, June 1973, Paper No. 91.

6. Prasad, J.,
"Hollow Structural Sections in Flexure", M. Eng. Thesis, McMaster University, 1972.

7. Shanley, F.R.,
"Strength of Materials", McGraw-Hill Book Company, New York, 1957, pp. 201-206.

8. Vann, W.P., Thompson, L.E., Whalley, L., and Ozier, L.D.,
"Cyclic Behaviour of Rolled Steel Members", Fifth World Conference on Earthquake Engineering, Rome, June 1973, Paper No. 145.

9. Nashid, M.,
"Hollow Structural Sections Subjected to Inelastic Strain Reversals ", M. Eng. Thesis, McMaster University, May 1974.

10. Munchener Ruckversicherungs-Gesellschaft,
"Earthquakes", D-8000 Munchen 40, Koniginstrabe 107, Published in 1973.

11. Berg, G.V., and Stratta, J.L.,
"Anchorage and the Alaska Earthquake of March 27, 1964", American Iron and Steel Institute.

12. Munchener Ruckversicherungs-Gesellschaft,
"Managua, a Study of the 1972 Earthquake",
D-8000 Munchen 40, Koniginstrabe 107, Published
in 1972.

13. Jennings, P.C.,
"Engineering Features of the San Fernando Earthquake, February 9, 1971", Earthquake Engineering Research Laboratory, California Institute of Technology, Pasandena, California.

14. Wood, F.J.,
"The Prince William Sound, Alaska, Earthquake of 1964 and Aftershocks", U.S. Department of Commerce, Environmental Sciences Services Administration, United States Government Printing Office, Washington, 1966.

15. Stratta, J.L., Chairman,
"Peru Earthquake of May 31, 1970, Preliminary Report", Earthquake Engineering Research Institute, 366 - 40th Street, Oakland, California 94609, September 1970.

16. Popov, E.P., and Bertero, V.V.,
"Cyclic Loading of Steel Beams and Connections", Journal of the Structural Division, ASCE, Vol.99, No. ST6, Proc. Paper 9790, June 1973, pp. 1189-1204.

17. Hudoba, J.,
"Plastic Design Capabilities of Hollow Structural

Sections", M. Eng. Thesis, McMaster University, January 1971.

18. American Society for Testing Materials, "Steel Piping, Tubing and Fittings", ASTM , Part 1, January 1966, Page 328.

19. Micro-Measurements, "Strain Gauge Applications with M-Bond AE-10/15 and M-Bond GA-2 Adhesive Systems", M-Line Accessories, Instruction Bulletin B-137-3, August 1974, P.O. Box 306 Romulus, Michigan 48174.

20. D.M.C. Specification Products, "Steel, Aluminum, Stainless Steel, Copper and Nickel", Drummond McCall, Reference Book 16, P.O. Box 219 - Montreal 101, Quebec.

21. Ramberg, W., and Osgood, W.R., "Description of Stress-Strain Curves By Three Parameters", Technical Note No. 902, NACA (National Advisory Committee for Aeronotics), July 1943.

22. Canadian Standards Association, "Steel Structures for Buildings - Limit States Design", CSA Standard S16.1-1974, pp. 31-32.

23. Hanson, R.D., "Comparison of Static and Dynamic Hysteresis Curves", Journal of the Engineering Mechanics Division, Vol. 92, No. EM5, Proc. Paper 4949, October 1966, pp. 87-113.

24. Seide, P. and Weingarten, V.I.,
"On the Buckling of Circular Cylindrical Shells Under Pure Bending", Journal of Applied Mechanics, Vol. 28, Series E, Number 1, March 1961, pp. 112-116.

25. Batdorf, S.B.,
"A simplified Method of Elastic Stability for Thin Cylindrical Shells II - Modified Equilibrium Equation", Technical Note No. 1342, NACA, 1947.